2022

Step Length Estimation in Daily Activities using RSSI-based Techniques

Zanru Yang

UNIVERSITY
OF WOLLONGONG
AUSTRALIA

Step Length Estimation in Daily Activities using RSSI-based Techniques

Zanru Yang

This thesis is presented as part of the requirements for the conferral of the degree:

Doctor of Philosophy

Supervisor:
A/Prof. Le Chung Tran

Co-supervisor:
Prof. Farzad Safaei

The University of Wollongong
School of School of Electrical, Computer and Telecommunications Engineering

August, 2022

This research has been conducted with the support of an Australian Government Research Training Program Scholarship.

Declaration

I, *Zanru Yang*, declare that this thesis is submitted in partial fulfilment of the requirements for the conferral of the degree *Doctor of Philosophy*, from the University of Wollongong, is wholly my own work unless otherwise referenced or acknowledged. This document has not been submitted for qualifications at any other academic institution.

Zanru Yang

June 5, 2023

Abstract

Step length, an essential component in gait analysis, is becoming appealing in many aspects of our life. It can reflect physical fitness among the young and the senior, e.g., obesity, falling probability and severity. It can also help predict the life expectancy of the elderly. Moreover, the disabled or patients with impaired cognitive functions also behave differently from healthy people in terms of step length. Another application of step length estimation is that it leverages non-GPS localisation where the global positioning system (GPS) is restricted or prohibited.

Accurate measurements of step length are thus important in numerous applications. Unfortunately, the existing step length measurement techniques are yet matured. Their common drawbacks could be expensive costs, specific location requirements, constraints of human activities to be measured and of the movement direction of the human under test, proneness to errors due to occlusions, modest accuracy, or a combination of these drawbacks. An accurate path loss model between two human feet is also missing.

Therefore, this thesis examines step length estimation and distance measurement between human body parts in wireless body area networks (WBANs). The thesis aims to overcome several above drawbacks by proposing novel techniques to estimate the step length of pedestrians, using our developed wearable, unobtrusive hardware during ambulation or other daily activities.

To this end, the thesis first proposes the channel model between two human ankles. The transceivers are built from off-the-shelf components, which are commercially available and well-developed. These developed transceivers are attached to the medial side of human ankles. Experiments are then carried out under different constraints to find the optimal hardware configurations for the distance estimation. The transmitted power at

0 dBm and the data rate at 9600 bps are found to be the optimal hardware configurations. The path loss between ankles, called on-ankle path loss, is investigated and characterised as the path loss in a free space model plus a correction factor. The proposed channel model jointly considers the path loss, non-linearity of the equipment, shadowing effect, multipath propagation, insertion loss and mismatch loss.

After the path loss model for the wireless channel between two ankles of the subject under test has been accurately characterised, this thesis proposes a novel step length measurement technique, using our developed wearable transceivers for various daily activities under different environments. In particular, experimental received signal strength (and thus path loss) data sets for both walking and jogging activities in either indoors or outdoors are collected and analysed to estimate human step length. A novel filtering technique, which sets up an upper threshold and a lower threshold, is proposed to filter out the on-ankle path loss outliers, thus creating a more reliable range of path loss values, which will be used for step length estimations. The histogram of the remaining on-ankle path loss between the two thresholds follows a two-Gaussian distribution. The upper threshold can be formulated based on the coefficients of the second hump of this two-term Gaussian distribution, while the lower threshold could be determined at the point where the survival rate of the on-ankle path loss reaches 0.68. Our experiments show that the proposed measurement technique can measure accurately the step length with errors at the sub-centimetre level.

Afterwards, this thesis advances the above measurement technique by proposing a novel exponential weighted moving average (EWMA) algorithm to update the upper and lower thresholds, and thus the step length estimation, recursively. The EWMA algorithm allows our measurement technique to process each shorter subset of the data set, called a time window, and estimate the step length, rather than having to process the whole data set at a time. The step length is periodically updated on the fly when the time window is 'sliding' forwards. Thus, the EWMA algorithm facilitates the step length estimation in real-time. Experiments are conducted for both indoor walking and outdoor walking conditions. The impact of the EWMA parameter is analysed and the optimal parameter is

discovered for different experimental scenarios. Our experiments show that the EWMA algorithm could achieve comparable accuracy as the initially proposed technique with errors as small as 1.90% and 0.30% for the indoor and outdoor scenarios, respectively, while the processing time required to output an estimation of step length could be significantly shortened by 53.96% and 60% for the indoor walking and outdoor walking, respectively. This means the EWMA algorithm helps save more than half of the time in outputting a step length estimation without compromising the accuracy.

Finally, this thesis compares the accuracy and feasibility of wearable smart devices on the market by carrying on experiments using the Apple watch and Fitbit watch with combined smartphones. The Apple watch is able to output step length directly with relative errors of 7.03% and 6.23% for indoor and outdoor scenarios, respectively. The Fitbit watch allows users to adjust their step length manually while having relative estimation errors of 10.58% and 7.93% for indoor and outdoor walking activities, respectively. Our proposed hardware using an RSSI-based method with novel filtering and EWMA algorithms could achieve relative step length estimation errors of 1.90% and 0.30% under the same setting. In addition, more features, such as wearing location, comfortability and possible cost, are evaluated.

In short, the thesis has tackled the challenging problem of estimating the human step length in daily activities by proposing a novel channel model and several novel measurement techniques. These contributions have laid some initial but important foundations for exploring the complete solution to the above problem. In the future, the proposed step length estimation hardware and the corresponding algorithm will be further improved to include more features, such as detecting different human activities and monitoring more gait parameters, including gait speed, step width and foot angle.

Acknowledgements

First and foremost, I would like to express my genuine appreciation to my principal supervisor, Associate Professor Le Chung Tran, and my co-supervisor, Professor Farzad Safaei, for their generous and patient guidance as well as continuous encouragement and inspiration. They have spent a lot of their precious time on training me how to conduct and record experiments in an efficient way, how to survey and solve research problems, as well as how to progress in academic writing and present work professionally. Their diligence and persistence in research have indeed set respectable models for me and have shaped my attitude as a researcher. Their innovative opinions and valuable comments always enlighten me. Apart from supervision, I am also thankful for their gentleness and wisdom throughout the journey, which placate my anxiety and help me overcome many difficulties. Without their creative thoughts and constructive suggestions in life and study, I would not have achieved this stage.

It is an honour to be a member of the School of Electrical, Computer and Telecommunications Engineering, University of Wollongong. I would like to thank for the financial support from the university for offering me the International Postgraduate Tuition Awards (IPTA) and University Postgraduate Award (UPA), as well as the lovely staff that I have met during these years.

I would like to show my thankfulness to my friends, Dr Yawen Zheng, Dr Melody Tan, Miss Chuanhui Tian, and Miss Rachel Chin, for the cheerful time that we have spent together and for the sorrowful moments that we have shared with each other. I would like to thank my office mates in Building 6.311, Dr Jiaman Li, Dr Yuxi Ruan, Dr Yiwen Mao, and Dr Yiwei Huang, for sharing valuable experiences and constantly encouraging one another.

I also would like to thank my housemate, Dr Zhuqin Feng. She is more than a flatmate but a big sister to me in my life and studies in Australia because of her caring and kindness. Her tasty cuisine makes me feel at home. Thanks to her lovely cats, Titan and Lucky, for enriching my life with their curious characters and fluffy furs.

Lastly, I would like to extend my heartfelt gratitude to my mother, Ms Ying Zhao and other family members back home. Although we are apart from each other, they never stop encouraging me for a second. They not only support me financially, but more importantly, they are my mental stronghold as they always trust and believe in me from the deepest heart.

Abbreviations

AE	Absolute Error
AFT	Access Point Faced Trilateral
AOA	Angle of Arrival
AP	Access Point
BMI	Body Mass Index
CAREN	Computer-Assisted Rehabilitation Environment
CDF	Cumulative Distribution Function
DFBM	Distance between the Fixed-nodes Based Model
DLT	Direct Linear Transformation
EMA/EWMA	Exponential (Weighted) Moving Average
GM	Gauss Model
GPS	Global Positioning System
IDE	Integrated Development Environment
IMU	Inertial Measurement Unit
IoT	Internet of Things
IR	Infrared Radiation
ISM	Industrial, Scientific and Medical
LNSM	Log-Normal Shadowing Model
LNSM-DV	Log-Normal Shadowing Model with the Dynamic Variance
LoS	Line of Sight

LR-WPAN	Low-Rate Wireless Personal Area Network
LSE	Least Square Estimation
MEMS	Micro Electrical Mechanical System
MIMO	Multiple Input Multiple Output
MISO	Multiple Input Single Output
ML	Maximum Likelihood
O-QPSK	Offset Quadrature Phase Shift Keying
PARP	Peak-to-Average Power Ratio
PDF	Probability Density Function
PDR	Pedestrian Dead Reckoning
RALE	RSSI-with-Angle-based Localisation Estimation
RF	Radio Frequency
RSS	Received Signal Strength
RSSI	Received Signal Strength Indicator
RTO	Re-Transmission Timeout
RTT	Round-Trip Time
SIMO	Single Input Multiple Output
SISO	Single Input Single Output
SMA	Simple Moving Average
SMVM	Statistical Mean Value Model
WBAN	Wireless Body Area Network
WMA	Weighted Moving Average
X-CTU	XBee Configuration & Test Unit

List of Symbols

a	amplitude of the Gaussian distribution
α	weight component of mean value μ
AE	absolute error
b	centroid of the Gaussian distribution
β	weight component of standard deviation σ
c	component relates to the peak width of the Gaussian distribution
d	distance between the antennas (estimated step length in this thesis)
$\overline{d}$	average estimated step length
d_0	actual distance
d_{0j}	real average jogging step length
d_{0w}	real average walking step length
ε	normalised error
f	radio frequency
$f(x)$	Gaussian distribution
G_r	antenna gain of the receiver
G_t	antenna gain of the transmitter
h	height of the placement of the hardware
l	length of the long edge of the rectangle
n	number of points
p	data point

P	power level
P_r	received power
P_t	transmitted power
PL_{FS}	free space path loss
PL_{Ins}	path loss caused by mismatch loss and insertion loss
PL_{Mul}	path loss caused by multipath propagation
PL_{NonL}	path loss caused by hardware non-linearity
PL_{OA}	experimental on-ankle path loss
PL_{Shad}	path loss caused by shadowing effect
q	weight degree
r	radius
γ	weight component
R_{far}	far field region
R_{near}	near field region
t	time
tw	time window
$Th^{(l)}$	lower threshold
$Th^{(u)}$	upper threshold
μ	mean
χ	point
Y_t	output at time t
π	mathematical constant
λ	signal wavelength
σ	standard deviation
Δ	absolute difference
Δd	absolute distance error

ΔPL correction factor

Contents

List of Figures

List of Tables

Chapter 1

Introduction

1.1 Background

To date, the growing population is a sign of prosperity but there are also challenges associated with it. The baby boom and the increased life expectancy lead to a population explosion, which may burden the current healthcare system.

A world population pyramid illustrated in [1] is shown in Fig. 1.1. It is visualised that the world population is becoming healthier. The median age is the midpoint of age among a population. The world median age in 1950 was 23.6 years. In 2018, the median age was 30 years, and it is predicted to be 41.6 years in the year 2100, which is almost doubled compared to the year 1950. So as the life expectancy, over 20 million population are expected to live over 90 years old. When the top of the pyramid (i.e., especially the yellow range representing the year 2018 till now) becomes wider and looks less like a pyramid and instead becomes more box-shaped, the population lives through younger ages with a lower risk of death and dies at an older age. It is expected that the global population reach to 11.2 billion at the end of this century.

Adversely, the expanded population may overload the medical care frameworks, essentially influencing personal comforts and wellbeing [2]. Many individuals die from cancer, cardiovascular disease, Parkinson's, asthma, obesity, diabetes and many more chronic or lethal sicknesses every year. The common problem with all current fatal diseases is that they have often been diagnosed in the late stage. Another example of the breakdown of the medical system is that, during the outbreak of COVID, with the exponentially growing

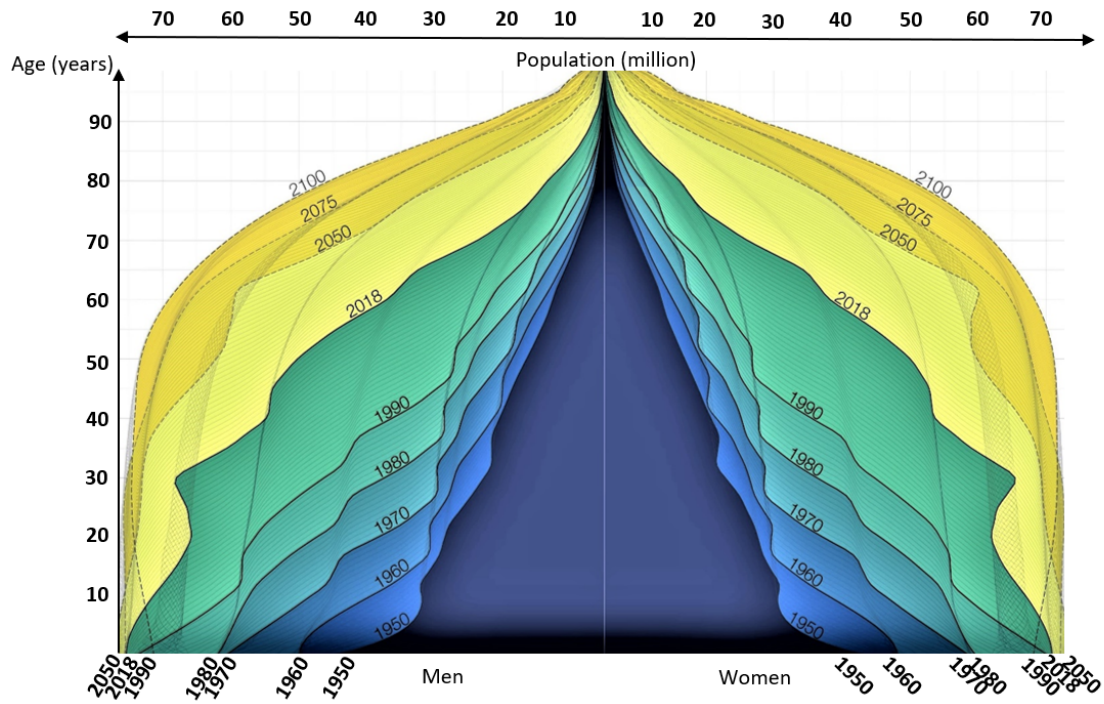

Figure 1.1: The demography of the world population from 1950 to 2100 [1].

number of confirmed cases, numerous patients could not receive appropriate treatments despite the health workers have already overworked.

Remote health diagnosis and monitoring are one of the solutions to alleviate the medical burden. Since most diseases can be prevented or treated at early stages, the importance of early detection is evident. Healthcare systems can be strengthened by monitoring, surveying, and providing wellness management and by concentrating on early detection as well as early prevention of diseases, which have become hot topics [2], [3], especially in the post-COVID era [4]–[6]. A more affordable and proactive healthcare system is one that is capable of early detection of abnormal conditions and signals. If individuals have access to such kind of personal healthcare monitoring products, the burden of the hospital monitoring system could be significantly eased. In this way, the excessive expense of in-hospital monitoring could be avoided.

With the increasing development and utilisation of the Internet of things (IoT), potential applications of the IoT in healthcare and remote monitoring for pandemic situations are proposed in the literature, e.g., [5], [6], to monitor a series of real-time body indexes of patients, such as the body temperature, respiratory rate, blood oxygen saturation, heart

rate, gait patterns, and step length (or stride length), to name a few.

Let us discuss the last two parameters in the above list in more detail. Safe walking requires intact cognition and executive control, thus monitoring the gait of dwellers, especially the elderly, is significant. Gait, and its related parameters, including the step length, could represent one's physical functioning ability. Step length is an important component of gait analysis, assisting health diagnostics, sports performance improvement, injury prevention, robotics and prosthesis structure design. Primarily, it is employed as a health indicator, helping diagnose injuries and other potential physical or mental diseases. Step length is able to predict the probability of slips and falls during walking or after perturbation. Step length and gait speed also vary between the healthy people and the disabled. They can even reflect mortality and predict the remaining years of life. Estimation of step length could also facilitate localisation and social distancing enforcement. In fact, in the early stage of COVID, without prescription and vaccination, social distancing is an important way to break the infection chain [5]. Correctly estimating the step length could contribute to personal localisation, especially in the indoor environment where the GPS is inaccurate. Step length estimation could also assist the measurement of the social distances between individuals, which could, in turn, help enforce the social distancing practice [7].

For the aforementioned reasons, this thesis focuses on step length estimation.

1.2 Motivation and Objectives

Step length estimation relies on extra hardware to collect data to assist the computation. The current deployments of such hardware pose some challenges and concerns as detailed below.

The first concern is the space requirement for the hardware deployment to measure the step length. Traditionally, the step length is estimated at a specific place. Patients are typically asked to perform a four-or-six-minute walk test or a ten-metre walking test in the clinics under the surveillance of nurses or other specialists. When more data is needed, the patients must come to the clinic to perform the walk on a sensing mat again. However,

it is reported that the gait patterns, including step length, extracted from the deliberate ambulation are different from the walking performance that occurs in the natural perambulation condition. Thus, it is important to measure the step length that reflects one's daily gait performance, i.e., the location should not be constrained in a specific room or on a specific sensing mat that pre-defines the direction of ambulation.

Meanwhile, the accessibility of the equipment, such as the commercial availability and the cost-efficiency, is another concern. As the ultimate goal is to monitor and estimate the user's step length timely and periodically, the wearable device should be reliable so that it is not only able to operate for a long time but also has no safety hazard. Thus, it is required that the hardware components of the device should be maturely developed to sustain precise estimation over a period of time, be off-the-shelf to purchase and cost-effective to maintain and utilise regularly.

At the same time, complexity and usability, e.g., of whether the estimation approach is very technical or user-friendly, the ease of initialising and setting up, are other challenges that should be considered. For example, therapists supervise the walkway-based measurement in the rehabilitation centre. The infrared image processing technique requires well-trained staff. These step length estimation methods are not suitable for the public without relevant experience and knowledge. Additionally, no current step length estimation method seems to be transparent and accurate enough for measuring human step length in the daily activities, while maintaining the portability and comfortability. Moreover, the long time exposure to laser may raise other health concerns, which makes the infrared radiation (IR)-based step length detection not suitable for step length measurements on a daily basis.

The disclosure of personal privacy and confidential information is the main concern of the vision-based technologies that deploy cameras for step length estimations. Besides, though being able to capture the posture of the walker during ambulation to promote the precision and reliability of the step length estimation, the installation of cameras disguisedly limits the movement range and direction of the person under test. The subject must move at least within the scope that cameras can capture. To grab the best resolution of the

picture or video and to estimate the target information as accurately as it can, the trajectory of the activity should be performed vertically to the filming direction of the camera. Any obstacle between the cameras and the subject under test would cause serious estimation errors.

Henceforth, this thesis aims to address the above concerns. Our approach is to develop the hardware from the commercially available off-the-shelf components and to propose novel measurement techniques to estimate the step length based on the radio frequency (RF) propagation between the hardware attached to the ankles of the subject under test. The results show that our hardware along with our novel measurement technique could measure accurately the step length in the daily human activities for both indoors and outdoors. To the best of our knowledge, our hardware and proposed measurement techniques are the first of their kinds.

1.3 Research Questions and Research Approaches

Given the above objectives, this thesis addresses the following research questions: (i) how to describe the path loss between two human ankles and how to optimally configure the hardware which is deployed to measure human step length? (ii) how to estimate human step length in daily activities under different indoor and outdoor environments? (iii) how to estimate the step length in real-time and what are the optimal parameters of the proposed techniques? and (iv) how is the performance of the developed hardware if compared to the smartwatches?

The following explains these questions and our corresponding research approaches in detail.

- The objective of the first research problem is to present the channel model between two human ankles, which has not existed in the literature. The free space path loss model computes the power attenuation in a single line of sight (LoS) path propagation, without considering reflections and shadowing. The two-ray ground reflection model is only suitable for the system with elevated antennas and a distance of several kilometres. For the human body, the IEEE 802.15.6 path loss models [8], [9],

are mainly used in laboratories and anechoic chambers, and they are not for channels between the human ankles. Therefore, we develop our RF hardware, attach the hardware to the medial side of the ankles of the person under test, collect the channel attenuation data sets, and predict the channel model. Since the hardware equipment is attached to the medial sides of human ankles, where an LoS path exists, considering the maximum distance (i.e., the step length that aims to be estimated) during the whole ambulation session is less than one metre, our path loss model is found to be the free space path loss model added with a correction factor, which is found empirically.

To address the optimal configurations of the hardware and to find the correction factor of the proposed path loss model, experiments are carried out for different settings, including the transmitted power, data rate, and different placements of the hardware on or off the human body, as well as different indoor and outdoor environments.

- The second research question aims to propose novel step length estimation methods that are able to calculate the average step length of the subject under test. To avoid miscalculations and to enhance the estimation accuracy, the experiments are consistently carried out with the optimal hardware configurations and they are repeated multiple times. Thus multiple data sets for each human activity (walking and jogging) and for each propagation environment (indoor and outdoor) can be collected. The core idea in our proposed estimation algorithm is the proposal of the upper and lower bounds, which can be either found empirically or formulated statistically based on the collected data sets, to filter out the outliers in order to form a reliable range of data values used for estimating the step length.

- Thirdly, this thesis proposes the step length estimation technique which could be used for the measurement in real-time. It is shown that long distance walks may contribute more valuable information beyond short walks [10]. Thus, we significantly expand the size of our experimental data sets, along with proposing a novel

exponential weighted moving average (EWMA) algorithm to continuously estimate the average step length and keep updating this estimation over a short period of time to simulate the real-time processing. The optimal parameters of this EWMA algorithm are empirically found in the sense that they minimise the measurement errors.

- The last research question is practical as there are smart devices on the market that provide step length measurements, such as Apple watches or Fitbit watches. This thesis promptly includes experiments using smartwatches, with combined smartphones under the same experimental environments, and then analyses as well as makes comparisons between a series of features and parameters of our proposed estimation techniques and those of the popularly used wearable devices.

1.4 Contributions

This thesis proposes a number of novel solutions/algorithms. Specifically, it contains the following contributions.

- In this thesis, we have developed wireless transceivers for our measurement campaign. The developed transceivers are portable and relatively comfortable to wear in daily activities. They are used to collect the path loss data that will be processed to estimate the human step length. To determine the optimal configurations of the developed wearable hardware system, different configurations regarding transmitted power and data rate are investigated. It is found that the transmission power of 0 dBm along with the data rate of 9600 bps are the optimal configurations of the developed transceivers.

- For the first time, a novel empirical path loss model between two transceivers attached to the ankles of the person under test is derived in this thesis. It is discovered in this thesis that the path loss of the wireless channel between two ankles can be described as the free space path loss model added with a corrections factor, which jointly considers the non-linearity of the equipment, shadowing effect, multipath, mismatch loss, and insertion loss of the hardware components. With the optimal

configurations of the hardware and the proposed empirical path loss model, the distance between two ankles (i.e., the step length) can be calculated accurately for both walking and running activities in either indoor or outdoor environments.

- To estimate the step length in the human walking and running activities and to ensure the accuracy of the estimation, a novel filtering technique is proposed to set up the two thresholds of path loss values in order to eliminate the path loss outliers. The remaining data is thus more reliable, which will be used to estimate the step length. It is discovered that the measured path loss between two ankles, namely, the on-ankles path loss, follows a two-term Gaussian distribution, and the two thresholds lie on each side of the second hump of this distribution. The lower threshold is determined at the corresponding point when the survival rate of the on-ankle path loss is 0.68. The mathematical expression of the upper threshold is found as $\mu + \gamma\sigma$, where μ and σ are the mean and standard deviation of the measured data set, respectively, while γ is the weight, whose value is different for indoor and outdoor environments. With the proposed filtering technique, the step length can be estimated under different situations, namely, indoor walking, indoor jogging, outdoor walking, and outdoor jogging, with the estimation errors of a sub-centimetre scale.

- To estimate the step length in daily activities and update the step length estimation periodically without having to collect the whole data set and then process it offline, a novel EWMA algorithm is proposed in this thesis. In this algorithm, the thresholds of the on-ankle path loss are computed and updated after a certain period of time. The optimal value of the weight component γ is investigated. The performance of the EWMA algorithm in estimating the step length is evaluated for both indoor and outdoor walking scenarios. It is revealed that the proposed method also achieves the step length estimation errors of 1.90% and 0.30% for the indoor and outdoor scenarios, respectively, while the step length can be computed and updated within a short time. Meanwhile, compared to our proposed step length estimation method mentioned above, it is observed that, with the application of the EWMA algorithm,

the processing time needed to yield a step length estimation result could be saved up to 53.96% and 60% for the indoor walking and outdoor walking, respectively. Thus, the proposed EWMA algorithm facilitates the step length estimation in real-time.

- To make a fair comparison between smart devices and the developed hardware using the RSSI-based method with novel filtering and EWMA algorithms proposed in this thesis, the walking step length of the person under test is examined in both the same indoor and outdoor environments using smartwatches combined with the pairing smartphones. There are two groups of experiments. One of them uses an Apple watch and an iPhone while the other one uses a Fitbit watch and an iPhone. Experimental results show that the relative walking step length estimated errors provided by this thesis, which proposes the RSSI-based method with novel filtering and EWMA algorithm, are as small as 1.90% and 0.30% for indoor and outdoor environments, respectively. Under the same circumstance, the indoor and outdoor relative walking step length estimated errors measured by iWatch are 7.03% and 6.23%, respectively, and by Fitbit are 10.58% and 7.93% for indoor and outdoor walking scenarios. Therefore, compared to Apple and Fitbit watches, the thesis proposed measurement techniques provides higher accurate estimation.

1.5 Thesis Structure

This thesis includes 6 chapters structured as follows.

1. In Chapter 1, the research background is firstly provided. The concerns and challenges of the current techniques, motivations of our research and the corresponding approaches are discussed, followed by the main contributions of the research, the thesis structure and the list of publications.

2. Chapter 2 provides an overview of the significance of step length, monitoring in numerous aspects of life, such as disease diagnostics, falling and injury prevention, rehabilitation, life expectancy prediction, non-GPS positioning and localisation. This chapter then provides an in-depth literature review of the existing works considering

step length estimations, which can be classified into three main approaches, namely walkway-based systems, vision-based systems, and wearable devices. This chapter then discusses more deeply the current works which study gait patterns, especially step length detection and distance measurement, using the received signal strength indicator (RSSI) technique. The research gaps related to step length estimations, overcoming which is the main objective of this thesis, are pinpointed.

3. Chapter 3 considers a static scenario and studies the channel properties between human ankles. The optimal hardware configurations of our developed wearable transceivers are examined. An empirical channel model that describes the path loss between two ankles is also proposed in this chapter.

4. Chapter 4 contains the step length estimation in both walking and jogging activities in both indoor and outdoor environments. The distribution of the on-ankle path loss is explored, based on which a novel filtering technique is proposed to form the boundaries of the reliable data used for the step length estimation. Accuracy analyses of the proposed measurement technique are then discussed.

5. Chapter 5 proposes a novel EWMA algorithm to update the step length estimation in a selected period of time. Analyses of the influence of the parameters on the performance of the EWMA algorithm, derivation of the optimal values of the parameters, and comparisons of the processing time in the step length measurement technique with and without the EWMA algorithm are then presented.

6. Chapter 6 compares the performance and features between currently prevalent smartwatches and the developed hardware using RSSI-based technique with novel filtering and EWMA algorithms proposed in this thesis, in terms of indoor and outdoor walking step length estimation accuracy, comfortability, possible cost, etc.

7. Chapter 7 concludes the thesis with a summary of our contributions, recommendations, and potential future research directions.

Fig. 1.2 provides readers with a visible structure of the thesis.

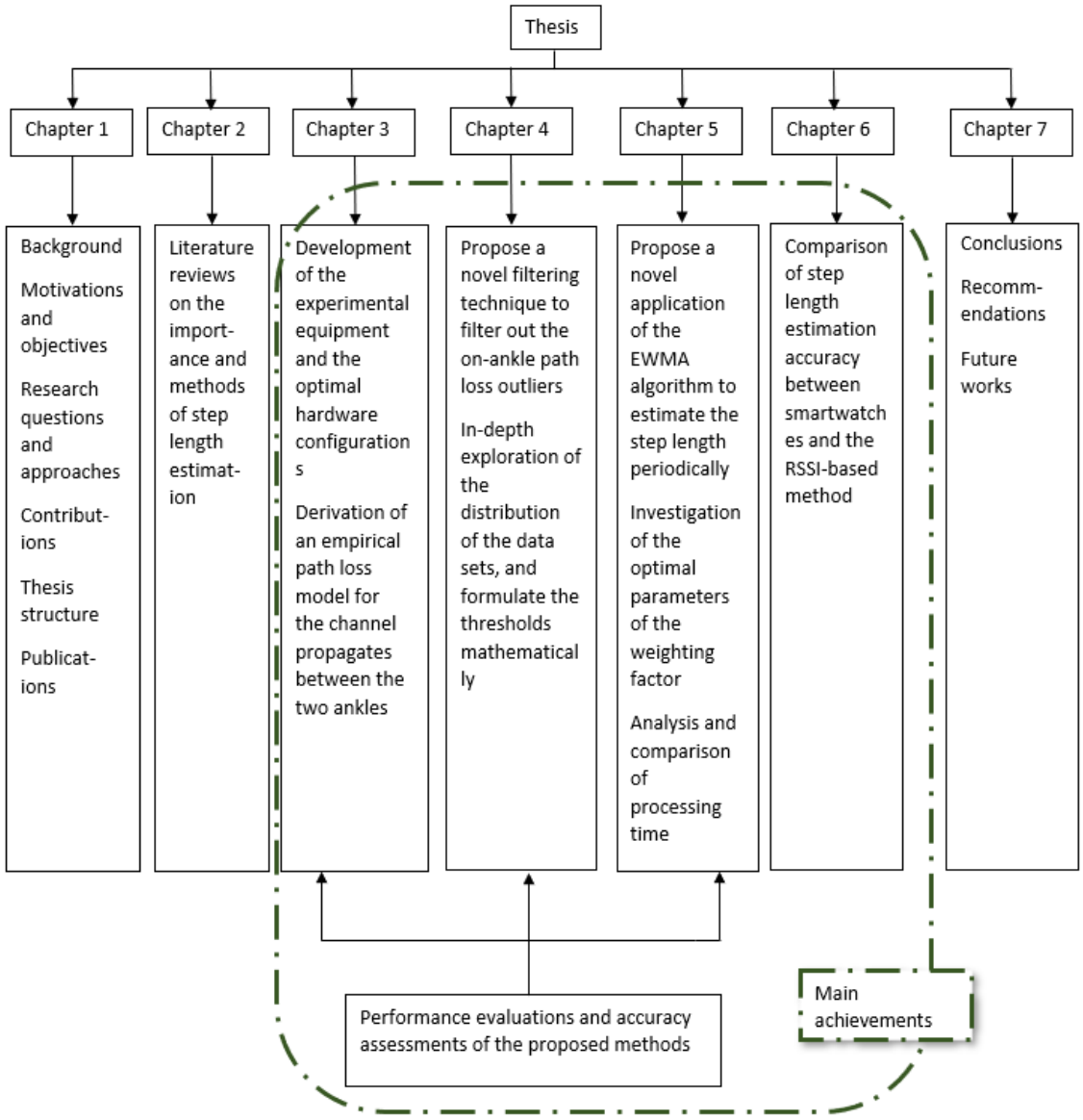

Figure 1.2: Thesis structure.

1.6 Publications

This thesis is based the following three journals, which two of them have been published at Sensors, and one is submitted under review.

1. Z. Yang, L. C. Tran, and F. Safaei, "Step length measurements using the received signal strength indicator," *Sensors*, vol. 21, no. 2, p. 382, Jan. 7, 2021.

2. Z. Yang, L. C. Tran, and F. Safaei, "Step length estimation using the RSSI method in walking and jogging scenarios," *Sensors*, vol. 22, no. 4, p. 1640, Jan. 2022.

3. Z. Yang, L. C. Tran, F. Safaei, A. T. Le and A. Taparugssanagorn, "Real-time step length estimation in indoor and outdoor scenarios," *Sensors*, vol. 22, no. 21, p. 8472, Nov. 2022.

Besides the above journals, the data sets collected and used in this thesis are accessible to the public via the website https://documents.uow.edu.au/ lctran/download/.

Chapter 2

Literature Review

2.1 Introduction

This chapter reviews prior works that study step length estimation. First, Section 2.2 provides an overview of the health monitoring at present and the important role of the gait analysis in the health monitoring system, especially for the elderly. Then, the definition of step length in general and in this thesis is introduced in Section 2.3. The significance of step length is highlighted in Section 2.4. Section 2.5 reviews and assesses the state-of-art step length detection and estimation technologies. Lastly, Section 2.6 compares the step length estimation methods and outlines the open research problems that need to be addressed, as well as the motivations and research objectives of this thesis.

2.2 Overview of Gait Analysis

As mentioned in Chapter 1, awareness regarding health monitoring, especially for daily activities, has been raised in the past decades due to the growing population, prolonged life expectancy, and the surging cost of healthcare and treatments [2], [3]. Consequently, with feasibly collectable data, health indicators are being statistically analysed. Then, recommendations that benefit and improve health are proposed based on the evaluation results. Leading health indicators may include life expectancy, mortality, morbidity, weight and obesity, physical activity and injury, diseases and mental health, etc. as shown in [11], [12].

The latest studies show that the human gait, which describes the walking patterns of

humankind, not only identify a person's lifestyle and quality, but are also of a great importance because they reflect the human health condition [13], [14].

First of all, gait could be observed in clinics and it could assist health diagnostics. Gait disorders and abnormalities can be assessed by observing the movements of patients in clinical settings and techniques. The inconsistency or asymmetry of walking, and abnormal postures, especially for the lower limbs, are cautious alarms for numerous physical problems, such as muscle strain, injuries, stroke, fracture, back pain, joint pain in the lower limbs, and even neurological disorder [15]–[17]. Thus, clinical gait analysis focuses on the patterns, cadences, and balanced force sharing in gait performance.

Apart from clinical and medical studies, gait analysis is also important in sports applications. On one hand, it helps to improve athletes' performance in various sports events, such as running, swimming, cricket, and baseball to name a few [18], [19]. Monitoring and assessing athletes' lower limb motion characteristics during games and training contribute to estimating their energy expenditure, so that athletes' kinetic styles and capabilities could be learned and personalised. Thereby, a more targeted training plan, which enables the improvement of the athletes' performance in an easier and more efficient way, can be developed and adjusted promptly. For example, coaches may use gait analysis to improve athletic performance and recommend proper gear, such as footwear. On the other hand, gait analysis is vital because accurate evaluations not only could prevent unnecessary injuries, but also extend a player's athletic career life. As an example, Schmid *et al.* [20] exam icing athletes' functional performance, as well as gait.It is observed that potential secondary injuries could be significantly decreased with lower vertical ground reaction forces values, which can be achieved by adding a knee joint cooling time and adjusting the gait during the performance.

Another promising prospect of gait analysis is robotic research. It is doubtless that rehabilitation is indispensable for post-operated patients who suffered physical impairments [21]. Assistive therapy could help them to recover limb movement functions to some extent. As shown in [21], robot-assisted therapy systems bring aids to the traditional gait training and restoration processes. In general, more than one therapist is required in

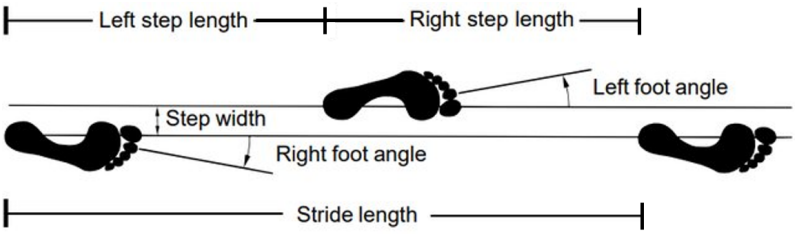

Figure 2.1: Gait analysis parameters [26].

a walking functions training session for each patient. Therapists can be released from repetitive work which can be replaced with properly designed ambulation-assisted robots or trajectories. Thus, human resources can be saved and used on more urgent occasions. At the same time, the accuracy, efficiency and reliability are also upgraded because the system is driven by precise instrumentation to measure and control positions and forces [22]. Alternatively, with well developed wearable robot-assisted exoskeleton, working performance and capabilities can be enhanced without muscle fatigue or spasm [23].

With the great advancement in health care and technologies, gait analysis unfolds a wide range of opportunities and applications in health monitoring and diagnosis, sports training and injury prevention, as well as robotic assistive rehabilitation.

2.3 Definition of Step Length and Stride Length

In gait analysis, step length and stride length are two fundamental and invaluable characteristics that are worthy of observation and investigation. Stride length is defined as the distance between two successive placements of the same foot [24] and it is twice the step length [25], i.e., a step is when a foot moves in front of the other foot and stride is a combination of two steps. Aggarwal *et al.* visually explain the relationship between step length and stride length in [26], as well as the representative parameters such as left and right step lengths and widths, feet angles and stride length, as shown in Fig. 2.1. Except for patients who suffer from strokes and thus would walk asymmetrically as a sequela [27], in normal gait, the walking of normal people is almost symmetric, which means that a person's left step length and right step length are similar though slightly different from each other [28].

For clarity, this thesis focuses on the average step length during continuous walking or jogging motions, rather than a typical right or left step length. Thus, in this thesis, the step is defined by the positions of opposite feet. The step length is calculated as the maximum anteroposterior distance between the medial sides of two ankles when the person under test walks or jogs at a normal pace. The reason for the step length to be referred to as the distance between two ankles is because, in our experiments mentioned later in this thesis, our developed hardware is attached to the ankles of the subject under test.

Statistically, the average walking step length for men and women are 2.5 feet and 2.2 feet, respectively [29], [30]. In reality, step length may vary slightly for individuals, depending on several factors, such as height, age, injury, illness, terrain, and environments surrounding the subjects. Generally, the walking step length for adults is within the range of 67.1 cm to 76.2 cm on average [29], [30]. As a result, in this thesis, our measurements and analyses will focus on the range of step length from 0.6 m to 0.8 m.

2.4 Importance of Step Length Measurement and Estimation

2.4.1 Work as a Health Indicator

As an essential component in ambulation and gait analysis, step length, or stride length, appears to be informative in many aspects of life.

First and foremost, step length could aid the diagnosis of injuries and other underlying conditions in both physical and mental layers. As an example, observation has been made among the elderly that, compared to non-fallers, fallers tend to have a slower gait speed. Their step length is shorter and has larger step length variability [31]. Gait speed is measured by letting the person under test walk over a predetermined distance and is calculated based on this distance and the time to complete that specified distance. It is commonly assessed with a 6-minute walk test [32] or a 10-metre walk test [33]. Gait speed is the same as walking speed, which is the product of step length and cadence which varies depending on the the size of the individual's lower limbs. In [25], gait speed is also declared

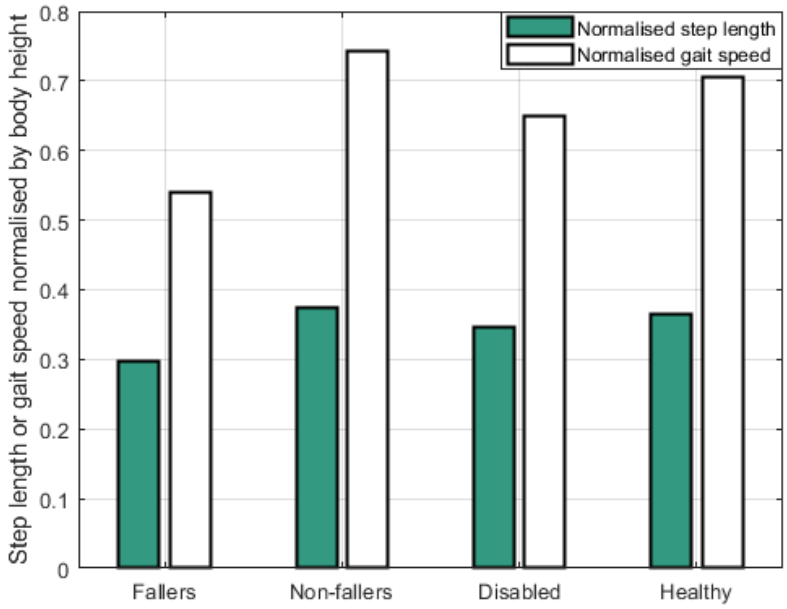

Figure 2.2: Comparison of step length and gait speed normalised by the body height for the fallers, the non-fallers, the disabled and the healthy.

in relation to stride length, thus, step length, having predictive capacity for adverse health outcomes in the elderly. Henceforth, step length could be used as an indicator to predict the probability of slips and falls when walking or after perturbation. In [34], a wide range of spontaneous gait parameters are reported for a group of senior citizens. As shown in Fig. 2.2, the green and white bars are representing the normalised step length and the normalised gait speed of the subjects under assessment, respectively. It is noted that, in this figure, step length and gait speed are expressed as the values normalised by the body height of the person under test. It is observed that both the step length and the gait speed of non-fallers are larger than those who fall. Similarly, the disabled participants perform a shorter step length and a slower gait speed than the healthier group. Moreover, Rosso *et al.* [35] unveil that not only step length itself, but its variability plays a significant role in reflecting the health condition of the elderly, especially in overt neurological diseases. Adults experiencing a slower walking speed and higher step length variability are likely to suffer poorer cognitive and executive functions which are also confirmed by their lower grey matter integrity.

The performance of gait may also reflect underlying diseases. In [36], gait speed, stride

Table 2.1: Gait patterns of subjects under test with and without pre-disability.

Variable	Normal	Pre-disability
Normal pace walking		
Gait speed, m/s	1.04 ± 0.12	0.83 ± 0.21
Stride length, m	1.18 ± 0.11	1.03 ± 0.18
Stride length variability	4.5 ± 2.0	3.8 ± 2.1
Walking-while-talking		
Gait speed, m/s	0.74 ± 0.22	0.61 ± 0.26
Stride length, m	1.11 ± 0.17	0.94 ± 0.19
Stride length variability	8.1 ± 14.0	6.0 ± 3.3

length and stride length variability are studied among the normal elderly and seniors with pre-disability. Pre-disability is defined in [36] for the dwellers are still able to manage and maintain their daily living but with self-reported difficulty. From Table 2.1, the pre-disabled group has a slower gait speed, a shorter stride length, as well as a smaller stride length variability for both the normal pace walking and walking-while-talking conditions compared to the healthy. Thus, with a properly settled baseline for various daily activities, stride length or step length can indicate the earliest stages of disablement.

Besides, Liu *et al.* [37] attempt to quantify the stability of gait variability regarding the step length, step width, cadence, as well as gait speed. They demonstrate that the gait parameters can also reflect the fitness of young adults. As shown in Fig. 2.3, the grey and white portions represent the youth with or without obesity. In this study, a normal weight person has a body mass index (BMI) between 18 kg/m^2 and 25 kg/m^2. If one's BMI exceeds 30 kg/m^2, then this candidate is considered as obese. In Fig. 2.3, the step length/width and gait speed are expressed as the values normalised by the body height of the participants. It is observed that the overweight group presents a slower self-selected gait speed, a less frequent cadence, and a shorter step length, accompanied by a wider step width.

Additionally, step length and related parameters work cooperatively in evaluating the severity of injuries and diseases. For instance, step length and the angle of the foot relative

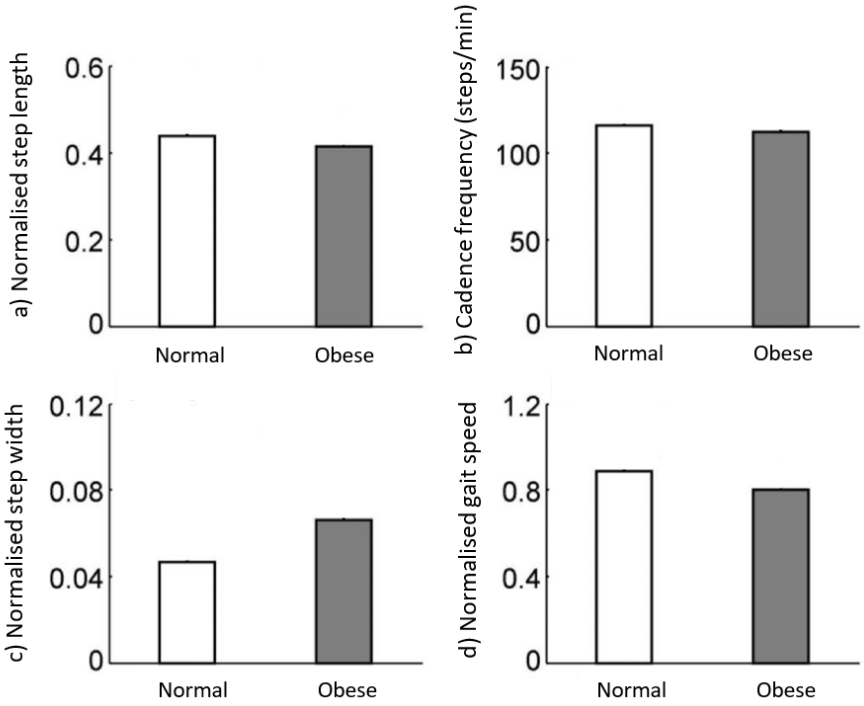

Figure 2.3: Comparisons of a) step length normalised by the body height, b) cadence, c) normalised step width and d) normalised gait speed between normal-weight and obese young adults [37].

to the floor while walking cooperate together to predict the severity of slips [14], accidental falls and fall-related injuries [38]. By monitoring these step-related patterns over time, one's walking nature could be characterised, so that potential health problems requiring further assessments could be noticed and indicated. Furthermore, based on these assessed walking characteristics, the recovery of postoperative patients could be more effectively evaluated [39].

Ultimately, step length and walking speed reflect the mortality, and predict the living years of senior citizens to some extent. It is experimentally proved in [40] that the timed walk performance measurement reflecting the walking speed and stride length for both sexes and various age groups could be used to predict the of dependency, mortality and institutionalisation. By employing a large number of participants to enrich the data samples, the authors in [10] conclude that gait speed is highly associated with survival among seniors. The median years of remaining life are predicted for males and females based on their age and gait speed. The pooled analysis results have been grouped into three areas as shown in Figs. 2.4 and 2.5. The red, orange and green areas are considered as the

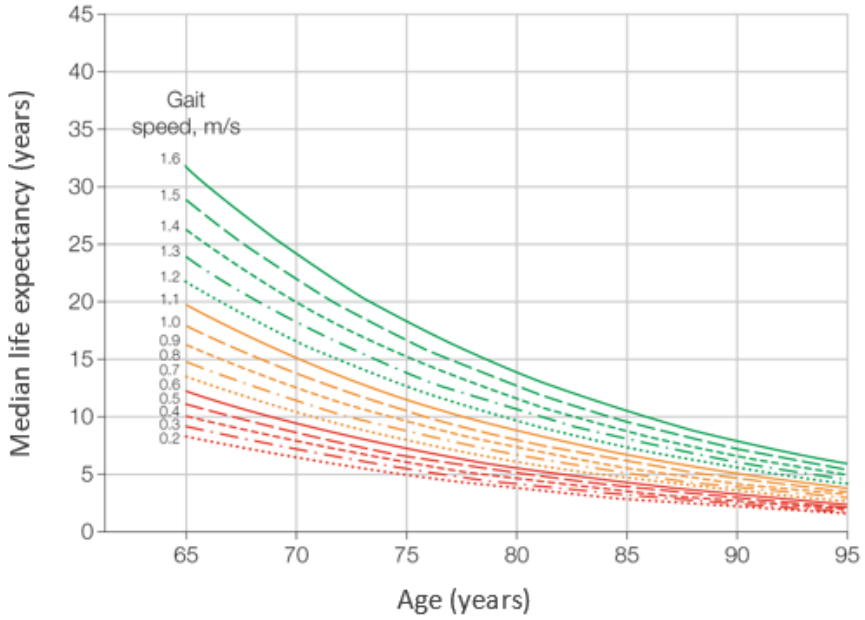

Figure 2.4: Predicted male median life expectancy by age and gait speed [10].

extremely high-risk level, the median high-risk level and the low-risk level, respectively. Generally, the predicted survival years for each gender and age decrease with a slower gait speed. In the age group of 65 to 75, the estimated remaining years in life are around 32 for men and 41.5 for women in the best case, i.e., if their gait speed is 1.6 m/s. If the median gait speed is 0.8 m/s, the predicted life expectancy is around 15 and 31 years for males and females, respectively. Risks are raised for those who walk less than 0.5 m/s, with a life expectancy of less than 13 and 18 years in life for males and females, respectively. Researches in [41], [42] use big data revealing that, the elderly with a walking speed slower than 1 m/s should be considered as the high-risk population, and extra attention and assessment in healthcare should be performed. If this number decreases below 0.6 m/s, there is an increased risk of leg injuries, hospitalisation or even death [10]. Thus walking patterns help identify mortality and even predict the life expectancy of the aged [10].

Therefore, step length and its relevant parameters, such as gait speed and step length variability, are considerably significant in monitoring, predicting and even preventing health conditions for the communities. As a result, exploring and investigating ways to measure and estimate step length efficiently and accurately are important.

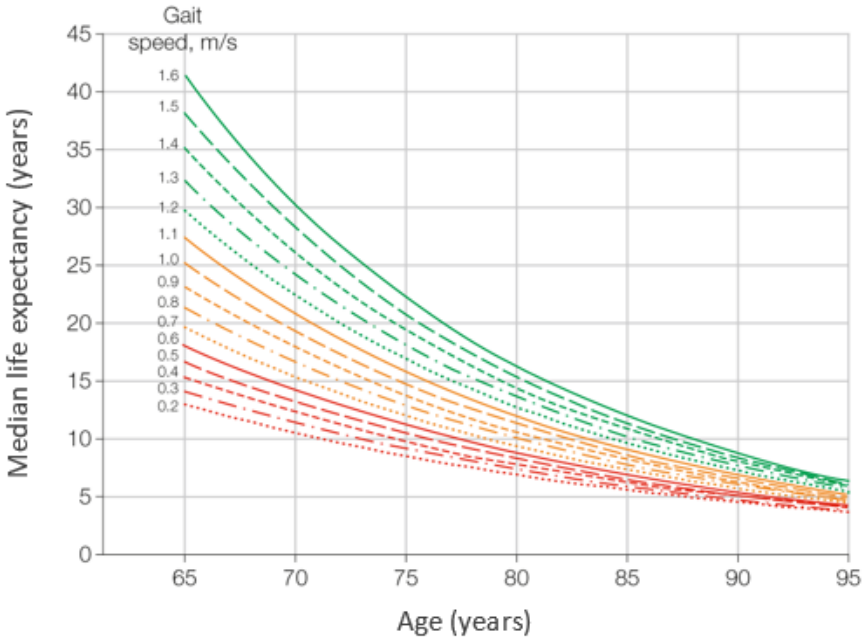

Figure 2.5: Predicted female median life expectancy by age and gait speed [10].

2.4.2 Assist Localisation and Positioning without GPS

Apart from working as a health indicator as mentioned above, the accurate estimation of step length also facilitates the localisation and positioning without using the GPS. GPS plays a dominant role for outdoor localisation [43]. Although GPS devices are becoming more portable, they may fail to meet the accuracy requirements for some indoor environments, because the electromagnetic wave is severely attenuated by physical barriers, such as walls, and other obstacles [44]. Their indoor performance is deficient due to the weakness of signals emitted by GPS and their disability to penetrate most building materials or water. Also, GPS signal is sometimes prohibited or denied in some situations, such as conflict zones or battlefields [44]. Due to those limitations, non-GPS localisation is much more preferred and is highly demanded [45], [46]. The estimation of step length, or the distance a person, e.g., a soldier, may walk at a particular time, could benefit the positioning of the target of interest, especially in the indoor environment. In addition, the study of step length and distance estimation also provides alternative ways to assist the public in maintaining social distancing [7].

In the following section, we will review the prior research on the state-of-art step length estimation technologies and evaluate the feasibility based on their practical experiments

and corresponding accuracy.

2.5 Step Length Measurement and Estimation

The problem of step length or stride length estimation could be traced back to the problem of distance estimation. Thus, when review the literature related to step length measurements and estimations, necessary review of distance estimations might be also provided in the following sections.

Current gait assessments used by physical therapists are subjective and restrictive, as gait parameters are traditionally observed and recorded by expensive equipment and well-trained staff in clinics [47]. They highly rely on the presence of a trained professional and equipment that is costly and not easily accessible. Meanwhile, the testing procedure only lasts for a short period, which could result in inconsistent performance and thus may lead to inaccurate conclusions [48]. Thereby, a system or method that can monitor and assess human step length in a continuous daily manner, offering reliable and quantifiable estimation, is worth exploring.

In general, step length can be estimated based on three systems, namely the instrumented walkway systems, the vision-based systems, and the wearable devices.

2.5.1 Walkway-based

The main advantage of walkway-based measurements is they output relatively accurate result in a straight forward way. Gait patterns can be monitored and data can be collected as long as the sensing mat is placed. It is welcomed in certain indoor environments such as hospitals, clinics, rehabilitation centres and laboratories. The sensing mat is laid specially to measure a group of instant gait characteristics and to warn any abnormal walking behaviours. Specific personnel could make decisions in terms of adjustments, treatments or medication based on the detected outcomes.

The walkway-based system, such as the instrumented walkway or instrumented treadmill, utilises pressure sensors embedded in mats where participants can get tested while walking on the specifically designed floor covering [49]–[51]. For example, the GAITRite

portable mat is a commercially available walkway. It relies on embedded pressure sensors to detect the foot positions of the subject under test. This kind of devices has been tested reliably in the measurement of temporal and spatial parameters of gait analysis among both young and old generations [49]. Moreover, the GAITRite mat is able to collect data in real-time for instant processing, such as step time, step length, swing, and toe in/out [52]. The mat is aimed for clinics to establish baseline function, documenting multiple gait patterns in pre and post-intervention, matching objective gait parameters with subjective findings, and justifying decisions for devices or services provided.

Li *et al.* [51] present an innovative pressure sensing mat that detects the foot pressure and positions of the subject under test. This study proposes a prototype that is cost-efficient compared to the costly GAITRite walkway. It can also collect real-time data including the foot pressure strength, and the location of the feet. However, this low profile and low cost textile smart mat can only output the position of feet in a blurred mapping performance with shades of colours to distinguish the feet' pressure. Thus the step length can hardly be estimated based on this mapping, which also points out that this work can be further strengthened by improving the sensing resolution to achieve a more visible performance.

In short, the walkway system is useful for quantifying the pressure patterns of feet over time [53], but it is constrained by its nature property, as the whole walking procedure must be performed on the walkway to assure the completeness of data collection. Since the walkway system is confined by locations, it is neither cost efficient nor realistic to pave the sensing mat ubiquitously. Thus, the pressure measurement system is mainly used in a specific indoor environment where the sensing mat is laid and precise results are needed, such as clinics, hospitals, rehabilitation centres, or specific laboratories. More importantly, instead of a long-term observation, the sensing mat is only suitable for collecting data in a certain walking session as the participant must walk on the fixed mat in a specific testing premise.

2.5.2 Vision-based

The vision-based monitoring system has been widely applied around the world. The key feature of vision-based step length detection and estimation is the image processing, which can be done through cameras and/or infrared radiation (IR) devices. With the development of computer vision technologies and visual sensors, such systems partly overcome the shortage of the walkway measurement in a specific setting.

Studies show that the camera-based system could provide a solution to continuous daily monitoring. Continuous monitoring can be used to track individuals' gait patterns and estimate the step length [48], [54]–[64]. With the deployment of cameras, step length can be detected and estimated. Both single-camera system [48], [57], [59]–[61] and multi-camera system [54], [65], [66] are able to extract gait parameters, thus the step length.

Specifically, the authors in [57], [60] study the marker-less image-based system to capture distinctive events during ambulation using a single web camera. Cai *et al.* formulate the step length symmetry ratio in [48] which can be used in unconstrained straight line walking. The objective in [48] is to build unconstrained monitoring environments, which allow the elderly to walk without strict restrictions on walking directions or routes. The step length symmetry ratio is the ratio of the observed step lengths of adjacent steps, which is a powerful gait parameter in representing gait symmetry and is not affected by ages. Their experiments are conducted in a clinical setting on a straight walkway, and focus on instantaneous gait parameters, aiming to offer the stride length of a senior and to reflect the health condition timely. To track the motions of the person under test, some markers are signified on the walkway in [48] to assist the measurement of the footprints, which help calculate the step length symmetry ratio. The stride length can be estimated by detecting and extracting several pieces of perspective information related to predefined markers. The experiment results imply that the camera-based method is a promising way to detect all steps when the user is moving slowly, especially in an indoor environment.

A static camera is used in [61] to film the experimental process in an indoor environment. By applying the direct linear transformation (DLT) method, the authors examine the variations in participants' heights and stride lengths. Results show that the height of

the subect under test can support the estimation of stride length as it is not affected by surroundings such as the clothing of the participant and the position of the camera.

Wang *et al.* [54] propose a two-camera system to extract valuable gait parameters, including the walking speed, step time and step length. The extracted parameters are validated with the data collected from experiments undertaken using a pricey GAITRite sensing mat and a Vicon motion capture system in a laboratory room. Their results show that, although the designed two-calibrated cameras can address the limitation of the walking path direction, and provide gait speed, step length and time with a small average difference from the reference database, the maximum discrepancy is large for all three parameters. For instance, the maximum difference between the system proposed in [54] and the GAITRite sensing mat and the Vicon camera are 9.47% and 9.91%, respectively. It is also noted that this particular experiment is carried out with a very slow walking pace, rather than a general walking pace in daily activities. In [65], the same authors refine their previous work in [54] by gathering data not only from a laboratory but also from a senior housing, so that actual daily performance could be assessed. It is found that subjects perform walking differently in the laboratory and in the senior house. The differences could be as large as 21% in walking speed, 12% in step time, and 6% in step length estimation. Thus, the importance of measuring and estimating the human step length in a real living environment is highlighted.

The researchers in [59] use cameras as additional sensors in pedestrian dead reckoning (PDR) to analyse step length and step frequency. Currently, PDR is a popular indoor localisation method [67], [68] due to the wide availability of smart devices. Recently, the researchers in [69] propose a machine-learning-based step length estimation algorithm with the use of cameras and smartphones. This research considers a systematic feature selection algorithm to determine the choice of user-specific parameters from a large collection of data. The mean absolute errors of the step length estimations are 3.48 cm and 4.19 cm for a known test person and an unknown test person, respectively. However, the above camera-based techniques are flexibility-constrained because the camera must be arranged at a certain place and has a limited horizon. Moreover, its accuracy may be

reduced in fast-moving situations or by obstacles appearing between the cameras and the person under test.

So far, many works have been done in vision-based systems to examine residents' ambulation patterns and gait parameters. However, challenges regarding the lower limbs are still conspicuous. For example, though the image could be captured, it is hard to distinguish the moving legs as they are crossing each other, especially in the side view gait analysis. Another drawback among current studies in camera-based monitoring is that the subject under test is required to walk perpendicularly to the observation direction of cameras or along some specified routes, whereas in reality, an individual does not walk perfectly along a straight line [48]. Lastly, the public is rising in concerns about their privacy intrusion when cameras are used [63], [70], which is also an issue that needs to be addressed in the step length estimation.

Ohta *et al.* [71] developed a health monitoring system for elderly people who live alone. By employing a number of IR sensors, which are installed within the experimental site, to monitor the in-house movements of the subjects under test for a long run (over 80 months in this study), big data helps generalise a specific pattern of movements for each participant. Thereby, if an abnormal stay or movement is surveyed, the unusual state would be analysed and reported to emergency contacts, such as family members.

The method of IR thermography is applied in [72] to detect the gait patterns of humans and an accuracy of 78% – 91% is achieved. IR-based communication is a low-cost protocol for the short-range exchange of data over infrared light. However, one of the most critical drawbacks is the requirement of the LoS path. In other words, the performance of an IR-based system can be severely degraded by opaque obstacles. More importantly, because the usage of laser requires well-trained staff, the pricey equipment, and the potential harm of a long time exposure, it is not an ideal method for step length measurements on a daily basis.

The ultrasonic technique measures the time required to send an ultrasonic signal and receive the reflected wave from the target object, which can then be transformed to the distance between two points [53]. Although the ultrasonic ranging system is accurate

with the errors in a sub-centimetre level over the range of 2 cm to 5 cm in general, it needs expensive hardware and will be affected by temperature and humidity [73], [74].

In short, the monitoring cameras are required to be located and installed at a specific place, which then limits the horizon of the observation and the range of the movements of the person under test. This is because the participants have to move in a way that the trajectory of the movement is vertical to the direction of the camera lens. There is also a general privacy concern during the operation of cameras. In addition, the IR-based system requires professional staff to operate the equipment and poses potential health detriment due to long time exposure. Consequently, this vision-based approach might not be an optimal choice for the daily step length estimation.

2.5.3 Wearable Device-based

Newer studies have concentrated on the use of wearable sensors to solve the challenges in step length measurements while still maintaining their accuracy and precision. This approach typically requires the deployment of simple hardware equipment. Accurate methods to estimate gait parameters, such as step length, is needed since it is an essential factor being used to determine if a person's walking pattern is symmetric and/or if there exists a balance disorder that may cause collapse.

A wearable inertial sensor can be utilised in an inertial measurement unit (IMU) to collect gait-related parameters, which then help to estimate the human step length. An IMU generally consists of an accelerometer, a magnetometer, and a gyroscope. Step length could be estimated by employing sensors on many body parts.

Initially, body parts that do not experience much movements during walking, running, or other daily functional activities are first considered in the literature. These parts may include the head, the chest, the pelvis and the lower back areas because they only involve little changes of orientation during the movements. The approach is then examined for other body parts. For example, the work in [75] proposes a head-worn device and uses the Gaussian process regression model to estimate the walking speed. The objective of [75] is to verify the feasibility and accuracy of the walking speed estimation using a head-

worn inertial sensor. Experiments in this study are conducted both indoors and outdoors with different walking speeds, namely slow, normal and fast. The normal walking speed is defined as between 100 cm/s to 150 cm/s. Speeds lower than 100 cm/s or higher than 150 cm/s are reckoned as the slow walking speed and the fast walking speed, respectively. With the collected data, the authors propose a Gaussian process regression model that considers both time domain and frequency domain features of the tri-axial acceleration norm signal, which is used to estimate the walking speed. By using the leave-one-out-cross validation technique, the developed model is assessed. The evaluation results show that, for the indoor environment, the mean absolute error of normal walking speed is 5.4% and the standard deviation is 2.4%; for the fast walking speed case, the mean absolute error is 6.5% while the standard deviation is 3.1%. The proposed system is less accurate for slow walking speeds with the mean absolute error and standard deviation of 10.4% and 5.1%, respectively. This means that the technique in [75] faces big challenges in estimating the gait speed and step length for the elderly.

The authors in [76] develop a step length measuring system, which consists of an exercise shirt with a chest belt and a portable measuring device called XPOD. Bluetooth is employed to realise real-time transmission and analysis. In [76], treadmills are used during the experiments. The subjects either walk or run on the treadmills. The authors measure the accelerometer signals on the chest and design three artificial neural networks. From the accelerometer signal, they segment each stride to obtain the ranges, and the differences between the minimum and maximum of three accelerations for this stride. With the obtained parameters, subject's personal factors such as height and weight are also adopted to train the proposed neural networks. At first, a classification network determines whether the subject is walking or running, and then the walking or running network can be employed to estimate the stride length. Experimental results in [76] consider both travelled distance error and walking speed error. From the scattered diagrams of the collected data and the estimated values, there are clear differences between them even for the same data set. Thus the correspondence between the travelled distance error and the walking speed error remains unclear. The average root mean square error of the travelled

distance error is about 13.22 cm within the actual walking distance range from 32.66 m to 617.30 m in the experiment. The average speed error is 0.54 km/s when the actual speed is in the range of 4.7 km/s – 17.14 km/s.

In [77], the feasibility of an analysis of spatio-temporal gait parameters using accelerometry is studied. Based on the collected data from the treadmill experiments and the assessment, the authors in [77] analyse the subjects' trunk acceleration patterns and their relationships with spatio-temporal gait parameters. They develop a geometric expression that relates the step length, the length of the user's leg, and the vertical displacement of the centre of mass during the stance phase, which is obtained by double integration of the high-pass filtered vertical acceleration of a sensor placed on the trunk. However, the authors reveal that this model tends to underestimate the step length and that a calibration parameter is needed to adjust the performance of each user. Other researchers propose several modifications of the model in [77]. For instance, Alvarez *et al.* [78] and Gonzalez *et al.* [79] make the use of heuristics to reduce the integration drift error in the inclusion of the length of the user's foot, as a predictor of the forward displacement during the double-stance phase.

Köse *et al.* [80] propose a system that requires a 3-axis accelerometer and a 2-axis gyroscope placed on one side of the pelvis. The objective of [80] is to use a single IMU to estimate the step length bilaterally during walking. To this end, the authors propose a novel signalling method by combining a Kalman filter and an optimal filtered direct-and-reverse integration. Then they apply the combined high-pass filter to the IMU signals. By using wavelet decomposition, the steps of each foot can be detected and differentiated. It is noted that the error may occur as a result of the pelvic rotation which leads to the displacement of the sensor during walking. The authors introduce a correction angle to compensate for the residual errors, and then compute the length of each step. Results show that, the step length can be estimated for all subjects with errors being less than 3%. Moreover, the authors also measure the traversed distance and the measurement error is less than 2%.

Currently, most smart devices have built-in inertial sensors, which provide useful infor-

mation and help position the body part of interest. Smartphones are getting popular in the wearable sensor-based step length estimation as they are frequently carried. The authors in [67], [68] study the human stride length based on the data collected from inertial sensor measurements in a smartphone. The experimental results demonstrate that the step length can be estimated with an error rate of 4.63% for indoor scenarios. Considering a general step length of 0.7 m, the corresponding absolute error would be 3.24 cm. The error of step length estimations is reduced to 2% in another work in [81] based on a back-propagation artificial neural network using an IMU that is placed on the feet.

The smart device can be held in hand as mentioned in [82] where the authors propose a novel step length estimation method with a handheld micro electrical mechanical system (MEMS). The proposed system uses the step frequency, height, and a set of three parameters to firstly detect a step event and then calculate the step length. Experiments are carried out on a soccer playground, which can be viewed as an open space. The experiments have demonstrated the percentages of error over the travelled distance between 2.5% and 5%. In particular, the signal is propagating every 2.5 seconds, suggesting that real-time implementation could be achieved based on the proposed handheld step length estimation model.

Besides smartphones, other wearable or portable devices, such as smartwatches or smart glasses, also facilitate step length estimation methods. For example, the work in [83] presents a wrist-worn device that aims to estimate the travelled distance, walking or running speed, and step length. Assuming that the stride length is proportional to the torque of legs, the authors propose an alternative step length estimation method to estimate the step length from the acceleration signals observed at the wrist. In [83], the authors utilise box-and-whisker diagrams, which provide a fast and easy way for visualising the mean and the main percentiles, identifying outliers and comparing several data sets. This study shows that, the relative errors of estimated travelled distance distribute between -1.2% and 1.4%. It should be noted that the larger measuring ranges are often found in the works using wrist-worn sensors because the upper limbs are the body parts which are expected to hav a greater range of motion during walking [83].

Apart from upper limbs, lower limbs, such as thighs, shanks, and ankles, also move in a wide range during gait and ambulation experiments. Hence, they are also considered as potential mounting locations of sensors for the gait analysis.

Innovatively, [84] focuses on long-term monitoring of stride length and gait speed. This is because long-term experiments are not subjected to short walking tests, so the gathered information would be more representative and valuable for analysis. Miyazaki [84] uses a simple geometric model in which the stride length is estimated based on the leg length and the opening angle during the stride. To measure this angle, a gyroscope sensor is mounted on the thigh. It is found that the stride length has a roughly linear relationship with the mean walking velocity. Moreover, the error of estimated step length in the developed ambulatory system model depends on the walking speed as well. Yet the proposed model has a $\pm 15\%$ maximum relative error in the estimation of walking velocities.

Instead of using acceleration to estimate step length, authors in [85] make use of the opening angle of the leg, which can be obtained from their proposed novel step detector. The developed step detector can be put in the front pocket to ensure the detected movement of the leg is in a forward direction, which is related to the occurrence of the steps. The experiment in [85] is conducted indoors on a treadmill and more than 15,000 steps are collected in the experiment. The relationship between step length and the opening angle is then formulated with a linear regression model. Experimental results and assessments show that the proposed method is able to detect all steps for the whole 69-metre walk, and the estimated step length error is about 10.37 cm.

Works in [86], [87] mount the sensors on the lateral side of the shank of the subjects under test. The authors use an 1-axis gyroscope and a 2-axis accelerometer in their proposed system. After segmenting stride circles among walking, by using the angle obtained by integrating the angular rate of the gyroscope, the shank linear accelerations and angular velocities can be generated and transformed into the navigation frame. It is assumed in these works that the initial velocity at mid-stance shank vertical event is zero, which may lead to the result of errors in speed estimations. This is because, at the mid-stance shank vertical event, the shank still rotates about the ankle joint. Thus the initial velocity would

be the product of the angular velocity of the shank and the distance from the sensor to the ankle joint. As a result, the travel distance error and root mean square error of the walking speed estimation in [86] are 4% and 7%, respectively. In [87], the root mean square error is improved to 5.6%. The shank-mounted sensors may be of a great value for estimating walking speed and step length with abnormal foot motions and for the embedded control of knee-mounted devices, such as prostheses and energy harvesters.

Zihajehzadeh *et al.* [88] study the influence of different factors on the step length and walking speed estimation. The comparison includes factors such as the mounting locations of the wearable sensors, features, as well as regression methods. In [88], experiments are performed indoors along a corridor. Raw data is collected from a tri-accelerometer and a tri-axial gyroscope at the rate of 100 Hz. In particular, compared to a least square regression analytical method called Lasso, Gaussian process regression achieves better accuracy. The accuracy does not affect much by sensor placement locations in [88]. By using the Gaussian process regression, with external acceleration to calibrate the measurements, the mean absolute error for waist-mounted and ankle-mounted systems are 4.5% and 4.9%, respectively. Moreover, the accuracy is also enhanced by using both time domain and frequency domain features. It is revealed in [88], [89] that the estimation performance would be severely degraded by about 15% if only time domain features are included in the estimation.

The research in [90] compares the accuracy of distance estimations between different placements of the IMUs. Firstly, this paper utilises only one inertial sensor on each shank, called the integrator-based method, providing an average accuracy of 91.21%. The accuracy is improved to 95.37% if two sensors are employed on each leg, namely the angle-based method. As a result, the maximum errors are 11.26 cm and 5.51 cm for the integration and angle mode, respectively. Although the integrator-based method is simpler, the angle-based method achieves better accuracy in terms of step length estimations since it is not sensitive to the initial conditions and errors caused by double integrations. However, experiments and analyses for the outdoor environments are still missing. Moreover, a major disadvantage of using IMUs is that they typically suffer from

an accumulated error, which means the accuracy will be degraded over time.

The received signal strength (RSS)-related technique is an inexpensive approach for step length measurements. It features a low communication overhead and low complexity. Based on the relation between the RSSI and distance in wireless signal transmissions, step length can be estimated [91]. Thus RSSI can be used for double purposes of distance measurement and node localisation technologies. RSSI has been well-researched in the aspects of indoor localisation and human tracking, such as in [92]–[109], thanks to its advantages, including simple and inexpensive hardware. The RSSI technique relies on the signal strength of the received signal, which is a function readily available (or simple to obtain) in most commercial transceivers [73].

The work [102] studies the RSS-based joint estimation of unknown location coordinates, using the distance-power gradient parameter in the path loss model. Similarly, the work [105] also aims to realise node localisation in an unknown environment. The parameters in the path loss model are extracted from the periodically transmitted signals. With the incremented number of beacon nodes, though the computation time is prolonged, the accuracy of distance measurement can be enhanced, which provides an option in the wireless sensor node localisation. To address the issue of external interference, which causes fluctuation of RSSI, Wang *et al.* [106] propose an RSSI-based ranging method. The distance between the transmitter and the receiver can be obtained based on the pre-established database of mapping relationships between the RSSI and the distance range. Pormante *et al.* [103] and Shi [108] consider a weighted-RSSI strategy to optimise the localisation, where the weight is obtained from the reciprocal of the sum of measured distances.

In [110], the authors attempt to avoid the instability of RSSI, so that the RSSI values could reflect the distance in a more accurate way. They propose three experimental data processing methods, including the statistical mean value model (SMVM), the distance between the fixed-nodes based model (DFBM) and the Gauss model (GM). The authors consider a simplified shadowing model and formulate the distance measurement based on RSSI, which is collected from practice. Then the Zigbee-based hardware platform is

used to test their measurement errors. With a data set of 100 samples in each experiment, the comparison of the performance of three methods indicates that GM outperforms the others with the error of 2 m for the distance range of 20 m. However, the accuracy of this approach is still very modest with the probability being as large as 10%.

In [96], the authors implement a distance estimation technique using RSSI in a sensor network, following the Zigbee standard. The distance is estimated based on the Zigbee hardware and the maximum likelihood (ML) detection method. With a sensor node density of 0.27 nodes/m^2, the estimation error can be reduced to 1.5 m in a 7.08 m $\times$ 10.60 m conference room. The study shows that Zigbee is able to assist the node localisation and distance estimation for both indoors and outdoors. However, all of the above experiments have collected a limited number of data samples, which may affect their confidence in the estimated accuracy. It is necessary to significantly expand the data sets to have meaningful observations and conclusions.

As RSSI itself is sensitive to noisy environments and the shadowing effect, an RSSI-based fusion framework may compensate partially for the weaknesses. The authors in [111] present a smartphone-based system for locating Wi-Fi access points. There is a great attenuation in receiving signals if the device holder's back is toward the Wi-Fi node, which causes inaccurate estimations. Zhang *et al.* [111] propose that the subject under test performs a uniform circular motion, whereas the work in [97] addresses this error-prone issue with a built-in gyro sensor in smartphones to collect the intensity value of the gyroscope while collecting Wi-Fi signals. The rotated angle and RSSI value can be obtained even when personal motion is not uniform. With consideration of the log-normal shadowing model (LNSM) and the proposed access point (AP) faced trilateral (AFT) algorithm, the localisation accuracy in [97] is improved with an average deviation of 0.8562 m in a laboratory environment.

To address the signal fading issue caused by the shadowing effect and the multipath propagation, works in [112], [113] propose a multi-antenna system that equally transmits the power at a low peak-to-average power ratio (PARP). Similarly, Hamdoun *et al.* applies multiple antennas in [98], employing a combined indoor propagation model that

considers both path loss and shadowing effect proposed by [114]. Both trilateration and triangulation algorithms are used to estimate the distance between four anchors and three target nodes based on the RSSI values. Then the estimation accuracy is compared between different systems, including single input single output (SISO), single input multiple output (SIMO), multiple input single output (MISO), and multiple input multiple output (MIMO). Simulation results show that the estimation accuracy is improved by applying multiple antennas at both transmitter and receiver. This study could be further evaluated by realising the experiments physically.

RSSI-based Bluetooth distance measurements are considered in [115]. The authors establish a mathematical model to address the relationship between RSSI values and the distance between two Bluetooth devices. Then they use a triangulation algorithm with the least square estimation (LSE) to measure the distance between two Bluetooth devices. The proposed scheme yields good results for an indoor environment but also shows about 6–8 dB attenuations when Bluetooth devices, such as mobile phones, are covered by the human body. In addition, choosing a reasonable weight in LSE in practice requires further study.

Unlike the aforementioned works which mostly focus on a static scenario, Zhang *et al.* [116] consider body motions in human daily activities and the impacts of characteristics in the dynamic on-body propagation model. The authors discuss the relationship between RSSI variations and different directions of the antenna in a walking scenario when the receivers are attached to the human's wrists. It is observed in [116] that the placement of the transmitter contributes to the shadowing effect. Generally, the path loss fluctuates more if the hub is placed on the back collar rather than the front of the abdomen. The change in the relative positions of the human's wrists with respect to the human's torso causes different shadowing levels. Moreover, path loss and some other characteristics, such as auto-correlation, cross-correlation and path loss discrepancy, change periodically while the subject under test is walking.

Xu *et al.* [117] improve the accuracy and self-adaptability of the LNSM by applying an LNSM with the dynamic variance (LNSM-DV) model, and formulate the relationship

between the variance of RSSI and the distance. The LSE is used to define the coefficients in the proposed model. In [117], experiments have been conducted for both indoor and outdoor environments. Results show that the proposed LNSM-DV is adjustable and could better describe the relationship between distances and RSSI, thus the distance could be estimated in an accurate manner. However, [117] only takes 100 data samples for each scenario, which may affect the accuracy of LSE. Moreover, there is also a concern in the outdoor scenario, as the proposed method does not perform the estimation correctly in a short distance range.

Work in [118] combines the RSSI and angle of arrival (AOA) method to estimate the position, thus the distance, of an unknown node. The proposed RSSI-with-angle-based localisation estimation (RALE) algorithm collects different RSSIs for different angles by rotating the node at the same place. The strength of the received signal indicates the main lobes of the radiation pattern and thus the zone of the unknown node. The estimation accuracy could be improved by increasing the number of pause directions to collect more information that can be used in the calculation. With nine pause directions in the experiments, the probability of accurately estimating the distance to the target in [118] is 83.68%. Similarly, the authors in [100], [119] rotate the antenna direction and then record the received power at different angles. By finding the strongest signal from the received power spectrum, the position of the unknown node, thus the distance to a reference node can be identified.

A weighted combination method of RSSI and AOA is explored in [46]. The observation indicates that the RSSI component is more sensitive to shadowing than the AOA component. In the simulation, the accuracy of correctly estimating distance from the anchor to the unknown node is claimed to be 83%.

Table 2.2 summarises the aforementioned works, comparing several RSSI-based distance estimation techniques in terms of channel model, hardware, measured data set, as well as the experimental range and accuracy. This thesis is also added to this table for comparison.

Table 2.2: The literature comparison of RSSI-based distance estimation, where ($\surd$) represents Applied/Discussed, (N/A) represents Not Applicable, and ($\diagdown$) represents Not Mentioned.

	[110]	[96]	[97]	[115]	[116]	[117]	[118]	[46]	This thesis
Measurement	RSSI	RSSI	RSSI	RSSI	RSSI	RSSI	RSSI + AOA	pAOA + qRSSI	RSSI
Channel model	$\diagdown$	$\diagdown$	LNSM	Experimental indoor propagation model	Experimental on-body channel model	LNSM -DV	$\diagdown$	LNSM, flat rayleigh fading channel	Experimental model
Size of experimental data set	100	$\diagdown$, claim to be small	60	$\diagdown$	192,000	100	$\diagdown$, claim to be large	N/A	50,000
Hardware	Zigbee + CC2430 chip	Ubiquitous device + CC2420 radio controller	3+ Wi-Fi access points	Bluetooth	Arduino UNO + Zigbee	Micaz nodes + CC2420 radio controller	Bluetooth + BLE device	N/A	Arduino UNO + Zigbee

Antenna	Omni directional whip antenna	monople antenna	Omni directional whip antenna	Patch antenna or antenna array	Integrated antenna	Dipole antenna	Dipole antenna	Antenna array	Integrated antenna
Shadowing effect	√	N/A	√	6 - 8 dB	√	√	N/A	√	√
Method to estimate the distance	GM	ML	Trilateration	Triangulation LSE	N/A	LSE	RALE	Trilater-ation + Triangu-lation	Driven by the proposed experimental path loss expression
Number of nodes	4	0.27 nodes/ m^2	4	4	3	3	2	Max (p, q)	2
Range	20 m	7.08 m× 10.60 m	8 m× 7 m	6 m× 8 m	N/A	7 m	360°	100 m× 100 m	1 m
Error	2 m	1.5 m−2 m	0.8562 m	1.2 m	N/A	N/A	16.32%	17%	Sub-centimetre level

Deep learning has been adopted to estimate human step length because it can learn the features of the data automatically and has shown excellent performance in different application domains with the cost of powerful computing facilities. The proposed deep-learning-based algorithm in [120] can adapt to different phone carrying ways and does not require individual stature information and spatial constraints. The average error of this method is 3.01%, which means if the actual step length is 0.7 m, then the corresponding error range is within 2.1 cm. Paper [121] defines a deep-learning-based framework with an activity recognition model to regress the user change in distance and step length. The average error of the proposed method is 2.1%, which is about 1.47 cm if the step length is 0.7 m. It is worth noting that the positions (e.g., handheld position or pocket position) of the smartphone have a huge influence on the estimation by around 5% [122].

Shin *et al.* [123] raise the importance of using optimal parameters including the walking frequency and the acceleration variance, which are linearly related to the walking step length. The authors propose an optimal parameters oriented algorithm to estimate one's step length. These optimal parameters are driven by their experimental study, in which a MEMS sensor module is used. The MEMS sensor module is attached to the waist of the person under test, and it comprises a microcontroller, a Bluetooth device and two accelerometers. The person under test walks or runs along a straight trajectory. After calculating the walking frequency and the acceleration variance, the pedestrian's step length can then be determined by a linear approximation. Results show that, without the proposed algorithm, the estimation error is as large as 20%, and this number is greatly improved to 4.8% with the movement status awareness algorithm. However, the placement of the sensor in this study may negatively impact accelerometers during the movement of the user. Moreover, noise and accumulative errors are also factors that degrade the performance of accelerometers.

Díaz *et al.* [124] investigate human step length and step width using wearable sensors in a computer-assisted rehabilitation environment (CAREN). Steps are detected by using the algorithm proposed in [125]. In particular, the authors in [124] propose a deep neural network to estimate the step length. The selected topology consists of two fully connected

hidden layers, where the first one has five neurons and the other one contains three neurons. After training and testing the network, the data collected from CAREN show that, for walking on a treadmill, the step length and step width could be estimated with the mean absolute errors of 0.2396 cm and 2.53 cm, respectively. However, it is observed in [124] that gait patterns are affected by the preset velocity of the treadmill. Moreover, the data in [124] is collected using a treadmill under a specific environment rather than normal indoor and outdoor propagation environments in daily human activities. Thus, the estimated step length and step width may not be solid enough to reflect the participants' real walking status.

2.6 Chapter Summary

To conclude, this chapter has stated the significance of monitoring gait characteristics continuously during normal daily activities as invaluable information can be provided for a variety of purposes, including automated fall risk assessments, early detection of illness or changes in health status, and better assessment of progress during rehabilitation or changes in medication. The prior works that study step assessment have been discussed. The existing techniques mainly use either the walkway-based, vision-based, or wearable device-based estimation approaches.

The walkway-based system is a prime option in laboratories and health centres because it provides accurate measurement outcomes directly to the therapists. However, such a system is generally costly and is unable to be used for the assessment on a daily basis. The vision-based step length estimation could be used in any place with installed cameras. Nevertheless, it is also subjected to physical obstacles, especially in indoor scenarios. The step length estimation using wearable devices is gaining much interest, and the importance of the mounting locations of sensors and the optimal parameters selections during modelling are discussed. The RSSI-based systems (either use RSSI alone or in combination with other approaches such as Bluetooth, Wi-Fi APs, and IMU) facilitate the estimation of the step length under different channel models for both indoor and outdoor environments. However, this approach also has drawbacks as RSSI is sensitive to

the shadowing effect and noisy environment.

Despite the great progress made in recent years, there are a number of open issues that need to be addressed. Examples include continuously tracking people travelling between indoor and outdoor environments to estimate their step length, solving synchronisation problems, reducing the impact of shadowing and noise effects, and improving the estimation accuracy and energy efficiency. Although some previous technologies have attempted to address these issues, they have various limitations, such as the increase of the cost of the whole system, precision deficiency, and severe computational overhead. The evaluation criteria may include security and privacy, cost, performance, robustness and fault tolerance, complexity, user preference, commercial availability, precision, conformability, usability or transportability, etc. An algorithm that meets all or most of these criteria does not exist because there are always some trade-offs. Innovative research efforts are sought to devise measurement techniques that meet as many of these criteria as possible.

Accurate estimation of the human step length is a challenging task, especially in human daily activities, due to the randomness of the propagation environments related to these activities. As a result, there are few research papers that explicitly address the problem of step length estimation, although the overarching topic of distance measurements has been intensively researched for general communication systems. In addition, no past work jointly considers estimating step length for both indoor and outdoor environments in human daily activities.

This thesis thus considers three research problems to partially fill the aforementioned gaps: (i) the optimal configurations of the hardware which is deployed to measure the human step length, (ii) novel techniques for measuring the step length in daily activities for both indoor and outdoor scenarios, and (iii) optimal parameters of these measurement techniques.

To this end, first and foremost, the best hardware configurations for measurements of the step length must be examined. The empirical path loss model between the two human ankles must also be derived. They will be discussed in the next chapter.

Chapter 3

Static Step Length Estimation Using the Received Signal Strength Indicator

3.1 Introduction

As mentioned in Chapter 2, a thorough analysis of estimating the distance between nodes attached to the human body in daily life activities is still missing. Therefore, it is worth to explore the performance of the RSSI-based method in distance measurement in wireless body area network (WBAN) with different hardware configurations. In this chapter, we focus on the distance measurement between two human body parts in WBANs scenarios using the hardware-based RSSI approach. Inspired by our previous related works [126]–[128], we first develop the transceivers and use them to measure their distance when they are attached to the human ankles. We then propose an experimental path loss model between the two ankles of the subject under test, that jointly considers the path loss, non-linearity, shadowing effect, multipath, mismatch loss, and insertion loss. The static scenario where the subject under test stands still with different step lengths is considered to explore the characteristics of the wireless channel between the two ankles. We will demonstrate that the channel between two ankles follows an empirical model, which is the free space model added with a correction factor ΔPL. Different configurations are taken into consideration to find the most suitable transmission power level and data rate for the distance measurement.

In this chapter, portable transceivers with micro-controllers and RF modules are de-

veloped to measure the received signal strength, path loss, and thus the distance between the human ankles for both indoor and outdoor environments. By comparing the experimental results and the theoretical model, a modified path loss model between transceivers attached to the subject's ankles is derived. With the developed experimental path loss model, the step length can be relatively accurate measured, despite the imperfections of hardware devices, with a centimetre level estimated distance error. This chapter, therefore, helps address the need for a distance measurement method that has fewer health concerns, is accurate, and is less affected by occlusions and confined spaces. Our findings possibly lay a foundation for some important applications, such as the measurement of gait speed and localisation of the human body parts, in wireless body area networks.

The main contributions of this chapter are listed as follows.

- Derivation of an empirical path loss model between two transceivers attached to the participant's ankles. The proposed model jointly considers the path loss, hardware non-linearity, shadowing effect, multipath, mismatch loss, and insertion loss.
- The distance between the transmitter and the receiver has been estimated based on the proposed path loss model between the two ankles and the accuracy of the distance estimation has been analysed and discussed.

The content of this chapter has been published in [129].

The rest of the chapter is organised as follows. Section 3.2 describes the system model. The experimental materials are detailed in Section 3.3, and the newly proposed path loss model is presented in Section 3.4. The experimental outcomes and analyses are detailed in Section 3.5. Section 3.6 concludes this chapter.

3.2 System Model

There are several radio propagation models to predict the received signal power, including the free space propagation, two-ray ground reflection, and IEEE 802.15.6 path loss models. The two latter models are not applicable because they are not suitable with the experimental settings in this thesis. More specifically, the experiments in this chapter are

carried out for distances less than one metre between the two human ankles in the realistic environment, rather than for elevated antennas over several kilometres apart from each other or for the propagation environment in an anechoic chamber [9]. Meanwhile, the free space model is close to the propagation environment in our experimental settings but requiring an adaptation via the correction factor ΔPL.

In this chapter, we estimate the distance between the transmitter and the receiver within the range of a human step length, i.e., no more than one metre in both indoor and outdoor environments. The transmitter and the receiver are attached to the ankles of the subject under test in a way that the antennas face each other. This means that there exists a LOS path between the transceivers. As a result, the experimental path loss, denoted as PL_{OA}, is conjectured to be the free space path loss, denoted as PL_{FS}, plus a correction factor ΔPL, which covers some extra losses, as a consequence of shadowing effect, multipath, mismatch loss, and insertion loss, i.e.,

$$PL_{OA}(dB) = PL_{FS} + \Delta PL. \tag{3.1}$$

The free space path loss, PL_{FS}, is derived from the Friis transmission equation [130], which states that the ratio of the received power P_r to the transmitted power P_t is

$$\frac{P_r}{P_t} = \frac{G_t G_r \lambda^2}{(4\pi d)^2}, \tag{3.2}$$

where G_t and G_r are the antenna gains of the transmitter and the receiver, respectively. λ is the wavelength of the signal, and d is the distance between antennas. Eq. (3.2) requires the receive antenna to be located at the far field of the transmit antenna, which will be further detailed in the next section. The free space path loss is defined as

$$PL_{FS} = \left(\frac{4\pi d}{\lambda}\right)^2. \tag{3.3}$$

From Eq. (3.3), the free space path loss can also be presented in dB as

$$PL_{FS}(dB) = 20\log_{10}(f) + 20\log_{10}(d) - 27.56, \tag{3.4}$$

where f is the radio frequency in MHz, and d is the distance between the transmit and receive antennas in metres. This formula will be used to calculate the theoretical free space path loss, which could be regarded as a benchmark in our experiments. Additionally, the path loss between two transceivers can be expressed in dB as

$$\begin{aligned} PL_{OA}(dB) &= P_t - P_r + G_t + G_r \\ &= P_t + RSSI, \end{aligned} \tag{3.5}$$

where $RSSI(dB) = |-P_r + G_t + G_r|$ with a note that P_r (dB) is a negative value.

3.3 Materials and Data Collection Setups

In this section, we will detail the materials required for the experiments from both software and hardware aspects.

Arduino integrated development environment (IDE), XBee configuration & test unit (X-CTU) and Matlab are the software used in the following experiments. They are used to program the Arduino UNO microprocessors and to configure parameters of the XBee-PRO S2C wireless transceivers. When programming the Arduino UNO hardware using Arduino IDE, it is noted that the baud rate must be declared to be the same as that of the transmitting and receiving Xbee-PRO S2C modules. These Xbee-PRO S2C modules are configured through X-CTU. In X-CTU, apart from the data rate and the power level, we should also configure the addresses of the source and destination to pair them. Then we set the transmitter as a coordinator, and the receiver as an end device.

The wireless system works in the 2.4 GHz industrial, scientific and medical (ISM) band, which is one of the carrier frequencies of the IEEE standard for local and metropolitan area networks [8]. The wireless transmitter and receiver are built by using commercial off-the-shelf components, which are portable, light, affordable, and easy to assemble. They also have little power consumption which enables the on-body usage. One of the Arduino UNO boards works as the coordinator and the other works as the end device. After all configurations, the Arduino UNO boards, XBee-PRO S2C modules, and micro SD card are assembled together. The construction of the transceivers is depicted in Fig. 3.1(a). The

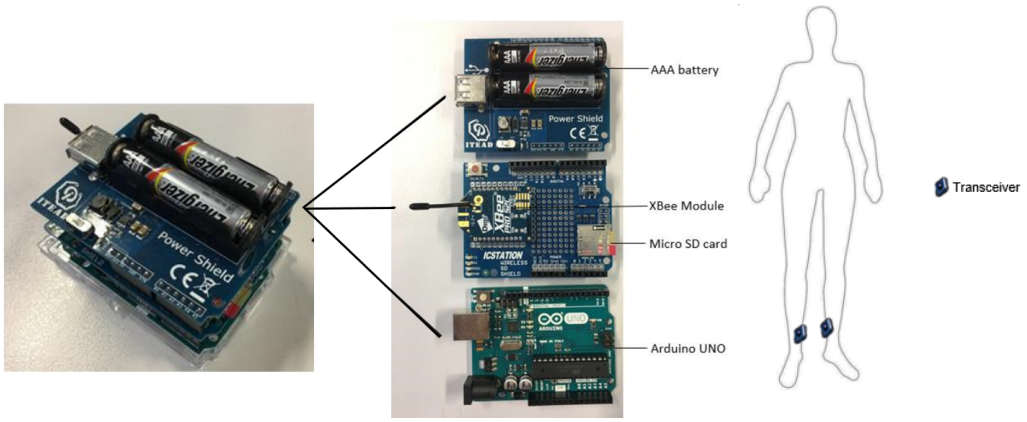

(a) Components of transceivers.

(b) Experiment on human ankles.

Figure 3.1: Hardware deployment.

main purpose of this system is to transmit and receive continuous data packets to/from each other, and a micro SD card is used to save the RSSI values.

During the experiment, a point-to-point link with one transmitter and one receiver is considered. Both transceivers are placed at the same height on human ankles as depicted in Fig. 3.1(b). The integrated whip antennas are used on the 2.4 GHz XBee-PRO S2C chips. The length of these integrated antennas is shorter than half of the wavelength. Therefore, these antennas are considered as electromagnetically short antennas. As a result, the reactive near field region is determined by

$$R_{near} < \lambda, \tag{3.6}$$

that is, $R_{near} < 12.5$ cm. Meanwhile, the far field is determined as

$$R_{far} > 2\lambda, \tag{3.7}$$

that is, $R_{far} > 25$ cm. Because our aim is to estimate the step length which is typically 0.4 m to 1 m, thus in this thesis, we only consider the far field region. From Eqs. (3.1) and (3.3), distance will be estimated as

$$d = \frac{\lambda \sqrt{10^{\frac{PL_{OA} - \Delta PL}{10}}}}{4\pi}, \tag{3.8}$$

where PL_{OA} is determined from Eq. (3.5).

The measurements start with the transceivers being placed at a distance of 0.4 m. The transmitter keeps sending sample packets at 9600 bps, with the power level of $P_0 = 0$ dBm. In our experiment, the packet length is 4 bytes. Thus, 300 frames will be sent each second. During the packet transmission, a three-column text file is saved in the micro SD card,. The first two columns are the packet sequence number and the packet time stamp, respectively. The last column is the RSSI values in dB. In this experiment, the hardware Arduino UNO is programmed in a way that, if an erroneous transmission occurs (i.e., the receiver does not receive the packet), a big value of RSSI would be recorded in the file. Thereby, in the later analysis, these erroneous transmissions will be easily detected and omitted.

The same measurement procedures at P_0 are repeated with the distance being increased every 0.1 m, from 0.4 m up to 1 m. We also repeat the experiment for different transmitted power levels and data rates. Our experiments have been carried out in both indoor and outdoor as shown in Fig. 3.2. The indoor experiments are conducted in a corridor, while the experiment environment for outdoor is a car park. The experiments are conducted for the static scenario, i.e., the subject under test stands still with different step lengths. These distances cover the normal step distance for human [39], while guaranteeing the RSSI measurement to be done in the far field of the transmit antenna. Therefore, the static measurement can symbolise the dynamic walking scenario.

3.4 Proposed Path Loss Model

In this section, an experimental path loss model will be derived. Based on this experimental model, the distance between the transmitter and the receiver can be estimated. Figs. 3.3 and 3.4 sketch the schematic diagrams where transceivers are attached to the human ankles and poles, respectively. The top view of the on-body measurement setup is shown in Fig. 3.3(a). The transmitter and the receiver are placed at the medial side of the ankles, while the antennas are pointing upward, orthogonal to the ground. The distance between them is denoted as d_0. Fig. 3.3(b) shows the side view of the on-body experiment, where

(a) Indoor.

(b) Outdoor.

Figure 3.2: Experimental environment.

the hardware is attached to the human ankles at a height of $h = 18$ cm. The schema of the off-body measurement is shown in Fig. 3.4, where the transceivers are attached to the poles at the same height as in the on-body experiments.

As stated in Section 3.2, it is conjectured that the path loss between two ankles, denoted as PL_{OA}, can be expressed as Eq. (3.1)

$$PL_{OA} = PL_{FS} + \Delta PL,$$

where PL_{FS} is the theoretical free space path loss, and ΔPL is the correction factor. The

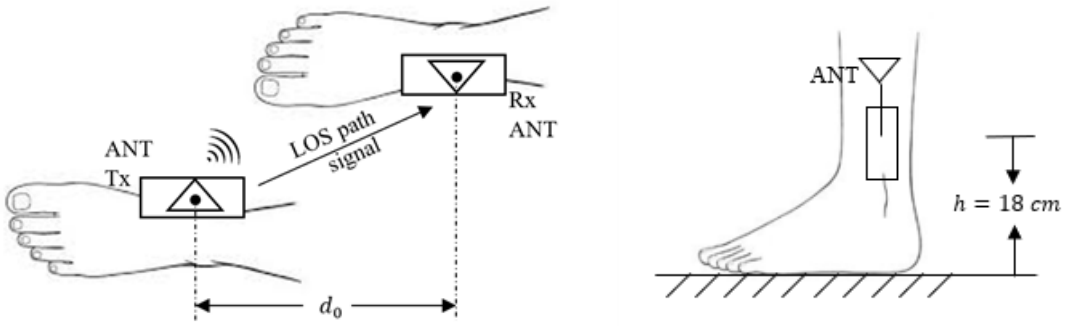

(a) Top view. (b) Side view.

Figure 3.3: Transceivers attached to the ankles.

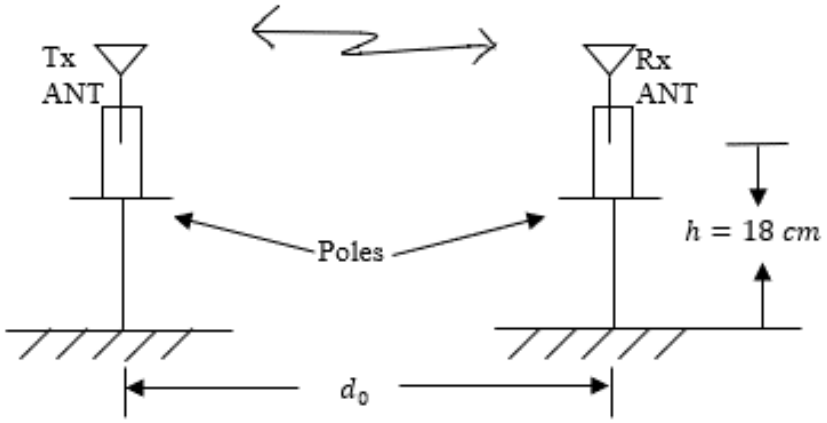

Figure 3.4: Transceivers attached to the poles.

correction factor can be presented as

$$\Delta PL = PL_{NonL} + PL_{Shad} + PL_{Mul} + PL_{Ins}, \tag{3.9}$$

where PL_{NonL} is the path loss discrepancy due to hardware non-linearity, PL_{Shad} represents the path loss of shadowing effect, PL_{Mul} denotes the path loss caused by multipath propagation, and PL_{Ins} denotes the mismatch loss and insertion loss. We will quantify these path losses in the following subsections.

3.4.1 Non-Linearity

Arduino UNO and XBee-PRO S2C are inexpensive commercial hardware, which may have a certain level of hardware non-linearity. The hardware non-linearity might include the power-dependent non-linearity and the rate-dependent non-linearity.

Table 3.1: Transmitted power of different settings for XBee-PRO S2C RF modules.

Power Level	Transmitted Power	Notation
0	0 dBm	P_0
1	+12 dBm	P_1
2	+14 dBm	P_2
3	+16 dBm	P_3
4	+18 dBm	P_4

The first experiment is conducted under the default data rate of XBee-PRO S2C, which is 9600 bps [131], along with the transceivers attached to the human body as depicted in Fig. 3.3. Fig. 3.5 demonstrates the relationship between the distance and the path loss between the transmitter and the receiver for different power levels at the same transmission rate. The transmitted power level can be found in Table 3.1 [131]. The blue line at the bottom is the free space path loss calculated by Eq. (3.4), which is used as the reference line to evaluate different hardware configurations. The black triangle markers and the green diamond markers are the average values of the measured experimental path loss at the power levels $P_0 = 0$ dBm and $P_1 = +12$ dBm, respectively. The corresponding coloured solid lines are the experimental fitted curves for these two power levels. From Fig. 3.5, it is clear that there is a little difference between the two experimental path losses corresponding to the two power levels. In theory, the path loss only depends on frequency and distance in Eq. (3.4), while, in practice, the experimental path loss may depend on the transmit power due to the power-dependent non-linearity of the hardware. However, the effect of the power-dependent non-linearity to the path loss is small as shown in Fig. 3.5; thus, it will be ignored in Eq. (3.9), i.e., $PL_{NonL} \approx 0$ dB. Fig. 3.5 also implies that the path loss between the two transceivers follows the same trend as that in the free space propagation.

The transmission rate is another variable in the experiment which may result in the discrepancy between the theoretical and practical path losses. To investigate the influence of data rate on the path loss between two ankles, the transmitted power is fixed at $P_0 =$ 0 dBm, so that the path loss is numerically equal to the RSSI (cf. Eq. (3.5)).

Fig. 3.6 describes the relationship between the distance and the path loss when the

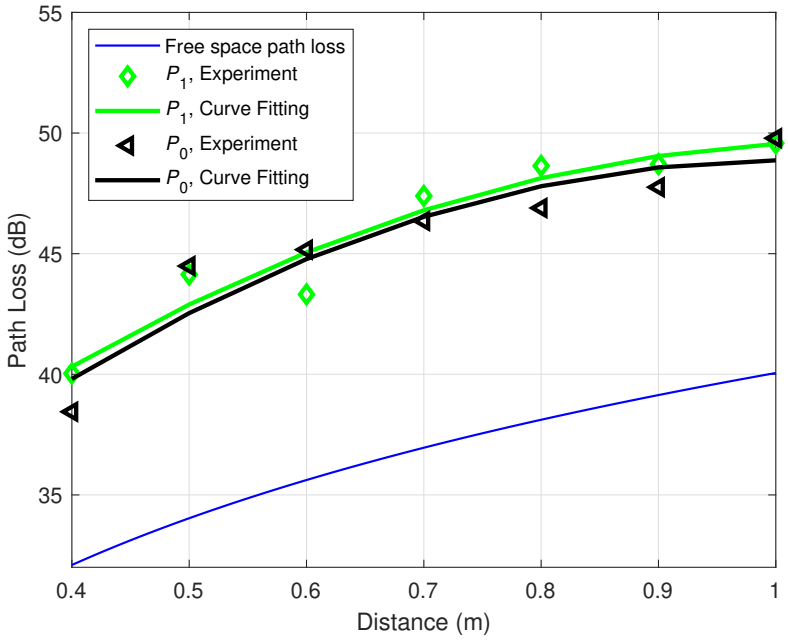

Figure 3.5: On-ankle path loss for different power levels at the data rate 9600 bps.

transmission rate is varied. Similarly, the black left-pointing triangles and the red circles are the average values of 50,000 measured experimental path losses at the data rates of 9600 bps and 19,200 bps, respectively. The corresponding coloured solid lines are the fitting curves for these two cases. The bottom blue line is the theoretical free space path loss. In theory, the path loss is influenced by distance and frequency only, while, in practice, according to Fig. 3.6, there is also a dependence on the data rate. With a steady increment of distance, the difference between the two cases of 9600 bps and 19,200 bps increases gradually. It is noted that within the step length 0.6 m to 0.8 m of our interest, which is the most common average range of step length for adults, as mentioned previously at the end of the Section 2.2. The path loss discrepancy between the 9600 bps and 19,200 bps is within this range is around 2 dB. Therefore, the non-linearity due to the transmission rate may contribute to the total correction factor ΔPL by about 2 dB, i.e., $PL_{NonL} \approx 2$ dB.

3.4.2 Shadowing Effect

To explore the shadowing effect caused by the human body, experiments are conducted for the off-body situation by removing the transceivers from human ankles (cf. Fig. 3.3) to two holding poles at the same height h of the human ankles as shown in Fig. 3.4. Other

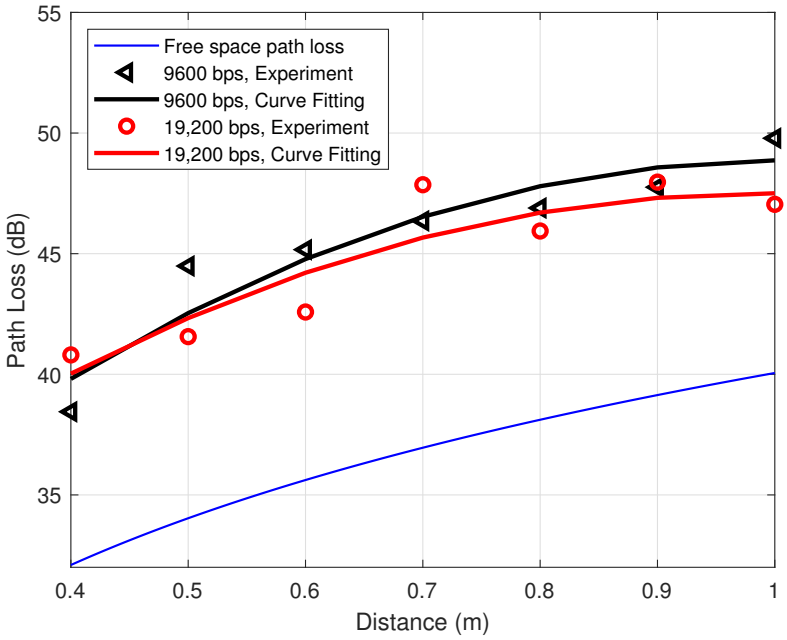

Figure 3.6: On-ankle path loss for different data rates at the transmitted power P_0 = 0 dBm.

configurations are kept the same as the previous experiments. Figs. 3.7 and 3.8 are the path loss for the off-body scenarios. More specifically, Fig. 3.7 depicts the experimental path loss at the data rate 9600 bps with different power levels. The left-pointing triangle markers are the experimental data, while the corresponding black curve is the fitting curve. Clearly, the off-body path loss curve for the power level P_0 matches very well with the on-body path loss one in Fig. 3.5 for the distance range 0.6 m – 0.8 m of interest.

Fig. 3.8 illustrates the experimental path loss data and the fitting curves for the power level $P_0 = 0$ dBm with different data rates. These two curves match well with the black and red curves in Fig. 3.6, especially in the range of interest 0.6 m – 0.8 m.

Figs. 3.5 – 3.8 indicate that the shadowing effect caused by the human body is not significant in our experiment, i.e., $PL_{Shad} \approx 0$ dB. This conclusion is reasonable and supported by our experiment configurations. In particular, in our experiments, the transmitter and receiver are placed on the inner side of the ankles as shown in Fig. 3.3. Thus, there is barely any body tissue between them to cause the shadowing.

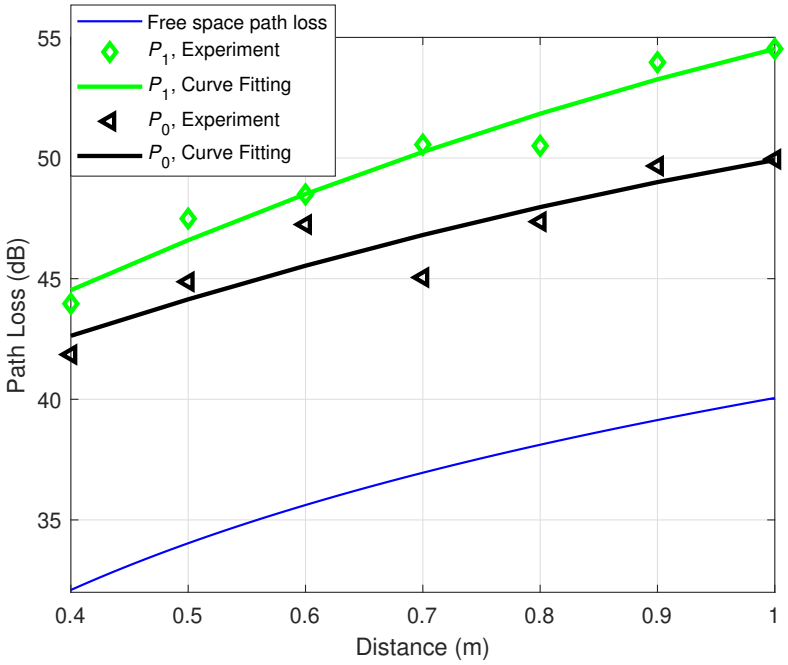

Figure 3.7: Off-body path loss for different power levels at data rate 9600 bps.

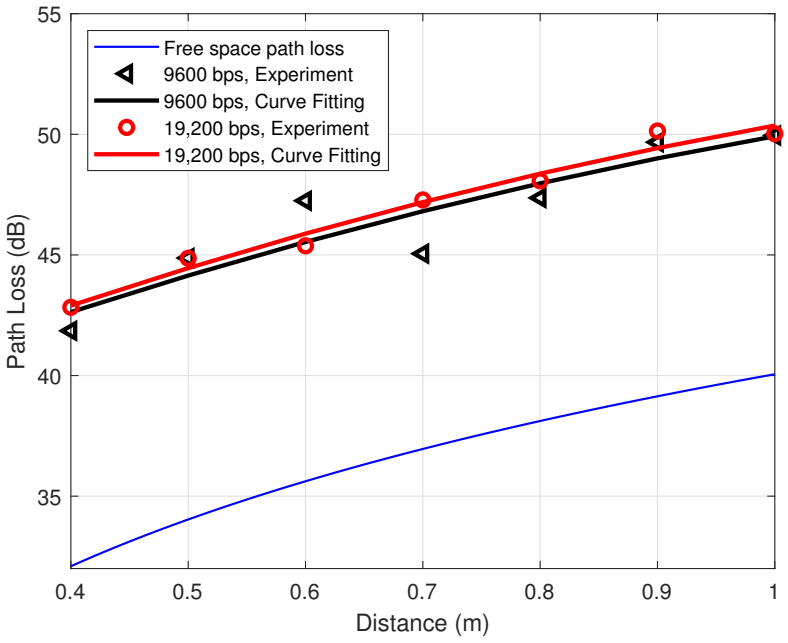

Figure 3.8: Off-body path loss for different data rates at transmitted power $P_0 = 0$ dBm.

3.4.3 Multipath Propagation

The influence of the multipath propagation is examined by repeating the experiment with the transceivers attached to the human ankles for the outdoor environment, which is shown in Fig. 3.2(b). Fig. 3.9 shows the relationship between the distance and the measured path

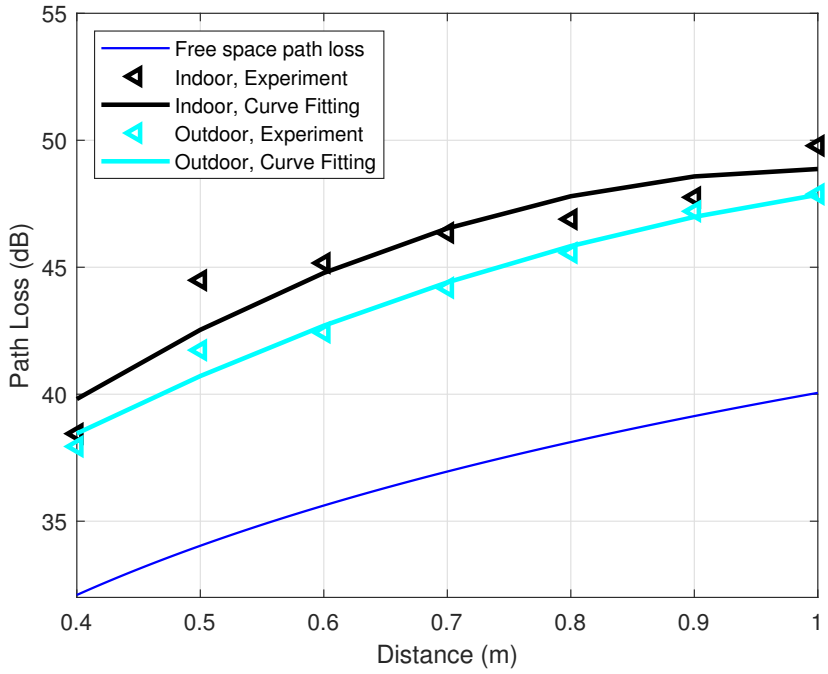

Figure 3.9: Indoor and outdoor comparison of path loss at transmitted power $P_0 =$ 0 dBm, 9600 bps.

loss between two ankles in the indoor and outdoor environments with the same configurations. The transmitted power is 0 dBm and the data rate is 9600 bps. The black and cyan left-pointing triangles are the average values of the measured path loss for indoor and outdoor, respectively. The blue line at the bottom is the theoretical free space path loss calculated by Eq. (3.4). The other two lines on top are the two corresponding curve-fitting lines for indoor and outdoor cases. Fig. 3.9 shows that the cyan curve is persistently below the black curve by 2 dB. This indicates that, for the indoor situation, the multipath contribute to the path loss correction factor by about 2 dB, i.e., $PL_{Mul} \approx 2$ dB.

3.4.4 Insertion and Mismatch Losses

In this section, both insertion and mismatch losses will be mentioned. Insertion loss is the loss of signal power due to the insertion of a component [132], while the mismatch loss happens due to impedance mismatches and signal reflections. In our experiments, the XBee SD shields are deployed on top of the Arduino UNO boards in order to connect the XBee RF modules to the Arduino boards as shown in Fig. 3.1(a). The insertion and mismatch losses due to hardware, including the XBee modules and the XBee SD shields,

are typically 3 dB at each transceiver. This results in a total insertion and mismatch losses of 6 dB, which are unavoidable because of the hardware, i.e., $PL_{Ins} \approx 6$ dB.

3.4.5 Overall Effects of Component Losses

In summary, the influence of the non-linearity is about 2 dB, the shadowing effect can be ignored, the multipath propagation contributes 2 dB to the total correction factor, and the insertion and mismatch losses are around 6 dB. Therefore, the correction factor in Eq. (3.9) can be written as:

$$\begin{aligned} \Delta PL(dB) &= PL_{NonL} + PL_{Shad} + PL_{Mul} + PL_{Ins} \\ &\approx 2 + 0 + 2 + 6 \\ &= 10. \end{aligned} \tag{3.10}$$

As a result, the path loss between the two transceivers on the human's ankles can be expressed as

$$PL_{OA}(dB) = PL_{FS} + 10. \tag{3.11}$$

As the experimental path loss model considerably fits with the practical path loss in our experiments for the transmitted power $P_0 = 0$ dBm and the data rate of 9600 bps, this configuration is adopted for the distance measurement below. It is worth noting that $P_0 = 0$ dBm and the data rate of 9600 bps are in fact the two default parameters of the Arduino UNO microprocessors. The hardware configuration where the transmitted power is 0 dBm, the data rate is 9600 bps, and the transceivers are attached to the inner sides of the human ankles is referred to as the optimal hardware configuration in this thesis. If other non-optimal configurations are chosen or the devices are not attached correctly to the inner sides of the human ankles, the correction factor of the proposed path loss model will require further amendments to avoid mismeasurement. For example, if the hardware is attached to the outer sides of the ankles, the shadowing effect will be more severe due to the presence of body tissues between the transceivers, which may result in the correction factor being no longer 10 dB.

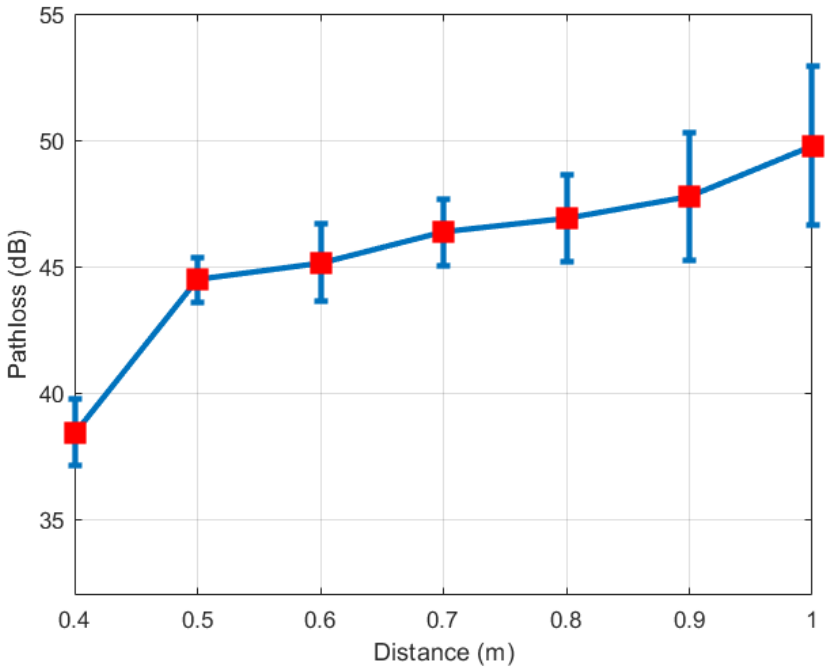

Figure 3.10: Standard deviation of path loss at $P_0 = 0$ dBm, 9600 bps.

3.5 Distance Measurement Accuracy

Fig. 3.10 illustrates the mean and standard deviation of the path loss for different distances at the transmitted power 0 dBm and the default data rate 9600 bps. The red square markers represent the mean values of the on-ankle path losses, while the blue vertical segments present the standard deviation of the measured path loss for each distance. A smaller standard deviation indicates the more consistent measured path loss values, while a bigger standard deviation means the measured path loss values spread over a wider range around the mean value. The mean value and standard deviation value together reflect the accuracy of the path loss measurement. It is observed that in general, the accuracy of the path loss measurement reduces with the increase of distance. The measurement accuracy of the path loss value PL_{OA} in turn affects the measurement accuracy of the step length based on the relationship in Eq. (3.8). Therefore, a deduction could be drawn from Fig. 3.10 is that, the distance measurement accuracy reduces when the real distance increases. This deduction will be confirmed by Figs. 3.11 and 3.12 mentioned later in this section.

From the measured RSSI values, the distance between the transmitter and the receiver can be estimated based on Eqs. (3.5) and (3.8). The estimated average distance is then

calculated by averaging 50,000 realisations. To evaluate the accuracy of the distance measurements, the absolute distance error is defined as

$$\Delta d(\mathrm{m}) = |\overline{\mathrm{d}} - \mathrm{d}_0|, \tag{3.12}$$

and the normalised distance error ε is expressed as

$$\varepsilon = \frac{\Delta d}{d_0} = \frac{|\overline{d} - d_0|}{d_0}, \tag{3.13}$$

where $\overline{d}$ and d_0 are the estimated average distance and the actual distance between the transmitter and the receiver, respectively. From Eq. (3.12), the relation between the estimated average distance $\overline{d}$ and the actual distance d_0 can be written as $\overline{d} = d_0 \pm \Delta d$.

Figs. 3.11 and 3.12 illustrate the cumulative distribution function (CDF) of the normalised distance error ε and of the absolute distance error Δd for different distances between two transceivers, respectively. From these two figures, the observation is that, in general, the accuracy of distance measurements decreases as the actual distance d_0 increases. For example, in Fig. 3.11, when the real distance d_0 is 0.5 m, the probability of estimating correctly this distance with the normalised distance error ε not exceeding 0.05 (i.e., $\Delta d \leq 2.5$ cm) is 55%. If this threshold expands to 0.15 (i.e., $\Delta d \leq 7.5$ cm), the probability would be 97%. Meanwhile, these probabilities for the real distance $d_0 = 0.8$ m are only 30% and 63%, respectively. This observation could be explained as follows: at a shorter distance, the signal is stronger and well-received, thus the path loss is smaller. Therefore, the probability of recovering accurate distances will be higher than that of long distances.

This behaviour is also reflected in Fig. 3.12. Overall, the accuracy of distance estimation reduces when the distance increases from 0.5 m to 0.8 m. As shown in Fig. 3.12, when the absolute error $\Delta d = 0.1$ m, the measurement accuracy of $d_0 = 0.7$ m is 95.21%, which is roughly the same as that of $d_0 = 0.5$ m. When $\Delta d = 0.15$ m, the accuracy reaches 100% in both cases.

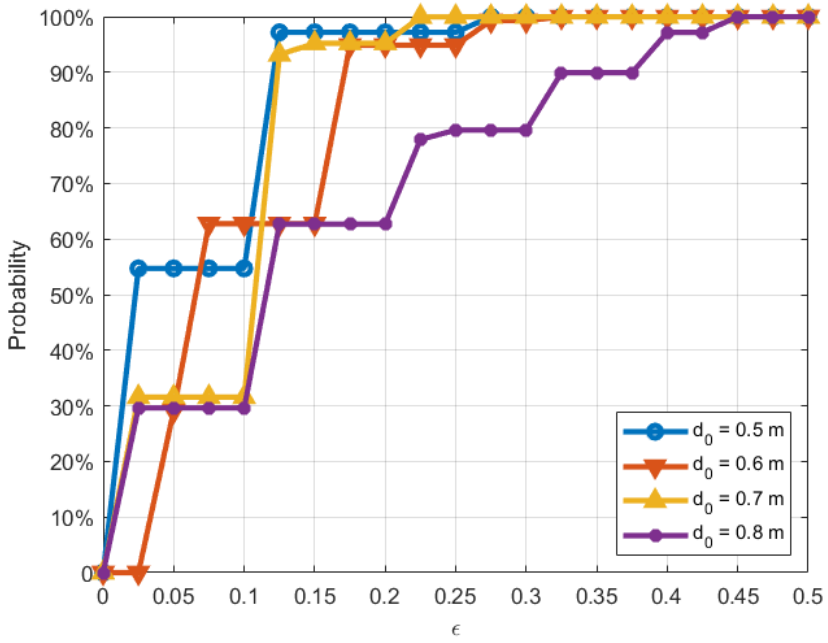

Figure 3.11: Cumulative distribution function of normalised error ε at different distances.

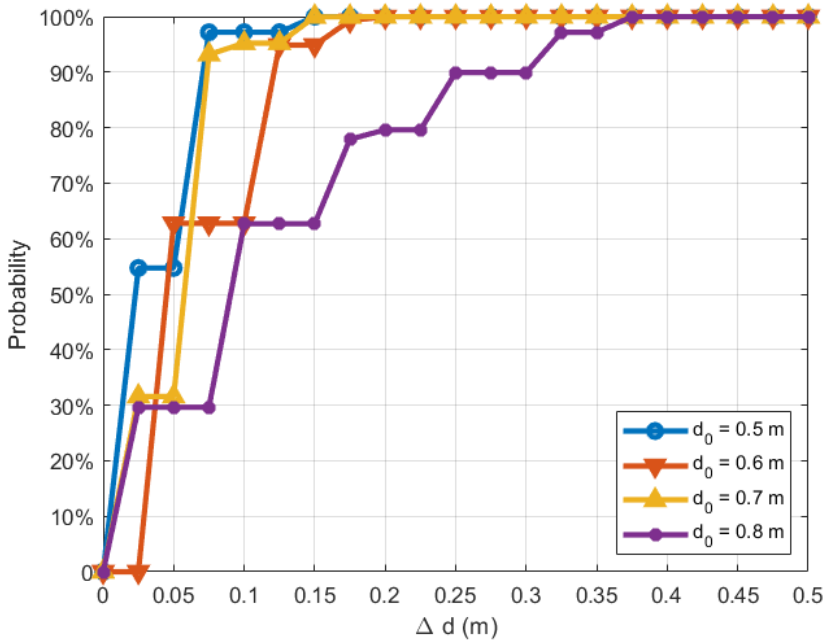

Figure 3.12: Cumulative distribution function of absolute distance error Δd at different distances.

3.6 Chapter Summary

In this chapter, we have developed portable transceivers using Arduino UNO and XBee-PRO S2C chips. The developed transceivers are used to measure the received signal

strength and to analyse the wireless channel between two ankles. We have also derived the experimental path loss model, which is equal to the path loss in free space plus a correction factor of 10 dB. This experimental path loss model is then used to estimate the distance between the transmitter and the receiver attached to the human ankles. The experimental results indicate that the distance can be calculated relatively accurately, despite the inexpensive hardware devices, with the distance errors of a centimetre scale.

The limitation of this work is that all the experimental data are collected under a static situation, i.e., the person under test stands still during the measurements. In the next chapter, we will conduct experiments to estimate the distance between human body parts in dynamic situations, where the person under test is walking or jogging in either indoor or outdoor environments.

Chapter 4

Step Length Estimation in Walking and Jogging Scenarios

4.1 Introduction

Our previous work presented in Chapter 3 proposed an empirical path loss model to estimate the human step length in both indoor and outdoor scenarios under a static context rather than in a dynamic one. To address this limitation, the main aim of this chapter is to estimate human step length in daily activities.

Step length (or stride length) plays an important role in coping with issues of human health conditions, especially for seniors. It is an indicator that predicts accidental falls and fall-related injury in the elderly [38], which may cause fatality [14]. A reduced step length has been found to be associated with the increased dependence, mortality, and institutionalisation of older people [40]. The variability of the step length also indicates the integrity of grey matter, which is closely related to personal memory and executive functions [35]. Furthermore, step length is one of the significant components in gait patterns. It can be converted to gait speed, which is useful in predicting life expectancy [10]. Therefore, monitoring the human step length is a vital topic that is worthy of investigating.

As mentioned in Chapter 2, the estimation of the step length can be traced back to the problem of distance estimation. Although distance estimation has been intensively researched for general communication systems, the existing publications that address the estimation of step length either have modest accuracy or follow privacy-invasive, health-

concerning, and strictly space-confined approaches. Specifically, camera-based technologies [48], [59] are privacy-invasive and prone to error as they may record images or video footage of the participants. The camera-based methods also require a specific experimental setting because any obstacle appearing between the camera and the person under test can cause measurement errors. Meanwhile, laser-based methods [72] may arouse health concerns because a long-time exposure to lasers in these methods may cause some health hazards. On the other hand, sensing mats [49]–[51] have been well adopted to improve the safety of patients, especially the disabled and those with disorders. However, the sensing mat approach is confined to particular spaces, such as clinics, hospitals, or a specific laboratory setting where the sensing mat is laid, because the person under test must walk or run on this mat. Therefore, a more-accurate, less-invasive, less-health-concerning, and less-space-confined, but also cost-efficient technique for step length estimations in daily activities is still missing.

Thus, this chapter aims to estimate the step length based on the RSSI method in both walking and jogging activities in indoor and outdoor scenarios. The RSSI has been widely employed in distance estimation [46], [92], [97]–[99], [133], providing reliable performance especially for measurements in LOS paths over short distances. The step length in this thesis refers to the average distance between two ankles of the person under test when the person is walking or jogging at a normal and equal pace. Unlike our previous work mentioned in Chapter 3 (and [129]), which only considers a static environment, this chapter undertakes experiments in actual moving activities. In particular, a novel filtering technique is proposed in this chapter, which is used along with the hardware transceivers and the empirical path loss model developed in Chapter 3 to estimate human step length correctly in both walking and jogging activities in both indoor and outdoor environments.

In this chapter, actual human step length is estimated based on wireless channel properties and the RSSI method. Path loss between two ankles of the person under test is converted from the RSSI, which is measured using our developed wearable transceivers with embedded micro-controllers in four scenarios, namely indoor walking, outdoor walking, indoor jogging, and outdoor jogging. For brevity, we call it on-ankle path loss. The

histogram of the on-ankle path loss clearly shows that there are two humps, where the second hump is closely related to the maximum path loss, which, in turn, corresponds to the step length. The histogram can be well approximated by a two-term Gaussian fitting curve model. Based on the histogram of the experimental data and the two-term Gaussian fitting curve, we propose a novel filtering technique to filter out the path loss outliers, which helps set up the upper and lower thresholds of the path loss values used for the step length estimation. In particular, the upper threshold is found to be on the right side of the second Gaussian hump, and its value is a function of the mean value and the standard deviation of the second Gaussian hump. Meanwhile, the lower threshold lies on the left side of the second hump and is determined at the point where the survival rate of the measured data falls to 0.68, i.e., the CDF approaches 0.32. The experimental data shows that the proposed filtering technique results in high accuracy in step length estimation with sub-centimetre scale errors.

The main contributions of this chapter are summarised as follows:

- A novel filtering technique is proposed to eliminate on-ankle path loss outliers and keep the remaining as a reliable range with a pair of upper and lower thresholds. This range of path loss values is used to estimate the human step length in daily activities, such as walking and jogging.

- The distribution of the on-ankle path loss is revealed to follow a two-term Gaussian distribution, and the two thresholds lie on each side of its second hump.

- The thresholds can be determined mathematically. The upper threshold relates to the fitting equation of the second hump of the two-term Gaussian distribution, which is found as $\mu + 0.5\sigma$ for an outdoor environment and $\mu + \sigma$ for an indoor case. The lower threshold relates to the survival rate of the collected data set, which is located at the point where the survival rate of the measured data is 0.68.

- The proposed filtering technique results in an accurate estimation of the step length, with errors of only 10.15 mm and 4.40 mm for walking and jogging in an indoor environment, respectively, and only 4.81 mm and 10.84 mm for the same activities

in an outdoor environment.

The content of this chapter has been published in [134].

The remaining of this chapter is organised as follows. Section 4.2 describes the proposed system model. In Section 4.3, the experimental procedures are detailed. Section 4.4 demonstrates a trial experiment with some preliminary observations. Section 4.5 presents the experimental results and analyses of the step length estimation accuracy in the indoor walking, indoor jogging, outdoor walking, and outdoor jogging situations. Finally, Section 4.6 summarises this chapter.

4.2 System Model

In this chapter, we adopt the transceivers and the experimental path loss model between two human ankles developed in Chapter 3. The experimental path loss PL_{OA} between two transceivers attached to the ankles of the person under test can be described as a modified free space path loss model with a correction factor ΔPL (cf. Eq. (3.1))

$$PL_{OA}(\text{dB}) = PL_{FS} + \Delta PL, \tag{4.1}$$

where PL_{FS} (dB) is the free space path loss and ΔPL (dB) is the correction factor, which accounts for the hardware non-linearity, multipath propagation, insertion, and mismatch losses. For the transceivers considered, the correction factor is empirically found as 10 dB in the previous chapter. Therefore, Eq. (4.1) can be written as

$$PL_{OA}(\text{dB}) = PL_{FS} + 10. \tag{4.2}$$

It is noted that the free space path loss [130] is defined as

$$PL_{FS}(\text{dB}) = 20\log_{10}\left(\frac{4\pi d}{\lambda}\right), \tag{4.3}$$

where d (m) is the distance between the two antennas and λ (m) is the signal wavelength. From Eqs. (4.2) and (4.3), this distance could be estimated as

$$d = \frac{\lambda}{4\pi} 10^{\left(\frac{PL_{OA}(\text{dB})-10}{20}\right)}. \tag{4.4}$$

This equation will be used to calculate the human step length in the subsequent experiments.

4.3 Experimental Setup

In this section, we detail our experimental settings. Similar to the previous experiments which have been described in Chapther 3, the Arduino IDE, X-CTU, Arduino UNO microprocessors, and XBee-PRO S2C wireless transceivers are employed in this experiment, and they are constructed as shown in Fig. 3.1. The parameters are configured as follows: transmission power $P_0 = 0$ dBm and data rate 9600 bps. This is the most proper configuration of the developed transceivers for measuring the distance between two ankles, as discovered from our previous experiments in Chapter 3. The core communication technology used in the XBee-PRO S2C modules is the spreading spectrum technique regulated by the IEEE 802.15.4 standard for low-rate wireless personal area networks (LR-WPANs) [135]. In particular, each group of four data bits is mapped into one of 16 nearly orthogonal spreading sequences, each of which is 32 chips long. The resulting chip sequence is modulated on the radio-frequency carrier in the 2.4 GHz band by the offset quadrature phase shift keying (O-QPSK) modulation scheme.

The transceivers are attached to the inner side of human ankles at the same height h, as shown in Fig. 3.2. The distance between two antennas is regarded as the real step length d_0 (m). In our experiments, the transmitter and the receiver are placed on the medial side of the ankles of the subject under test in a way that the antennas face each other, as shown in Fig. 3.2. This means that there exists a LOS path between the transceivers throughout the whole duration of the experiment, even when the person under test is walking or jogging, and that there is no human body part appearing between them. As a result, this

placement of equipment can eliminate the shadowing effect caused by any body parts. This intuitive prediction has been confirmed in Section 3.4.2, where experiments are performed both off-body and on ankles to compare the shadowing effect. Therefore, it is showed that the shadowing effect caused by the human body is negligible in our experiments.

The main purpose of this system is to transmit and receive continuous data packets to/from each other, and the assembled micro SD card in the receiver would record the RSSI values continuously. From the RSSI values, the on-ankle path loss can be calculated as (cf. Eq. (3.5))

$$PL_{OA}(\text{dB}) = P_t + RSSI, \tag{4.5}$$

where P_t (dBm) is the transmitted power. From Eqs. (4.4) and (4.5), the distance between the two transceivers is

$$d = \frac{\lambda}{4\pi} 10^{\left(\frac{P_t(\text{dB}) + RSSI(\text{dB}) - 10}{20}\right)}. \tag{4.6}$$

4.4 A Trial Experiment

This section presents a trial experiment of the indoor walking activity to explore the relationship between the measured path loss values and the positions of the two ankles. Fig. 4.1(a) plots the on-ankle path loss over time. During the first 0.64 s, the transmitter and the receiver initialise themselves and synchronise with each other. Once the transmitter and the receiver are synchronised, it takes around 0.02 s for the hardware to measure and record each RSSI value into the micro SD card, as shown in Fig. 4.1(a).

After the initial synchronisation phase, the Arduino may encounter erroneous transmissions from time to time due to temporarily being out-of-synchronisation. To cope with this, in our experiments, the Arduino UNO hardware is programmed in a way that, if an erroneous transmission occurs (i.e., the receiver does not receive the packet successfully), a very big value of path loss (120 dB is chosen in our experiments) would be recorded to the data file in the micro SD card to flag this erroneous transmission. Thereby, in the later analysis, any erroneous transmission would be easily detected and omitted. As shown

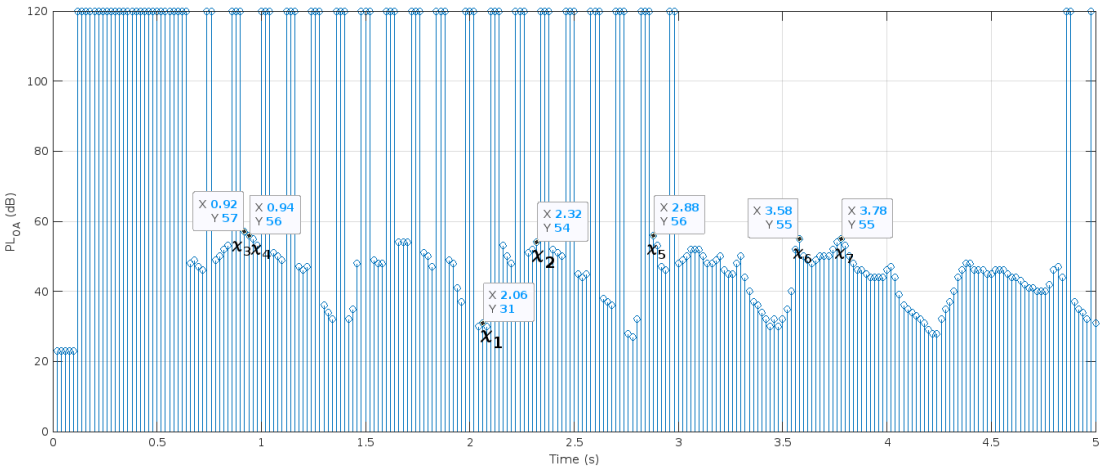

(a) On-ankle path loss at different time instants.

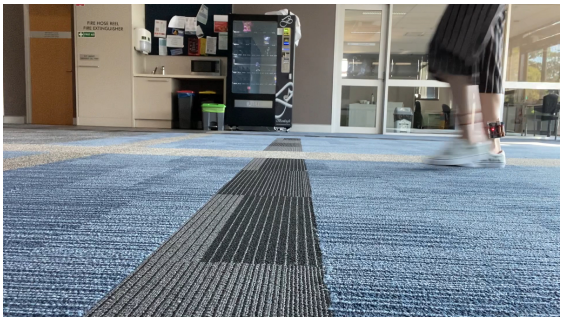

(b) Feet positions at χ_1 (t = 2.08 s).

(c) Feet positions at χ_2 (t = 2.32 s).

Figure 4.1: Trial indoor walking experiment.

in Fig. 4.1(a), the temporary out-of-synchronisation status is normally very short, and the transceivers could quickly synchronise again with each other. Hence, in general, the Arduino UNO transceivers are relatively stable and reliable.

Because of the modest computation capability of the Arduino UNO, the transceivers in our experiments are programmed to only transmit and receive data packets to record the RSSI values in order to avoid any unnecessary delay. Processing of the raw data is performed offline on a computer using Matlab instead. It is also noted that we aim to estimate the average step length over a certain period, rather than outputting the instantaneous estimated step length values, to mitigate the randomness in the measurement process. As a result, the processing time of our algorithm has a negligible effect on the RSSI calculations.

It is observed that the measured path losses have a periodical pattern. To explore the meaning of the peaks and troughs of the path loss, let us consider two points χ_1 (2.08 s,

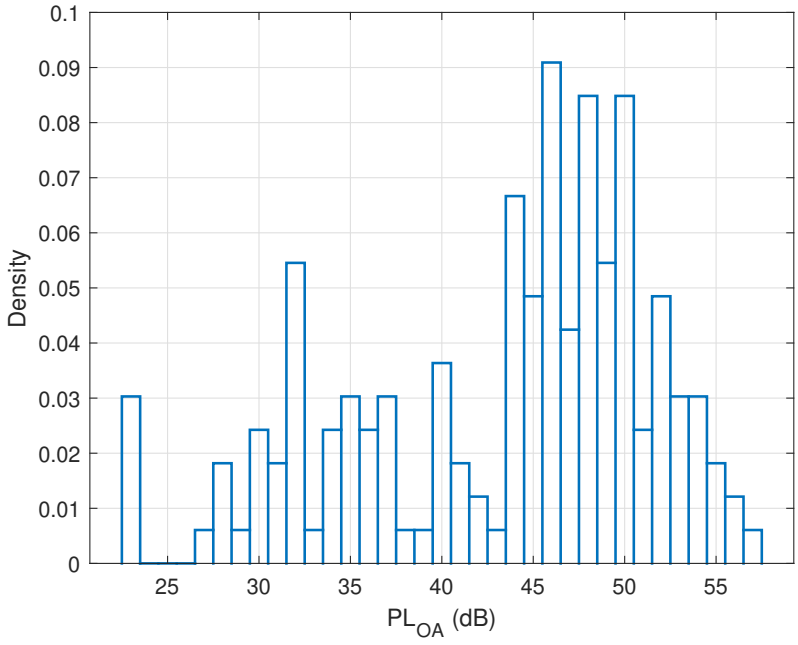

Figure 4.2: The probability histogram of the trial indoor walking experiment.

30 dB) and χ_2 (2.32 s, 54 dB) from the plot, where χ_1 is at a trough and χ_2 is the following peak. A video of the footage is captured in tandem with the path loss measurements. Based on the time stamps, we obtain the corresponding video frames, which correspond to χ_1 and χ_2, as shown in Figs. 4.1(b) and 4.1(c). In Fig. 4.1(b), two feet are aligned with each other. In other words, at χ_1, the distance between two ankles is the shortest, which indicates the pedestrian has moved the left leg from behind to the middle position and is about to step forward. Hence, a step is half-finished at the bottom points of Fig. 4.1(a). This step is fully finished as shown in Fig. 4.1(c). The ankles are at the largest distance from each other, where χ_2 is located. This means the peak path loss value at χ_2 in the time duration [2.08 s, 2.32 s] coincidentally corresponds to the step length. Note that $PL_{OA} = 54$ dB is not the global largest value of path loss in Fig. 4.1(a). For example, the peak path loss values at the points $\chi_3 - \chi_7$ at the time instants 0.92 s, 0.94 s, 2.88 s, 3.58 s, and 3.78 s are even bigger than 54 dB. In other words, the path loss corresponding to the step length is expected to be in a high range of the path loss values, but not necessarily the largest value. Hence, to find the step length, it is necessary to examine the histogram of the experimental data.

The bar chart in Fig. 4.2 depicts the probability histogram of the on-ankle path loss in

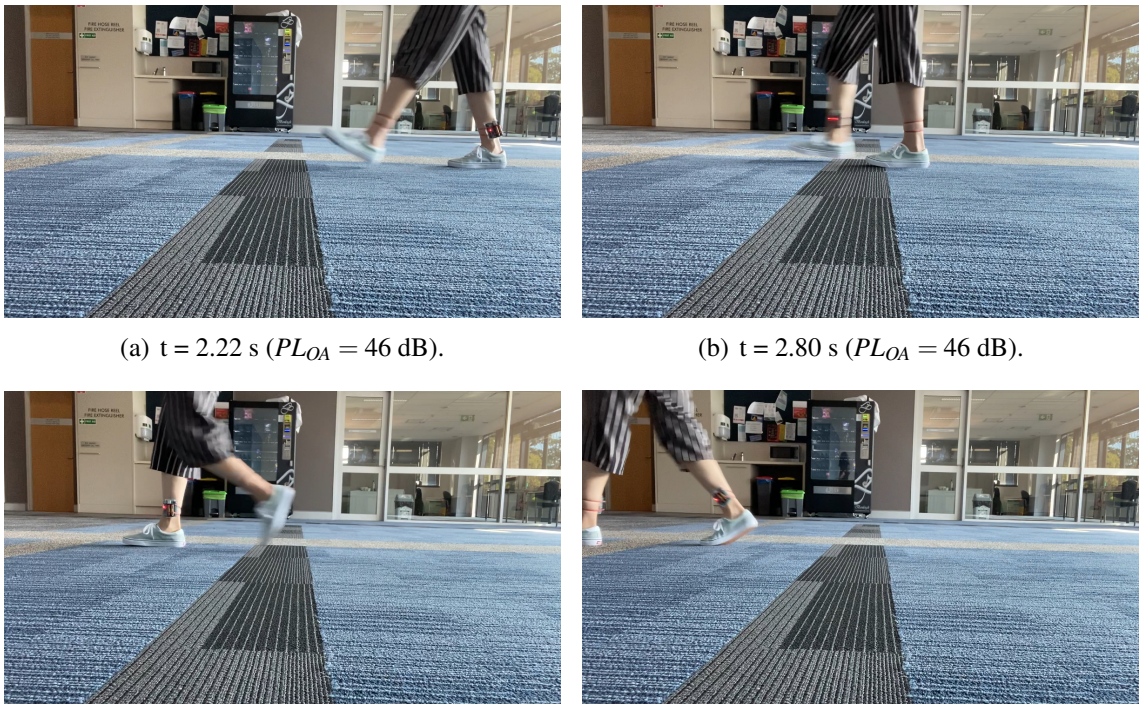

(a) t = 2.22 s ($PL_{OA} = 46$ dB). (b) t = 2.80 s ($PL_{OA} = 46$ dB).

(c) t = 3.12 s ($PL_{OA} = 50$ dB). (d) t = 3.72 s ($PL_{OA} = 50$ dB).

Figure 4.3: Feet positions at different time stamps of the indoor walking experiment.

this trial experiment. Clearly, the histogram shows a two-hump shape with the most likely path loss occurring at the peak density $PL_{OA} \approx 46$ dB. The first, smaller hump corresponds to the half-finished steps, i.e., when the two feet are about to cross each other. The second, bigger hump corresponds to the events when the two feet are likely most separated from each other. The step length (i.e., the maximum distance between the two transceivers) may occur somewhere around the peak density rather than always at the peak density in the histogram. To demonstrate this point, let us consider the two different moments $t = 2.22$ s and $t = 2.80$ s when the path loss of 46 dB takes place (cf. Figs. 4.3(a) and 4.3(b)). These two figures suggest that, although the on-ankle path losses at these time instants are the same and both correspond to the peak density in the histogram, the feet of the person under test are not in the identical posture. This means that the path loss corresponding to the peak density does not always correspond to the step length due to the random variations of the propagation channel. This observation is confirmed again in Figs. 4.3(c) and 4.3(d), where we show the two maximum distance events at the time instants $t = 3.12$ s and $t = 3.72$ s when $PL_{OA} \approx 50$ dB. The path loss $PL_{OA} \approx 50$ dB

corresponds to the second maximum density, rather than the peak one in Fig. 4.2.

From the aforementioned observations, we conjecture that the human step length can be estimated within a certain range around the peak density of the histogram. This is because the actual step length may occur before or after the peak density due to the random variations superimposed on the propagation channel caused by the dynamic motions of the person under test. Therefore, in the following experiments, we propose a filtering technique to discard outlier data to form a range of reliable path loss values for estimating the step length. The accuracy analyses will also be mentioned in the next section.

4.5 Experimental Results and Analyses

In this section, experiments are conducted in four dynamic scenarios, including indoor walking, outdoor walking, indoor jogging, and outdoor jogging. The indoor experiments are carried out in a corridor of a building, while the outdoor ones are conducted along a pavement, which could be seen as an open area in Fig. 4.4. The participant walks or jogs along a straight path with a length of 35.7 m. There are 50 steps and 38 steps in the walking and jogging scenarios, respectively. Therefore, the real average step length for walking is $d_{0w} = 35.7 \div 50 = 0.7140$ m, while for jogging, it is $d_{0j} = 35.7 \div 38 = 0.9395$ m. In each scenario, the experiments are carried out 10 times with over 1500 data in each data set. Altogether, there are more than 15,000 data values for each scenario. In our previous work in Chapter 3, an empirical path loss model for the wireless channel between the two ankles in a static situation has been derived, as shown in Eq. (4.1). As mentioned above, there exists randomness of the path loss in dynamic situations where the person under test is walking or jogging. Thus, we propose a filtering technique to apply along with the empirical model in Eq. (4.1) in order to eliminate the on-ankle path loss outliers. The resulting ranges of on-ankle path loss will then be used to estimate the step length in the four motion scenarios. The following subsections are the experiment results and analyses for the four motion circumstances.

(a) Indoor.

(b) Outdoor.

Figure 4.4: Experimental environments.

4.5.1 Empirical Threshold Pair

We propose a novel filtering technique to filter out the path loss outliers by setting a threshold pair, which consists of an upper threshold and a lower threshold. As these two thresholds work together, we find both thresholds simultaneously. As shown in Figs. 4.1 and 4.3, the path loss of the step length would be in the vicinity of the peak of the histogram. This is because the random variations of the propagation channel is caused by the dynamic movements of the person under test. Thus, it is important to consider a suitable range of the path loss values that might possibly correspond to the maximum distance between two ankles. To this end, based on the collected data sets, we first examine different combinations of the lower bound and the upper bound of this range to find the pair of

boundaries that minimise the error between the average estimated step length and the true step length. The path loss values higher than the upper threshold or lower than the lower threshold are considered as outlier values.

Fig. 4.5 demonstrates the normalised errors of the step length estimations in the indoor walking and indoor jogging scenarios for different lower and upper thresholds. The relative (or normalised) error ε in percentage is defined as

$$\varepsilon = \frac{|\overline{d} - d_{0i}|}{d_{0i}} \times 100\%, \tag{4.7}$$

where $\overline{d}$ is the average estimated distance between two ankles under a certain experimental scenario, which involves 10 data sets in each scenario. d_{0i} is the real step length, where i is either w for the walking scenario or j for the jogging scenario. Fig. 4.5 shows that the (lower, upper) threshold pairs of (40 dB, 52 dB) and (40 dB, 56 dB) result in the average estimated step lengths being the closest to the true step lengths (i.e., the smallest normalised error ε) in the indoor walking and indoor jogging scenarios, respectively.

Along with Fig. 4.5, Tables 4.1 and 4.2 show in more details about the estimated step length (cf. Eq. (4.4)), averaged over all ten data sets for some different pairs of the (lower, upper) thresholds for the indoor walking and indoor jogging scenarios. In each cell of the table, there are three numbers. The average estimated step length in metres, which is the average result based on 10 experimental data sets, is located outside of the brackets. Inside the brackets are the average absolute error in millimetres and the average relative error in percentage, respectively.

The average absolute error is calculated as $|\overline{d} - d_{0i}|$. Tables 4.1 and 4.2 confirm further the observation gained from Fig. 4.5 that the best pairs of (lower, upper) thresholds of the path losses are (40 dB, 52 dB) and (40 dB, 56 dB) for the indoor walking and indoor jogging cases, respectively. The average absolute and normalised estimation errors are just 10.15 mm and 1.42% for the indoor walking case, while these numbers are 4.40 mm and 0.47% for the indoor jogging case.

Similarly, Fig. 4.9, Tables 4.3 and 4.4 clearly show that the best (lower, upper) thresholds of the path losses used for estimating the average step length in the outdoor walking

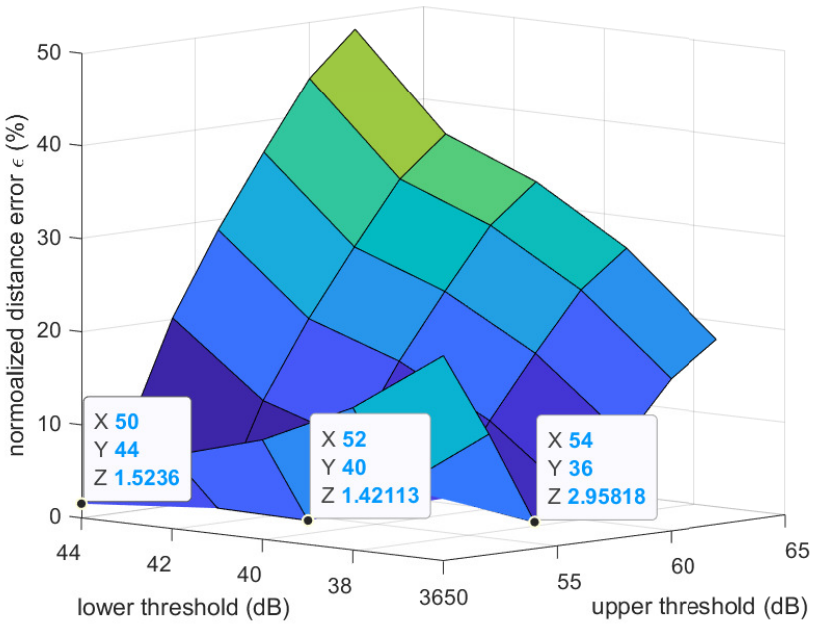

(a) Indoor walking.

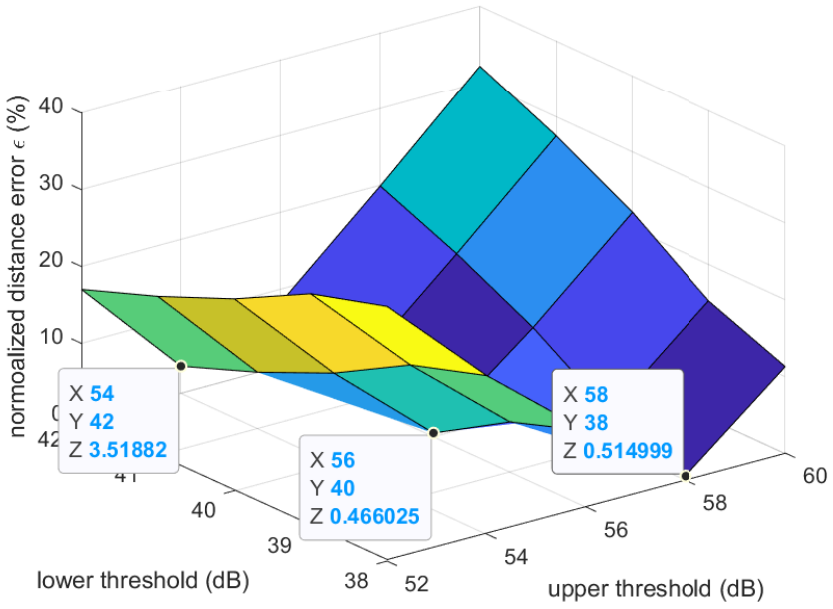

(b) Indoor jogging.

Figure 4.5: Normalised step length estimation errors of the indoor experiments.

and jogging scenarios are (39 dB, 51 dB) and (42 dB, 54 dB), respectively. The average absolute and relative estimation errors for the former case are just 4.81 mm and 0.67%, while they are 10.84 mm and 1.15% for the latter case.

The contour curves of the four experiments are shown in Fig. 4.7. The darker curves

Table 4.1: Estimation of the step length (m) in the indoor walking scenario for different pairs of upper threshold $Th^{(u)}$ (dB) and lower threshold $Th^{(l)}$ (dB). Two values in the brackets of each table cell are the corresponding absolute estimation error (mm) and relative estimation error (%), respectively.

$Th^{(l)}$ \ $Th^{(u)}$	**50**	**52**	**54**	**56**	**58**
36	0.5556 (158.39, 22.18)	0.6206 (93.41, 13.08)	0.6929 (21.12, 2.96)	0.7452 (31.21, 4.40)	0.7896 (75.55, 10.58)
38	0.6040 (109.96, 15.40)	0.6701 (43.86, 6.14)	0.7448 (30.83, 4.32)	0.7997 (85.65, 12.00)	0.8466 (132.56, 18.57)
40	0.6372 (76.83, 10.76)	**0.7039 (10.15, 1.42)**	0.7802 (66.19, 9.27)	0.8368 (122.82, 17.20)	0.8856 (171.60, 24.03)
42	0.6577 (56.30, 7.88)	0.7251 (11.14, 1.56)	0.8029 (88.92, 12.45)	0.8610 (146.98, 20.59)	0.9112 (197.21, 27.62)
44	0.7031 (10.88, 1.52)	0.7746 (60.60, 8.49)	0.8578 (143.82, 20.14)	0.9207 (206.66, 28.94)	0.9755 (261.53, 36.63)

Table 4.2: Estimation of the step length (m), absolute estimation error (mm), and relative error (%) in the indoor jogging scenario for different pairs of upper threshold $Th^{(u)}$ (dB) and lower threshold $Th^{(l)}$ (dB).

$Th^{(l)}$ \ $Th^{(u)}$	**52**	**54**	**56**	**58**	**60**
38	0.6282 (311.28, 33.13)	0.7458 (193.70, 20.62)	0.8461 (93.37, 9.94)	0.9443 (4.81, 0.51)	1.0450 (105.55, 11.23)
39	0.6557 (283.77, 30.20)	0.7758 (163.66, 17.42)	0.8785 (61.03, 6.50)	0.9791 (39.59, 4.21)	1.0825 (143.03, 15.22)
40	0.7050 (234.47, 24.96)	0.8288 (110.70, 11.78)	**0.9351 (4.40, 0.47)**	1.0397 (100.21, 10.67)	1.1477 (208.21, 22.16)
41	0.7450 (194.48, 20.70)	0.8708 (68.73, 7.32)	0.9795 (40.01, 4.26)	1.0870 (147.48, 15.70)	1.1984 (258.86, 27.55)
42	0.7795 (160.00, 17.03)	0.9064 (33.09, 3.52)	1.0170 (77.51, 8.25)	1.1268 (187.30, 19.94)	1.2410 (301.49, 32.09)

are where the better threshold pairs located, which result in the smaller measurement errors. The four pairs of thresholds and the corresponding measurement errors found in Figs. 4.5 – 4.6 are also shown in these contour figures. From Figs. 4.5, 4.7(a), 4.7(b) and Tables 4.1, 4.2, it is noted that the estimation error in the indoor walking scenario is higher than that in the indoor jogging one. This can be explained as follows. In general, one might expect that the error of the walking scenarios is smaller than that of the jogging ones as walking is a slower and more stable activity than jogging. This expectation is confirmed from the experimental results of the outdoor scenarios, where the errors for

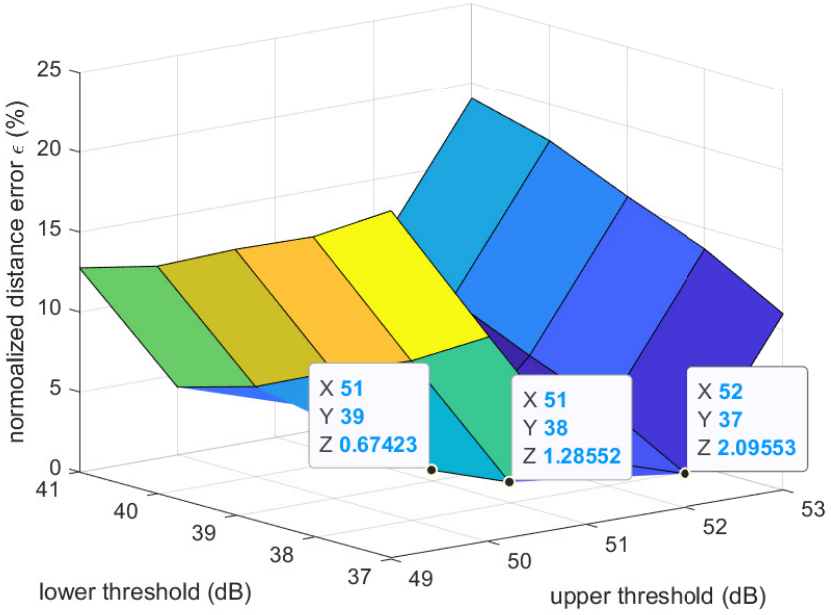

(a) Outdoor walking.

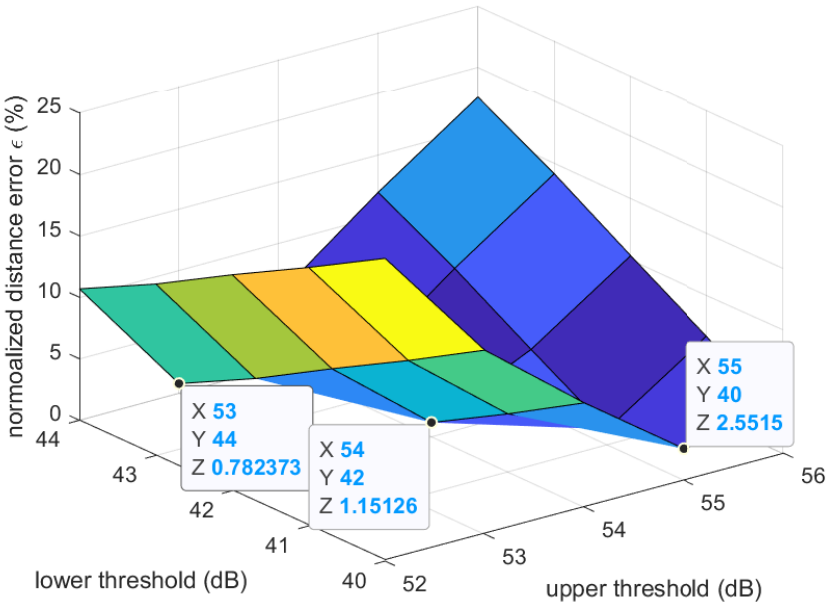

(b) Outdoor jogging

Figure 4.6: Normalised step length estimation errors of the outdoor experiments.

outdoor walking and jogging are 4.81 mm and 10.84 mm, respectively. However, this expectation may not always be the case for an indoor environment since there are more multipath indoors than outdoors. Because walking takes a longer time than jogging to complete a step, when multipath propagation occurs, more affected RSSI (thus path loss)

Table 4.3: Estimation of the step length (m), absolute estimation error (mm), and relative error (%) in the outdoor walking scenario for different pairs of upper threshold $Th^{(u)}$ (dB) and lower threshold $Th^{(l)}$ (dB).

$Th^{(l)}$ \ $Th^{(u)}$	**49**	**50**	**51**	**52**	**53**
37	0.5584 (155.56, 21.79)	0.6225 (91.54, 12.82)	0.6851 (28.93, 4.05)	0.7290 (14.96, 2.10)	0.7925 (78.54, 11.00)
38	0.5798 (134.16, 18.79)	0.6430 (71.02, 9.95)	0.7048 (9.18, 1.29)	0.7484 (34.40, 4.82)	0.8118 (97.79, 13.70)
39	0.5952 (118.81, 16.64)	0.6576 (56.41, 7.90)	**0.7188** **(4.81, 0.67)**	0.7622 (48.15, 6.74)	0.8254 (111.38, 15.60)
40	0.6125 (101.55, 14.22)	0.6740 (40.05, 5.61)	0.7345 (20.46, 2.87)	0.7775 (63.52, 8.90)	0.8406 (126.59, 17.73)
41	0.6229 (91.06, 12.75)	0.6839 (30.07, 4.21)	0.7440 (30.02, 4.21)	0.7869 (72.94, 10.22)	0.8499 (135.95, 19.04)

Table 4.4: Estimation of the step length (m), absolute estimation error (mm), and relative error (%) in the outdoor jogging scenario for different pairs of upper threshold $Th^{(u)}$ (dB) and lower threshold $Th^{(l)}$ (dB).

$Th^{(l)}$ \ $Th^{(u)}$	**52**	**53**	**54**	**55**	**56**
40	0.7082 (231.29, 24.62)	0.7990 (140.54, 14.96)	0.8599 (79.64, 8.48)	0.9155 (24.00, 2.55)	0.9651 (25.58, 2.72)
41	0.7420 (197.45, 21.02)	0.8338 (105.70, 11.25)	0.8952 (44.30, 4.72)	0.9515 (11.98, 1.28)	1.0018 (62.32, 6.63)
42	0.7745 (164.97, 17.56)	0.8669 (72.56, 7.72)	**0.9287** **(10.84, 1.15)**	0.9855 (45.95, 4.89)	1.0365 (96.96, 10.32)
43	0.8085 (130.98, 13.94)	0.9013 (38.16, 4.06)	0.9632 (23.74, 2.53)	1.0205 (80.98, 8.62)	1.0721 (132.64, 14.12)
44	0.8391 (100.41, 10.69)	0.9321 (7.38, 0.79)	0.9941 (54.60, 5.81)	1.0517 (112.21, 11.94)	1.1040 (164.46, 17.51)

values during that step would be recorded to the data set in the walking scenario than in the jogging one. As a result, the histogram of the path loss data set collected for the indoor walking scenario may have some (local) peaks that are distinct from the remaining non-peak values, compared to the indoor jogging case. This phenomenon can be observed in Fig. 4.8(a) (mentioned later in Section 4.5.2), where the density of the path loss value of 46 dB is much more prominent than other non-peak values, while the local peaks in Fig. 4.8(b) are less prominent compared to their surrounding values. This leads to a slightly worse accuracy in average step length estimation in the indoor walking compared to the indoor jogging.

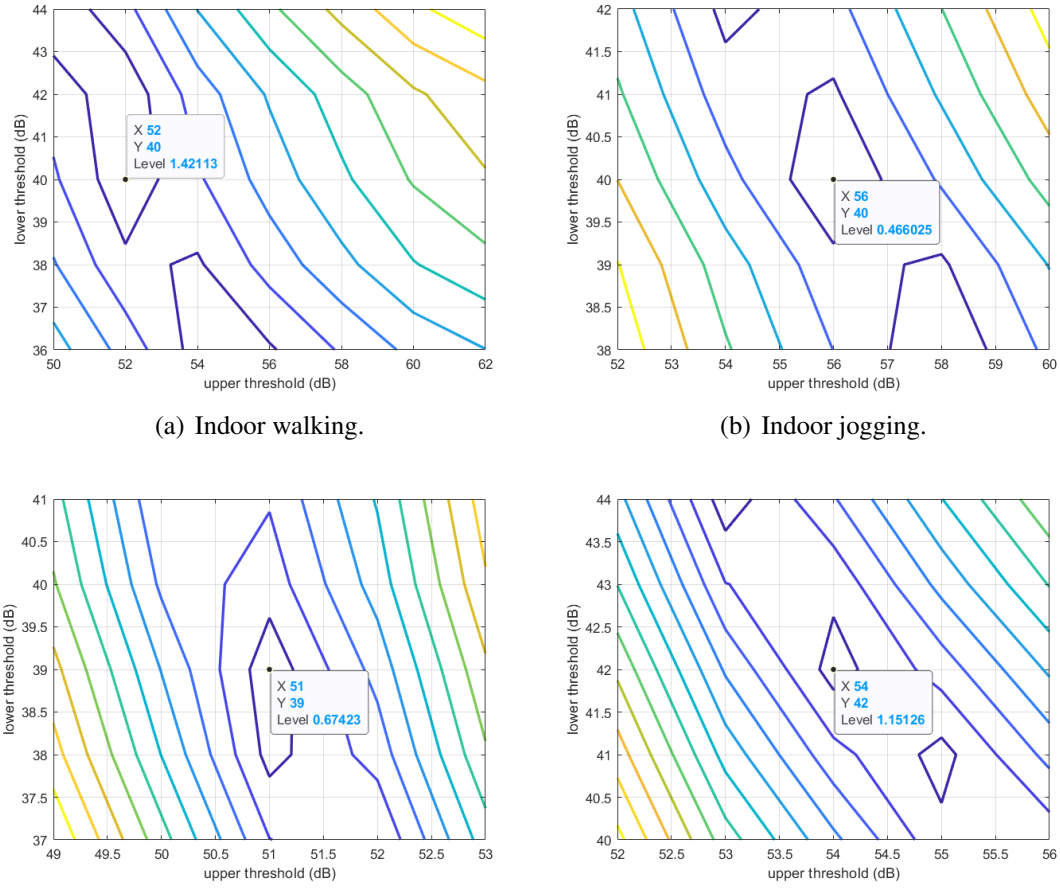

(a) Indoor walking.

(b) Indoor jogging.

(c) Outdoor walking.

(d) Outdoor jogging.

Figure 4.7: The contour curves regarding the normalised estimated step length error of different pairs of upper threshold and lower threshold for different experimental scenarios.

4.5.2 Upper Threshold Analysis

The data analyses mentioned in Section 4.5.1 are critical as they allow us to devise the novel filtering technique, which is detailed below.

In order to formulate the thresholds mathematically, we firstly depict the probability histogram for all the data sets (around 15,000 samples in each data set) collected in each experimental scenario, as shown in Fig. 4.8. The probability histogram of the measured on-ankle path loss is represented by blue bars. It is observed that, as the measured on-ankle path loss increases, its probability has a 'rise-fall-rise-fall' trend. It is noted that the plotted histogram has two humps (or local peaks), which correspond to the half-finished step, where the two feet are about to pass each other, and the fully finished step, when the two feet are most apart from each other, respectively. In order to describe this trend

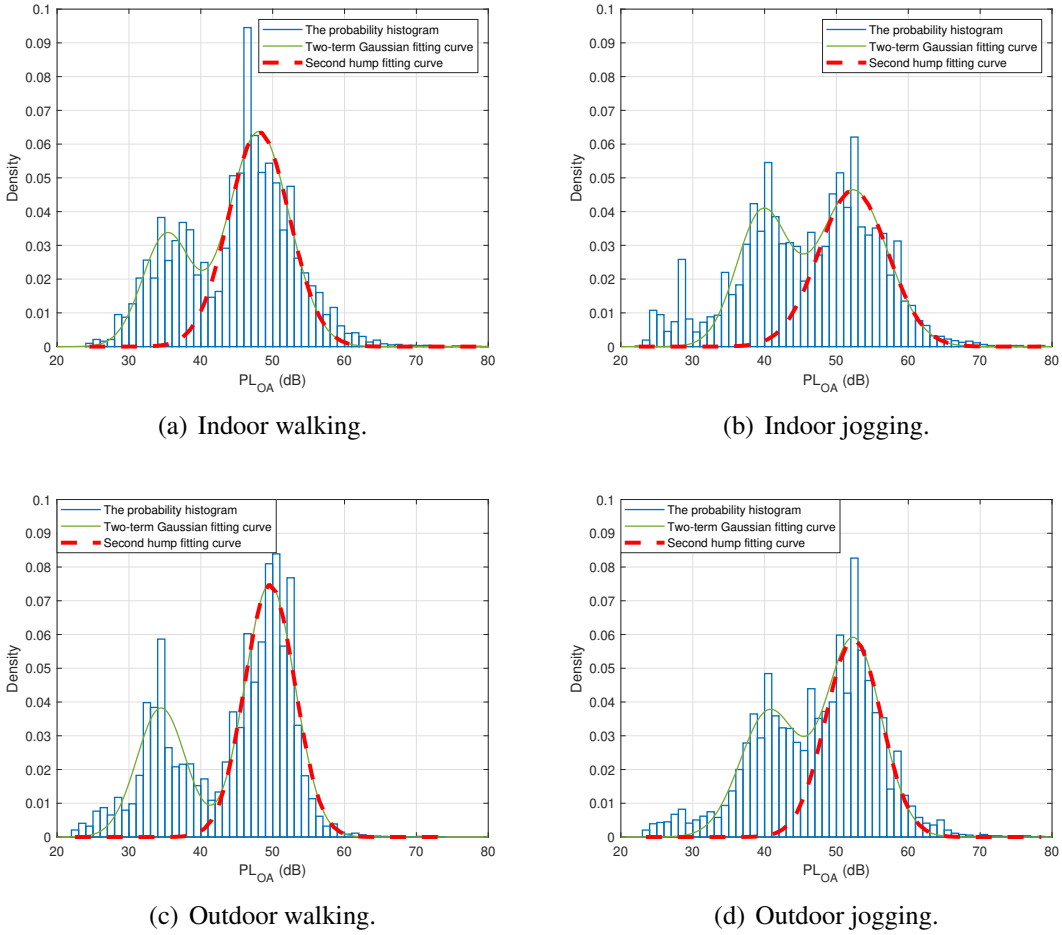

(a) Indoor walking.

(b) Indoor jogging.

(c) Outdoor walking.

(d) Outdoor jogging.

Figure 4.8: The probability histogram, the two-term Gaussian distribution, and the fitting curve of the second hump for the indoor and outdoor experiments.

mathematically, we use the inbuilt application Curving Fitting in Matlab. This application supports different fitting options, allowing users to adjust the resulting Gaussian approximation. The Gaussian curve fitting model in Matlab fits peaks and is written as

$$f(x) = \sum_{i=1}^{n} a_i e^{-}(\frac{x-b_i}{c_1})^2, \tag{4.8}$$

where a is the amplitude, b is the centroid (i.e., location), c relates to the peak width, n is the number of peaks to fit and $1 \leq n \leq 8$. In the application Curve Fitting, the number of peaks is also called the number of terms, which could be specified from 1 to 8. In this thesis, the experimental data follows a two-peak distribution, thus $n = 2$, which means the Gaussian curve fitting model being used here is a two-term Gaussian curve fitting model.

Ideally, the step length is related to the maximum on-ankle path loss. However, due

to the random variations superimposed on the propagation channel, the actual step length may correspond to a non-peak path loss around the peak of the second hump. This means that the pair of the (lower, upper) thresholds should capture a suitable range of the path loss values around the peak of the second hump. The values bigger than the upper threshold or smaller than the lower threshold are considered as outliers in estimating the path loss that corresponds to the step length. To capture the suitable range of the possible path loss values for estimating the step length, intuitively, the upper threshold should be located somewhere at the right slope of the second hump, while the lower threshold lies somewhere at the left slope of the second hump, i.e., in between the first hump and the second hump.

From Fig. 4.8, it is observed that the impact of the first hump on the right slope of the second hump is negligible. Thus, we can extract the second hump and approximate its right slope by the Gaussian distribution

$$f_2(x) = a_2 e^{-(\frac{x-b_2}{c_2})^2}. \tag{4.9}$$

This observation is confirmed in Fig. 4.8(a), where the bell-shaped red dashed curve representing the Gaussian distribution in Eq. (4.9) coincides with the right slope of the second hump of the two-term Gaussian distribution. As a result, we can obtain the mean μ and the standard deviation σ of the second hump based on the above Gaussian distribution in Eq. (4.9) as

$$\mu = b_2, \tag{4.10}$$

$$\sigma = \frac{c_2}{\sqrt{2}}. \tag{4.11}$$

The above observations and analyses hold for all indoor/outdoor walking and indoor/outdoor jogging cases, as shown in Fig. 4.8.

The curve fitting parameters a_2, b_2, c_2, μ, and σ for the second hump in the four scenarios can be found in Table 4.5. Since the path loss, which corresponds to the step length, is a random variable, its upper threshold should be determined as a function of both the mean value μ and the standard deviation value σ of the second term of the two-

Table 4.5: Coefficients for the second hump-fitting equation.

	Indoor Walking	**Indoor Jogging**	**Outdoor Walking**	**Outdoor Jogging**
a_2	0.06369	0.04639	0.07489	0.05866
b_2	48.0900	52.3400	49.6100	52.3900
c_2	5.9990	6.7870	4.9330	5.4610
μ	48.0900	52.3400	49.6100	52.3900
σ	4.2419	4.7991	3.4882	3.8615

Table 4.6: Absolute difference Δ (dB) between the function $\mu+\gamma\sigma$ and the empirical upper threshold (indoor walking: 52 dB; indoor jogging: 56 dB; outdoor walking: 51 dB; outdoor jogging: 54 dB).

	Indoor Walking	**Indoor Jogging**	**Outdoor Walking**	**Outdoor Jogging**
$\mu(\Delta)$	48.0900 (3.9100)	52.3400 (3.6600)	49.6100 (1.3900)	52.3900 (1.6100)
$\mu+0.5\sigma(\Delta)$	50.2110 (1.7890)	54.7396 (1.2604)	**51.3541 (0.3541)**	**54.3208 (0.3208)**
$\mu+\sigma(\Delta)$	**52.3319 (0.3319)**	**57.1391 (1.1391)**	53.0982 (2.0982)	56.2515 (2.2515)
$\mu+1.5\sigma(\Delta)$	54.4529 (2.4529)	59.5387 (3.5387)	54.8422 (3.8422)	58.1823 (4.1823)
$\mu+2\sigma(\Delta)$	56.5738 (4.5738)	61.9383 (5.9383)	56.5863 (5.5863)	60.1130 (6.1130)

term Gaussian distribution in Eq. (4.9). This philosophy is similar to the well-known concept of calculating the retransmission timeout (RTO) on the Internet where the RTO is the function of both the mean value of the round-trip time (RTT) and its deviation value.

We will find the upper threshold in the form of $\mu+\gamma\sigma$ where γ is a certain coefficient for all four walking and jogging scenarios. Table 4.6 presents the values of function $\mu+\gamma\sigma$ ($\gamma=0$, 0.5, 1, 1.5, 2), and the corresponding difference, denoted as Δ (dB), between these values and the upper thresholds, which have been worked out empirically from the actual measured data in Section 4.5.1. Table 4.6 clearly shows that the empirical upper thresholds in the indoor walking and jogging scenarios are both very well approximated by $\mu+\sigma$ with the differences Δ of only 0.3319 dB and 1.1391 dB, respectively. This finding makes sense because the upper threshold is equal to the mean path loss value μ plus a margin, which is equal to the standard deviation σ in this case.

Similarly, the empirical upper thresholds in the outdoor walking and jogging scenarios are both close to $\mu+0.5\sigma$ with the difference Δ of merely 0.3541 dB and 0.3208 dB,

respectively. The variations of the upper threshold in the two indoor cases are higher than those in the outdoor scenarios due to the fact that there are more multipath indoors than outdoors; thus, the actual path loss that corresponds to the step lengths might vary more widely around its mean value. As a result, the upper threshold could be formulated as

$$Th^{(u)} = \mu + \gamma\sigma, \tag{4.12}$$

where γ is 1 and 0.5 for indoor and outdoor scenarios, respectively.

4.5.3 Lower Threshold Analysis

As mentioned in Section 4.5.1, the lower threshold is located between the first hump and the second hump of the two-term Gaussian distribution, which means its value would be affected by both humps. Consequently, it is impossible to analyse the lower threshold based on a single hump as for the upper bound mentioned above. Thus, other techniques should be used to analyse the lower threshold. One of the possible techniques is based on the CDF or the survival function. The survival function is complementary to the CDF. It indicates the probability of the path loss value greater than or equal to a certain value. Fig. 4.9 depicts the probability histogram, the CDF (the red curves), and the survival function (the bold green curves) of the measured path loss data for all four scenarios together with the lower thresholds (the black dashed lines), which have empirically been found to be 39 dB and 42 dB in the outdoor walking and jogging cases, respectively, and 40 dB in the indoor cases, as detailed in Section 4.5.1.

Fig. 4.9 reveals an interesting fact that the intersections between the empirical lower thresholds and the survival curves are around 0.68 in all four cases. In other words, the measured path loss value is bigger than or at least equal to the value of the lower threshold 68% of the time in all four scenarios. Path loss values between the lower threshold and the upper one should be considered as the potential path losses corresponding to the step length. Based on the above empirical measurements and statistical analyses, we deduce that the lower threshold can be numerically found as the corresponding path loss value when the survival rate reaches 0.68.

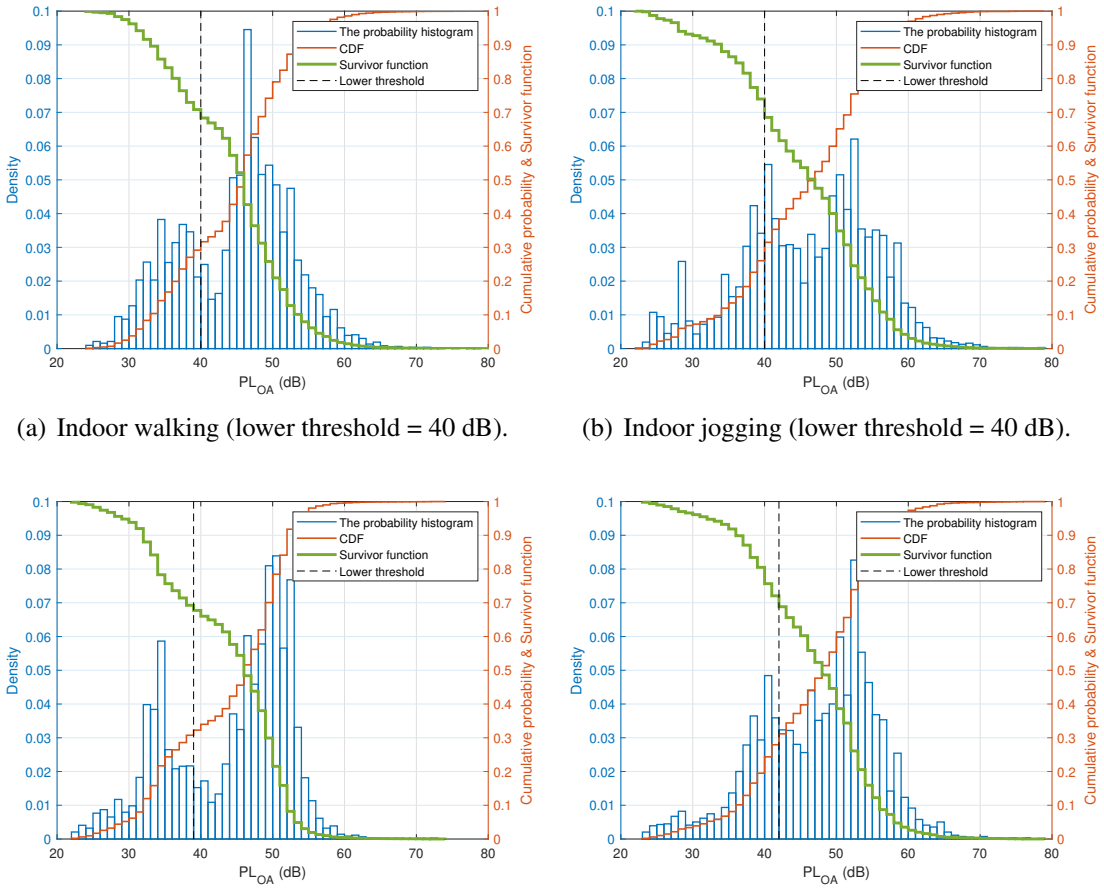

(a) Indoor walking (lower threshold = 40 dB).

(b) Indoor jogging (lower threshold = 40 dB).

(c) Outdoor walking (lower threshold = 39 dB).

(d) Outdoor jogging (lower threshold = 42 dB).

Figure 4.9: The probability histogram, the CDF, and the survivor function with respect to the lower threshold for the indoor and outdoor experiments.

4.6 Chapter Summary

This chapter estimates the human step length in daily activities based on our developed wearable transceivers and the RSSI method. We conduct experiments for both walking and jogging activities in both indoor and outdoor environments. By analysing the statistical properties of the collected data sets, for the first time, we propose a filtering method to set up the lower and upper thresholds in order to eliminate the path loss outliers. The resulting range of path loss values between the two thresholds is used to estimate the step length. Mathematically, the upper threshold for an indoor environment is $\mu + \sigma$, while this value for an outdoor scenario is $\mu + 0.5\sigma$. The lower threshold relates to the survival function of the experimental data sets. This threshold is found numerically to be the path loss value where the survival rate is around 0.68 for both the indoor and outdoor envi-

ronments and for both the walking and jogging activities. Our experiments show that the step length can be accurately estimated with errors of only 10.15 mm and 4.40 mm for the indoor walking and jogging activities and errors of 4.81 mm and 10.84 mm for the outdoor walking and jogging activities, respectively.

Observations from our experiments in this chapter indicate that the proposed system along with the proposed filtering technique can estimate the average human step length with a sub-centimetre error.

A limitation of this chapter is that we need to collect the data set for the whole intended period of time, then proceed to the offline data processing phase, rather than processing data to estimate the step length and updating this estimation in a continuous manner while the person under test is moving. Overcoming this limitation is the motivation for our work in the next chapter. More specifically, to guarantee both accuracy and efficiency, instead of waiting for the whole data set to be collected, we may apply the weighted moving average algorithm to continuously estimate the average step length and keep updating the step length over a certain period of time. In this way, the dynamic characteristics of human daily activities will be captured more accurately than the simple averaging method.

Chapter 5

Real-Time Step Length Estimation in Indoor and Outdoor Scenarios

5.1 Introduction

As presented in Chapter 4, human step length is estimated based on wireless channel properties and the RSSI method. The path loss between two ankles of the person under test could be converted from the RSSI, which is measured using our developed wearable transceivers with embedded micro-controllers in both walking and jogging activities for both indoor and outdoor scenarios. For short, we call it on-ankle path loss. The histogram of the on-ankle path loss has two humps, where the second one is related to the maximum path loss, which is corresponding to the step length. In addition, the histogram could be well approximated by a two-term Gaussian fitting curve model. Based on the histogram of the experimental data and the two-term Gaussian fitting curve, a novel filtering technique has been proposed to filter out the path loss outliers, which contributes to ranging the boundaries of the path loss values that are used for the step length estimation. In particular, the upper threshold is found to be on the right side of the second Gaussian hump, and its value is a function of the mean value and the standard deviation of the second Gaussian hump. Meanwhile, the lower threshold lies on the left side of the second hump and is determined at the point where the survival rate of the measured data falls to 0.68, i.e., the CDF approaches 0.32.

In previous chapters, we propose the step length measurement technique which can

overcome the limitations on health-concerning, space-confined, shadowing sensitivity, and daily usage of the aforementioned existing methods. Our technique works based on our developed RF wearable transceivers, our experimental path loss model, and our proposed data filtering method. The results of our previous work show that the proposed system along with the proposed techniques in Chapters 3 and 4 could estimate the average human step length with a sub-centimetre error. However, a limitation of those techniques is that we need to collect the data set for the whole intended period and then proceed to the offline data processing phase, rather than processing data to estimate the step length and constantly updating this estimation while the person under test is moving.

Overcoming this limitation is the main motivation of the work in this chapter. More specifically, to guarantee both accuracy and efficiency of the step length estimation, and to simulate real-time processing, we propose a novel EWMA technique to continuously estimate the average step length and keep updating this estimation over a shorter period of time. Thereby, the dynamic essence of human activities could be captured more accurately than the simple average used in our previous techniques. Real-time estimation of human step length is important, especially for life-critical applications such as fall detection and non-GPS localisation for soldiers on battlefields. The problem at hand is to accurately estimate the human walking step length in real-time so that individuals' walking patterns could be tracked and timely updated.

Estimating human step length in real-time poses some challenges. The first challenge is the accuracy of step length estimation. If less data is to be processed each time to output an estimation of step length, there might be some concerns about data quality and thus the estimation accuracy. Another challenge is the time required to generate a real-time output. Ideally, with less data being processed, less time is required. However, the real-time estimation algorithm is more complicated, thus there will be an increase in the processing time of the algorithm. Because of these two challenges, the proposed real-time estimation algorithm must have a reasonable compromise between the complexity and the accuracy, and the overall processing time must be evaluated.

This chapter is experimentally based, and data sets have been collected from both in-

doors and outdoors. With the increased size of the collected data sets, we assume that a sliding time window could be an effective adjustment to the proposed filtering technique. By employing the EWMA algorithm to eliminate the path loss outliers in each period of time, the human walking step length could be updated periodically.

This chapter makes the following contributions.

- The measurement is refined in terms of significantly expanding the size of data sets, so that the estimation of step length could be more realistic and better reflect the daily activities, including indoor walking and outdoor walking situations.
- A novel EWMA algorithm is proposed to determine the threshold pair of the path loss and to update the estimated step length for each segment (or time window) of the data set. Though the data is collected offline, the proposed EWMA algorithm provides a perspective to simulate the step length estimation process in real-time.
- The optimal upper threshold for updating the step length estimation for both indoor and outdoor walking scenarios is examined.
- The step length estimation results show that the accuracy of the proposed EWMA algorithm for indoor walking has a centimetre-level error, which is close to the estimations in our previous chapters. Interestingly, for outdoor activities, the proposed technique could further minimise the error to only a few millimetres, which is as small as 0.30% of the real step length.
- The processing time of the proposed EWMA algorithm is analysed in comparison with that of our measurement technique mentioned previously in Chapter 4. Our experiments show that the proposed EWMA algorithm could save up to 53.96% and 60% of the time required to estimate a step length for indoor and outdoor walking scenarios, respectively, while it can still provide comparable accuracy, compared to our previous technique.

The rest of this chapter is organised as follows. Section 5.2 provides an overview of moving average algorithms. Section 5.3 presents the experimental setups, including

hardware and software. Section 5.4 introduces the experimental system model and the proposed EWMA method. The experimental results containing analysis and evaluation are detailed in Section 5.5, for both indoor and outdoor environments. Lastly, Section 5.6 concludes this chapter.

5.2 Heuristic Algorithm: Moving Average

Moving average is a favoured tool in statistics for calculating and analysing data by creating a series of averages of different subsets of the full data set. There are several methods, including simple moving average (SMA), weighted moving average (WMA), and exponential moving average (EMA).

The SMA is the unweighted mean of a numbered data stream. The SMA of a data set containing n points is calculated as

$$SMA = \frac{1}{n}\sum_{i=1}^{n} p_i, \tag{5.1}$$

where p_i is the i-th data point, and every point contributes the same importance to the outcome. SMA was the strategy that we utilised in Chapter 4 to estimate the step length over a data set. Statistically, SMA is straightforward and relatively accurate when data points do not experience much fluctuation, yet the key limitation is that all data points must be included in the assessment even for those out-of-date ones.

The basic idea of the WMA is as follows. The weighted average is an average that has multiplying factors to give different weights to data at different positions in the sample time window. Mathematically, it is calculated by multiplying the value of given data by its associated weighting and totalling the values. In general, WMA assigns a heavier weight to more current data points and less to the past ones. This is because the recent data are more relevant than the data points in the past. The WMA for a time window of n data

points can be expressed as

$$WMA = \frac{q_n p_n + q_{n-1} p_{n-1} + ... + q_2 p_2 + q_1 p_1}{\frac{n(n+1)}{2}}, \\ = \frac{\sum_{i=1}^{n} q_i p_i}{\frac{n(n+1)}{2}}, \tag{5.2}$$

where q_i is the weight of each data point p_i, and $\sum_{i=1}^{n} q_i = 1$.

An EMA is also known as an EWMA. The EWMA for a series Y could be calculated recursively as

$$EWMA_t = \begin{cases} Y_0, & t = 0 \\ qY_t + (1-q)EWMA_{t-1}, & t > 0 \end{cases} \tag{5.3}$$

where the coefficient q represents the degree of weighting. It is a constant smoothing factor between 0 and 1. The effect of old data samples in Eq. (5.3) reduces exponentially fast. A higher q discounts the past observations faster. Y_t is the value at a time period t, and $EWMA_t$ is the value of the exponential weighted moving average at the time period t.

Though the basic smoothing provided by the SMA may be effective for a finite number of data, it is concerning that the effects of lags in data may reduce the responsiveness of the moving average indicator. The WMA and EWMA are more responsive to the change of data as they rely more heavily on the freshest data and place less value on older ones. This suggests that EWMA might be a better approach to estimate the step length in a daily human activity. As a result, this chapter proposes a novel EWMA algorithm to estimate the step length in both indoor and outdoor walking scenarios. It is worth noting that the pure EWMA technique already exists, but has not been used in step length estimations. Thus, this chapter is the first work that uses the EWMA technique to estimate step length. In addition, apart from updating the mean value μ and the standard deviation value σ in each time window as in the pure EWMA technique, the upper threshold of our data filtering technique is found to be in the form of $\mu + \gamma\sigma$. To estimate the human step length accurately, the optimal value of γ also needs to be explored. The whole process of estimating μ, σ, γ, and thus, the upper threshold of the corresponding time window is called our novel EWMA algorithm.

5.3 Experimental Setup

In this chapter, the experiments are carried out by deploying the same hardware, as well as software and under the same environments as in Chapter 4. This means that two Arduino UNO microprocessors are programmed by Arduino IDE as a transmitter (coordinator) and a receiver (end device), respectively. XBee-PRO S2C wireless transceivers are configured by XCTU, including destination and source addresses, interface data rate and power level. Signal will be transmitted with the power of $P_0 = 0$ dBm, at a rate of 9600 bps, from the coordinator to the end device. The data samples are received and stored in a micro SD card, then imported to and analysed in Matlab.

After assembling the transceiver hardware, the equipment will be attached to the medial side of human ankles at the same height h as illustrated in Fig. 3.3. The distance between the two antennas of the transceivers in Fig. 3.3 is defined as the real step length d_0.

The indoor experiments are conducted along a corridor in one of the university buildings, while the outdoor ones are performed on a pavement next to a car park, which can be considered as an open area as shown in Fig. 4.4. To improve the data reliability, unlike previous chapters, more data is collected for the work in this chapter. In the previous chapter, each data set contains ten separate experiments. One experiment only records the RSSI of an one-way direction walking or jogging. In this section, we have significantly increased the size of each data set by prolonging the experimental procedure in terms of time and distance.

With the purpose of making the path of the experiment identifiable and improving the reliability of the work, the route is traced with conspicuous cords stuck on the ground. As shown in Fig. 5.1, the path has the shape of a rectangle, with two semi-circles on its left and right sides with the radius of $r = 0.96$ m. The length of the long edge of the rectangle is $l = 32.53$ m. The person under test is instructed to walk along the marked route. There are three remarks in the experimental procedure. First, in order to collect a data set with continuous and abundant samples, the subject under test is required to walk along the path for twenty rounds in each experiment session. The total number of walking steps is counted to calculate the average walking step length d_{0w}, which will be used as a ground

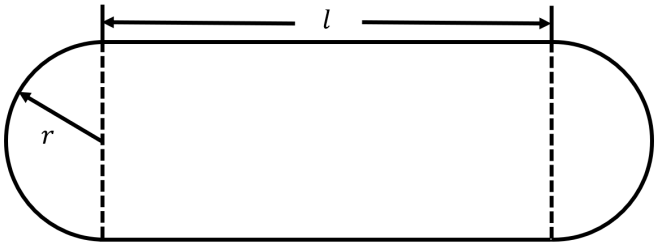

Figure 5.1: Schematic diagram of the experiment route.

truth. Second, the participant performs the walk at a normal and steady pace at all times, especially during the arc areas, and does not make sharp turns at the semi-circle portions to assure that the stride would not experience significant fluctuation. Third, new or newly charged rechargeable batteries are used before commencing a new set of experiments to guarantee the completeness of the data collection and the data reliability. Considering the time duration of each experiment, and two AAA batteries powering the hardware, the electricity may be extensively drained and consumed after each set of experiments.

5.4 System Model

The system model in this chapter is the same as in Chapters 3 and 4. As stated in our previous works, the transmitter and the receiver are fastened to the inner side of the ankles of the participant, thereby, an LOS path exists between the equipment throughout the time of the experiment. Moreover, no body tissue or other obstacles would appear between the transceivers, thus, the space between two ankles, could be regarded as a nearly free space. An experimental path loss model which measures the path loss between human ankles in daily activities has been proposed in Chapter 3. It could be described as a modified free space path loss model with a correction factor ΔPL

$$PL_{OA}(\text{dB}) = PL_{FS} + \Delta PL, \tag{5.4}$$

where PL_{FS} (dB) is the free space path loss and ΔPL (dB) is the correction factor, which consists of the hardware non-linearity, multipath propagation, insertion loss, and mismatch loss. From the observations in Chapter 3, the correction factor is empirically found

as 10 dB [129]. Therefore, Eq. (5.4) can be written as

$$PL_{OA}(\text{dB}) = PL_{FS} + 10. \tag{5.5}$$

It is noted that the free space path loss is numerically defined as

$$PL_{FS}(\text{dB}) = 20\log_{10}\left(\frac{4\pi d}{\lambda}\right), \tag{5.6}$$

where d (m) is the distance between the two antennas and λ (m) is the signal wavelength. From Eqs. (5.5) and (5.6), this distance could be estimated as

$$d = \frac{\lambda}{4\pi} 10^{\left(\frac{PL_{OA}(\text{dB})-10}{20}\right)}. \tag{5.7}$$

Seeing from the end device, the on-ankle path loss can be calculated as

$$PL_{OA}(\text{dB}) = P_t + RSSI, \tag{5.8}$$

where P_t (dB) is the transmitted power, and RSSI is presented as a positive decibel value. From Eqs. (5.7) and (5.8), the distance between the two transceivers is

$$d = \frac{\lambda}{4\pi} 10^{\left(\frac{P_t(\text{dB})+RSSI(\text{dB})-10}{20}\right)}. \tag{5.9}$$

For the purpose of improving the accuracy of the step length estimation, a filtering technique has been proposed in Chapter 4 to remove path loss outliers by establishing a pair of path loss thresholds. Any path loss that is greater than the upper threshold or smaller than the lower threshold would be abandoned. The path loss values within the two thresholds are used to estimate the step length. The lower threshold is found to correspond to the point at which the survival rate of the data set drops to 0.68 [134]. The upper threshold is found from the second hump of the PDF of the measured data [134]. This hump could be approximated as a Gaussian distribution

$$f_2(x) = a_2 e^{-(\frac{x-b_2}{c_2})^2}, \tag{5.10}$$

where a_2, b_2 and c_2 are all curve fitting coefficients. These coefficients have relation with the mean μ and the standard deviation σ of the second hump based on the above Gaussian distribution in Eq. (5.10) as follows

$$\mu = b_2, \tag{5.11}$$

$$\sigma = \frac{c_2}{\sqrt{2}}. \tag{5.12}$$

As mentioned in Eq. (4.12) of Chapter 4, the corresponding upper threshold is found as $\mu + \gamma\sigma$, where γ is the key factor in specifying the upper threshold.

The aim of this chapter is to estimate the walking step length and update the estimation after each certain time period. This time period is the duration of each sliding time window. Thus, the collected RSSI data set is truncated into different time windows $tw_i, (i = 1, 2, ..., k)$. The upper threshold of each time window tw_i is determined as

$$Th_i^{(u)} = \mu_i + \gamma\sigma_i. \tag{5.13}$$

Meanwhile the lower threshold is fully dependent on the current time window sample

$$Th_i^{(l)} = Th_{sample}^{(l)}, \tag{5.14}$$

where $Th_{sample}^{(l)}$ is the lower threshold value calculated for the current time window. $Th_{sample}^{(l)}$ is determined at the point where the survival rate of the data in this time window falls to 0.68. We propose here an EWMA algorithm, where the mean μ_i and standard deviation σ_i in Eq. (5.13) for the time window tw_i are calculated recursively as

$$\mu_i = \begin{cases} \mu_{sample}, & i = 1 \\ \alpha\mu_{i-1} + (1-\alpha)\mu_{sample}, & i \geq 2 \end{cases} \tag{5.15}$$

$$\sigma_i = \begin{cases} \sigma_{sample}, & i = 1 \\ \beta\sigma_{i-1} + (1-\beta)\sigma_{sample}, & i \geq 2 \end{cases} \tag{5.16}$$

where the subscript $sample$ indicates the corresponding value for the current time window. In the following analyses, the influence of γ will be explored in different environments.

Table 5.1: Real walking step length and the number of time windows in the data sets.

Date set	Description	Real walking step length (m)	Number of time windows
1	Indoor walking 1	0.6627	12
2	Indoor walking 2	0.6844	11
3	Outdoor walking 1	0.6633	15
4	Outdoor walking 2	0.6561	11

5.5 Experimental Results

In this section, human daily walking activities are examined in both indoor and outdoor environments. The data sets of path loss values are collected to estimate the participant's walking step length in both scenarios. Besides, the influence of the key parameter, γ, on the upper threshold in Eq. (5.13) is investigated, assuming that the weights α and β in Eqs. (5.15) and (5.16) are $\alpha = 0.125$ and $\beta = 0.25$, respectively. The values $\alpha = 0.125$ and $\beta = 0.25$ were chosen for illustration purposes. They had small values to have more impact on the current sample values of μ and σ, denoted as μ_{sample} and σ_{sample}, on the average values of μ and σ. The rationale was that the current data samples were more significant than the old samples in the human step length estimation. Recall that μ_{sample} and σ_{sample} are the mean and standard deviation, respectively, which could be found from the second Gaussian hump of the current time window.

In each indoor or outdoor scenario, two data sets are collected for the completeness of the experiments. Hence, there are four data sets in total, and the real walking step length of each data set is shown in Table 5.1.

Considering a time window size of 60 seconds, corresponding to 3000 samples, each of these data sets has around 11 or 12 time windows. This means, compared to the experimental data sets in Chapter 4, the data sets in this section contain twice the amount of data. In Table 5.1, the range of the real walking step length of the person under test was from 0.66 m to 0.68 m, which lies in our range of interest (i.e., 0.6 m - 0.8 m). Though the measurements are carried out in the same scenarios, there is still a slight discrepancy of the total walking time in different measurement trials. Therefore, the number of collected data samples varied, resulting in the different numbers of time windows among different experiments. Considering a time window size of 60 s, corresponding to 3000 samples per

time window, each of these data sets had 11 to 15 time windows. It is noted that, due to the slight difference of total walking time and the difference of the hardware synchronisation time, the number of collected data samples, thus the number of time windows, may vary among different experiments. Moreover, compared to the experimental data sets in Chapter 4, the data sets in this chapter contained twice the amount of data.

The benefit of increasing the size of the data sets is twofold. Firstly, it overcomes the limitation of the data samples in the previous experiments (around 15,000 samples in each experimental scenario), which may not be sufficient for applying the sliding time window and EWMA. Secondly, the reliability of the collected data is likely to be improved with a more extensive data set.

5.5.1 Indoor Walking

In our previous study [134], the histogram of the on-ankle path loss can be well approximated by a two-term Gaussian fitting curve model, whose second hump is closely related to the maximum path loss, which helps estimate the step length. An innovative filtering technique has been proposed in Chapter 4 to filter out the path loss outliers by setting a pair of thresholds, namely the lower and upper thresholds. Recalling from the previous chapter, the lower threshold could be numerically found as the corresponding path loss value when the survival rate reaches 0.68. Meanwhile, the upper threshold was calculated as (cf. Eq. (4.12))

$$Th^{(u)} = \mu + \sigma, \tag{5.17}$$

which indicates $\gamma = 1$ in Chapter 4. In this chapter, along with the proposed EWMA algorithm, we also investigate the optimal range of γ to obtain a more accurate step length estimation following Eq. (5.13).

Fig. 5.2 compares the absolute error between the real step length and the averaged estimation, calculated for the last time window (tw_{12}), with respect to the variation of γ from 0 to 1 for the indoor walking case based on the data set 1. The marker on each error bar in Fig. 5.2 represents the average estimated absolute error, while the two caps present the variation of the estimated absolute error around the average value, i.e., the deviation of

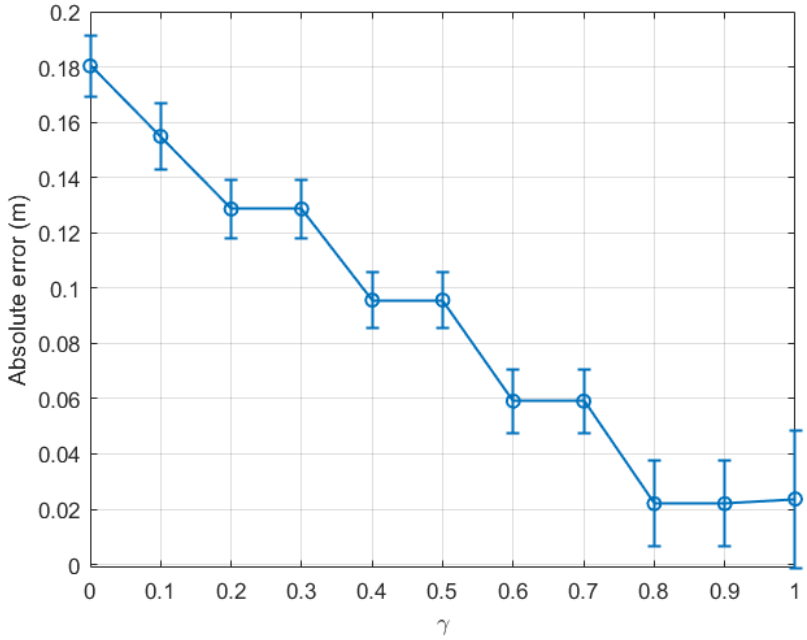

Figure 5.2: Indoor walking (data set 1): absolute error of the last time window (tw_{12}) with respect to $\gamma \in [0,1]$.

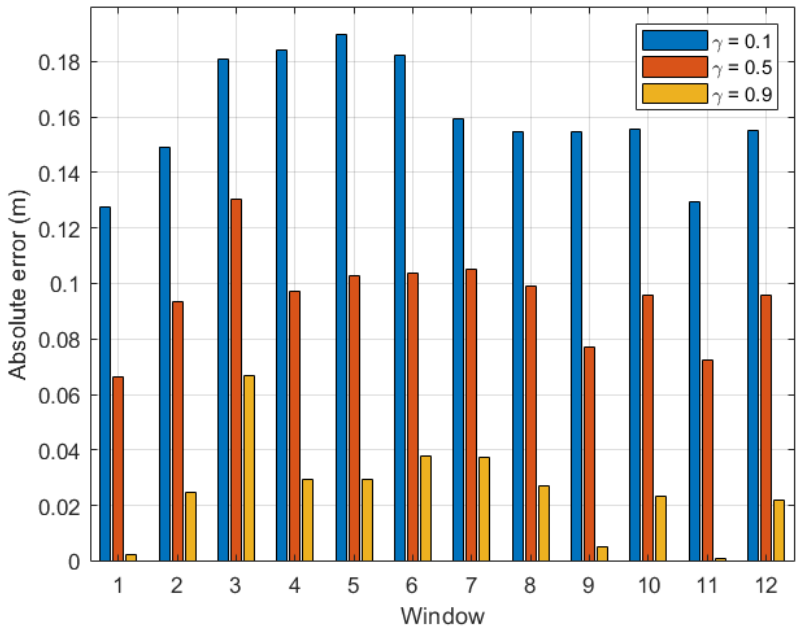

Figure 5.3: Indoor walking (data set 1): absolute error with respect to time windows $tw_i, i \in [1,12]$.

the estimation. The result shows that, when only the last time window tw_{12} is considered, the absolute error (AE) drops constantly from 0.18 m at $\gamma = 0$ to nearly 0.02 m at $\gamma = 0.8$. This error remains stable at $\gamma = 0.9$ and then slightly rises at $\gamma = 1$.

For more comprehension, Fig. 5.3 plots the absolute error calculated for each time win-

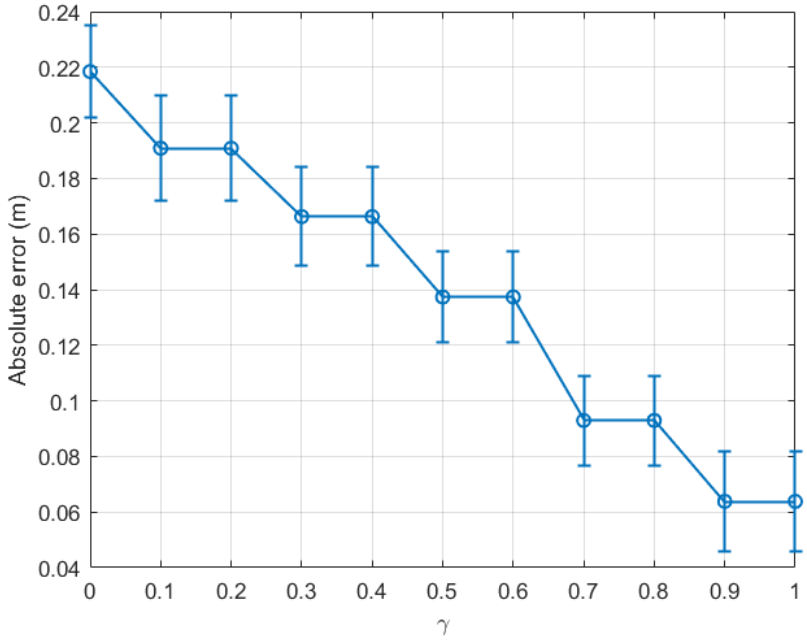

Figure 5.4: Indoor walking (data set 2): absolute error of the last time window (tw_{11}) with respect to $\gamma \in [0,1]$.

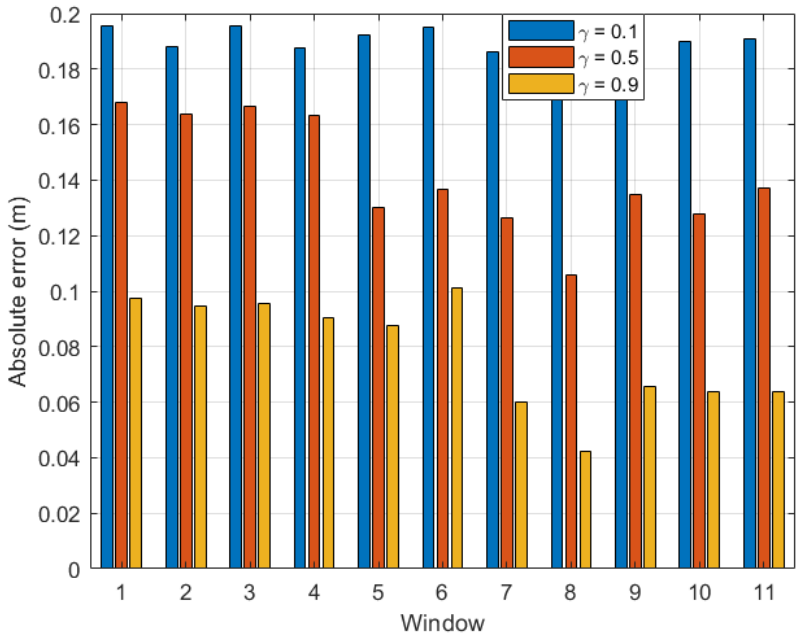

Figure 5.5: Indoor walking (data set 2): absolute error with respect to time windows $tw_i, i \in [1,11]$.

dow with $\gamma = 0.1$, 0.5 and 0.9 in a bar diagram. The same tendency as shown in Fig. 5.2 can be seen in Fig. 5.3. For instance, at the last time window, $AE^{(tw_{12})}_{(\gamma=0.1)} > AE^{(tw_{12})}_{(\gamma=0.5)} > AE^{(tw_{12})}_{(\gamma=0.9)}$.

From the above experiment, it is clear that the optimal γ locates between 0.8 and 0.9

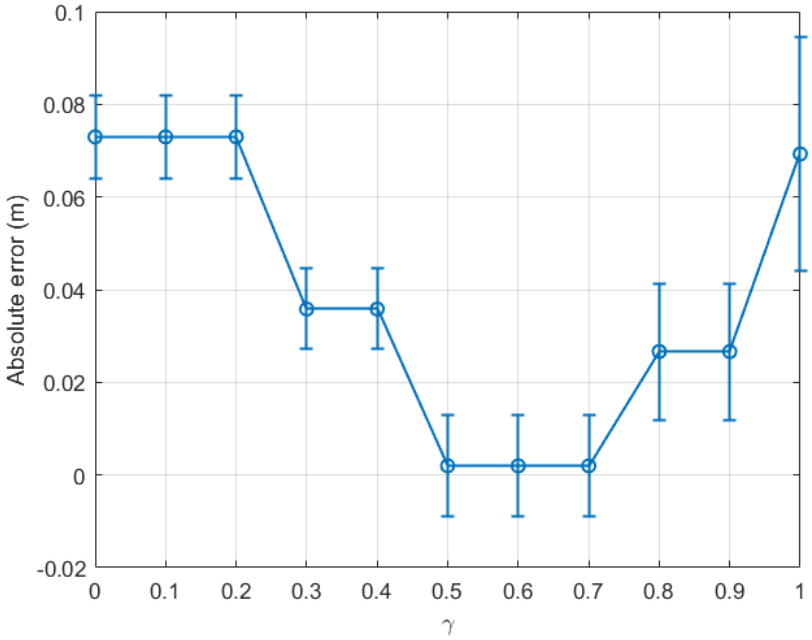

Figure 5.6: Outdoor walking (data set 3): absolute error of the last time window (tw_{15}) with respect to $\gamma \in [0,1]$.

for indoor environments. For completeness, we plot a graph similar to Fig. 5.2 for the data set 2 for the same indoor walking scenario as shown in Fig. 5.4. Clearly, the absolute error calculated for the last time window decreases consistently with γ, and the optimal γ is within the range [0.9, 1.0]. Further, it is confirmed in Fig. 5.5 that the optimal γ of this data set is 0.9 and the absolute error could be as small as 0.064 m.

As a result, the optimal γ for calculating the upper threshold for an indoor walking activity in Eq. (5.13) is found to be 0.9, which is relatively close to the sub-optimal value $\gamma = 1$ chosen in Chapter 4. The above estimation error could be as small as 3.02% of the real step length.

5.5.2 Outdoor Walking

Regarding the outdoor case, it is predicted based on Chapter 4 that the optimal γ could be around 0.5, because the multipath effect is less serious than the indoor case. This is confirmed by our experiments as detailed below.

Fig. 5.6 presents the absolute error of the step length estimation with respect to γ for the data set 3. From Fig. 5.6, at the last time window tw_{15} of the data set 3, it is observed

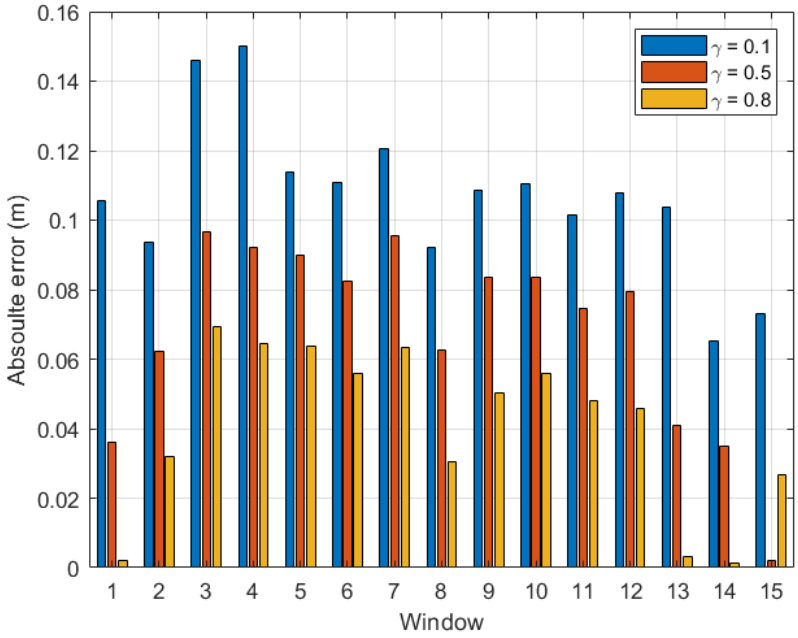

Figure 5.7: Outdoor walking (data set 3): absolute error with respect to time windows $tw_i, i \in [1, 15]$.

that the estimation error reduces to only 0.002 m when γ is within the range [0.5, 0.7]. Fig. 5.7 depicts the absolute error of the step length estimation with respect to the sliding time windows for data set 3. From this figure, it is clear that the best γ for the outdoor walking scenario is around 0.5, which turns out to be the same value chosen in Chapter 4.

For completeness, Figs. 5.8 and 5.9 present the estimation error of another data set of outdoor experiments, namely the data set 4. From Fig. 5.8, it is noticed that the line graph shares the same trend as that for the data set 3 as presented in Fig. 5.6. From the two figures, the smallest absolute error of the last time window tw_{11} is 0.0155 m when γ is within the range [0.4, 0.5]. This error is around 0.30% of the real step length.

In order to confirm the validity, accuracy, repeatability, and reliability of our proposed method, two more experiments have been conducted to collect bigger data sets than the four data sets 1 – 4 mentioned previously in our analysis, for indoor and outdoor walking scenarios, respectively. The two newly collected data sets, namely data sets 5 and 6, contained 18 time windows each. The absolute step length measurement errors calculated based on the last time window tw_{18} for data sets 5 and 6 are shown in Figs. 5.10 and 5.11 for the indoor and outdoor walking scenarios, respectively.

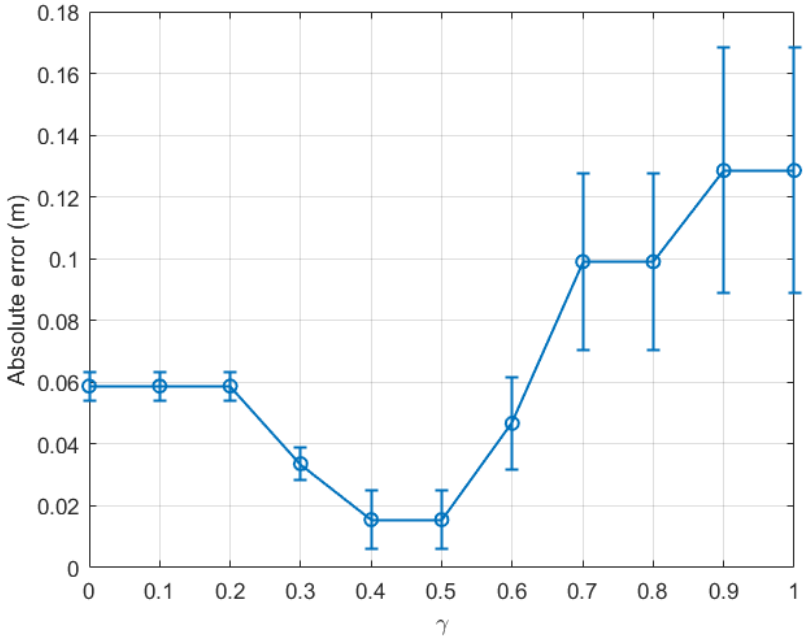

Figure 5.8: Outdoor walking (data set 4): absolute error of the last time window (tw_{11}) with respect to $\gamma \in [0,1]$.

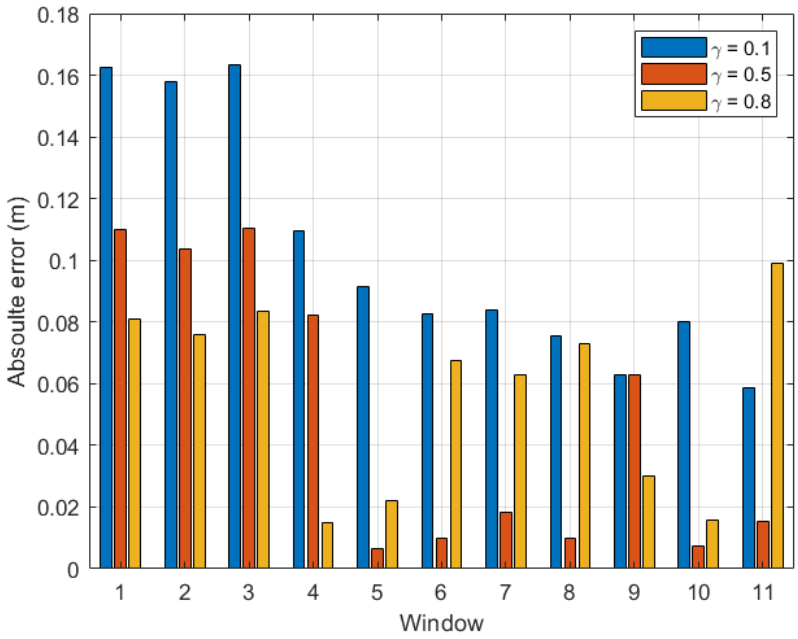

Figure 5.9: Outdoor walking (data set 4): absolute error with respect to time windows $tw_i, i \in [1,11]$.

Figs. 5.10 and 5.11 show that the new results agree with those mentioned previously in this chapter. Let us consider Fig. 5.10 for illustration. The real step length for data set 5 is 0.6679 m. As shown in this figure, when γ varied, the smallest absolute step length measurement error of 0.0127 m, i.e., 1.90% of the real step length, could be achieved when γ

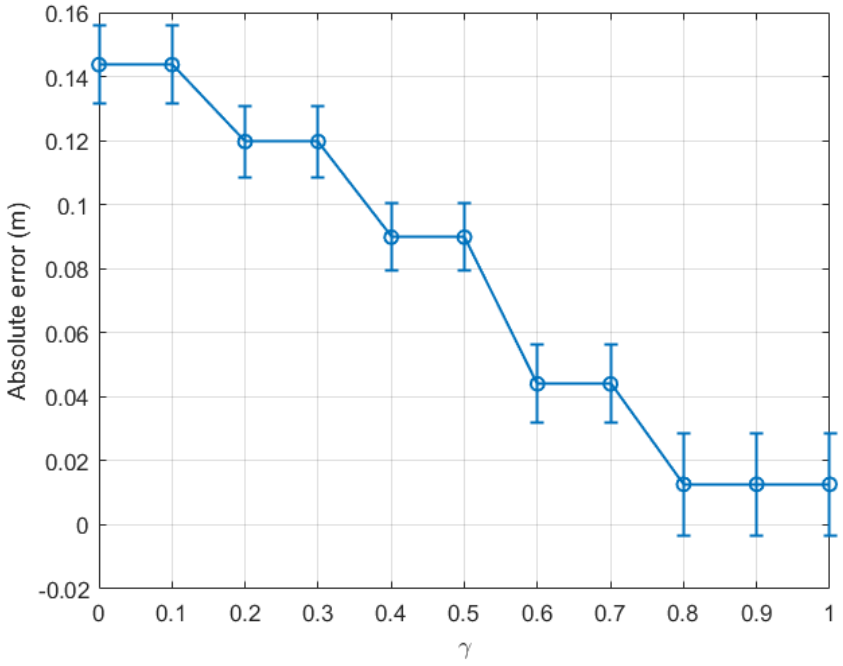

Figure 5.10: Indoor walking (data set 5): absolute error of the last time window (tw_{18}) with respect to $\gamma \in [0, 1]$.

was in the range [0.8, 1]. Similarly, in Fig. 5.11, the smallest absolute measurement error of 0.0096 m, i.e., 1.45% of the actual step length (0.6599 m), could be achieved when γ was in the range [0.4, 0.5]. These optimal γ ranges and the centimetre-level accuracy are similar to those mentioned previously for data sets 1 – 4.

To sum up, from the six groups of experiments, it is possible to achieve a centimetre-scale absolute error in step length estimation for both indoor and outdoor walking scenarios. Furthermore, the estimated absolute error of the outdoor walking case could be as small as a few millimetres (cf. Figs. 5.6 and 5.7, and 5.11). In general, the step length estimated in the outdoor walking scenario is more accurate than in the indoor walking one, as shown in Table 5.2. For instance, for indoor walking, from data sets 1, 2, and 5, the smallest absolute estimation error between the real step length and the corresponding estimated step length is 0.0127 m. Meanwhile, for outdoor walking, the largest absolute step length estimation error based on data sets 3, 4, and 6 is just 0.0155 m. It is observed that the estimated step length has a centimetre-level error for indoor scenarios, whereas it has a sub-centimetre-level error for outdoor ones. This observation agrees with the finding in Chapter 4, where the SMA method was applied and the absolute errors are 10.15 mm

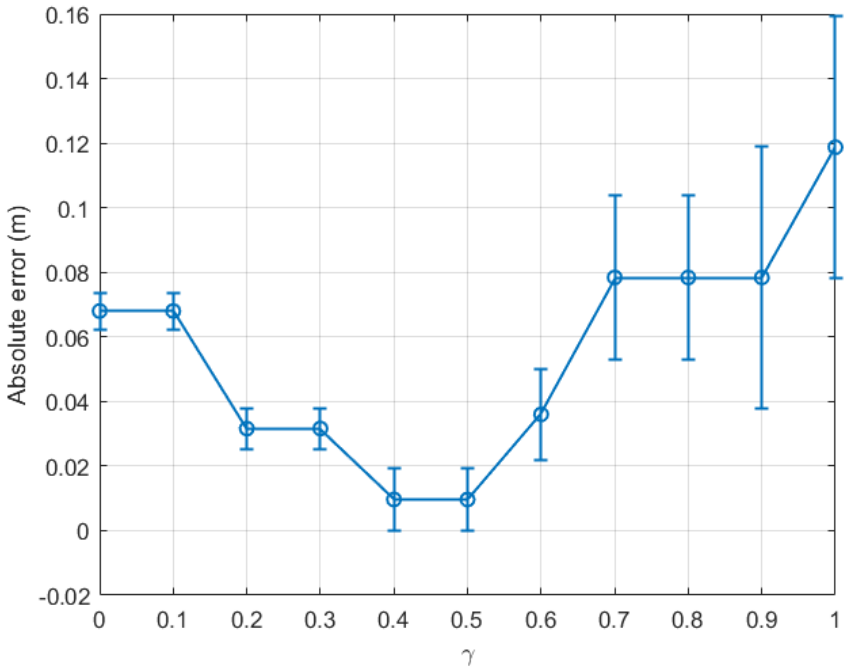

Figure 5.11: Outdoor walking (data set 6): absolute error of the last time window (tw_{18}) with respect to $\gamma \in [0, 1]$.

and 4.40 mm for indoor and outdoor walking, respectively. The comparative results validate the hypothesis proposed in this chapter that the proposed EWMA algorithm could be employed to update the upper threshold periodically. The estimated step length within each time window is estimated based on the updated pair of thresholds. The estimation accuracy is slightly worse than the experimental outcomes in Chapter 4 because the data being used in each time window is downsized. However, the proposed EWMA algorithm is promising because it allows real-time step length estimation without sacrificing much accuracy.

Table 5.2: Comparison of the real step length, estimated step length, and absolute and relative estimation error for both indoor and outdoor walking environments.

Environment	Data set	Real Step Length (m)	Estimated Step Length (m)	Absolute Estimation Error (m)	Relative Estimation Error (%)
Indoor	1	0.6627	0.6427	0.0200	3.02
	2	0.6844	0.6204	0.0640	9.35
	5	0.6679	0.6552	0.0127	1.90
Outdoor	3	0.6633	0.6613	0.0020	0.30
	4	0.6561	0.6409	0.0155	2.36
	6	0.6599	0.6503	0.0096	1.45

Recall that the work in [65] using a two-camera system had step length estimation outcomes with an error of 6%. The estimation error in the IR thermography technique is 9 – 22% [72]. By using the IMU sensor, the step length estimation error in the work [80] was about 3%, while the work [88] mounts the wearable sensor on the wrists of the subject under test, gaining an estimation error of 4.5%. From Table 5.2, the median relative estimation errors for indoor and outdoor walking scenarios in our EWMA technique are 3.02% and 1.45%, respectively. Compared with the existing techniques, the proposed EWMA algorithm could achieve a comparable or even better accuracy level in the step length estimation, while overcoming some main limitations of the existing techniques.

5.5.3 Comparison of the Processing Time

Apart from the accuracy evaluation, the processing time, which is the time used to estimate the step length, is analysed to assess the effectiveness and the feasibility of the proposed EWMA algorithm. In this section, we compare the processing time of our measurement technique in the cases of with and without applying the proposed EWMA algorithm. It is noted that the measurement technique without applying the EWMA algorithm is the technique proposed in Chapter 4. For a fair comparison, we use data sets of the same sizes. The data sets are those for the indoor and outdoor walking experiments in Chapter 4, which have 6 time windows and 4 time windows, respectively. Each

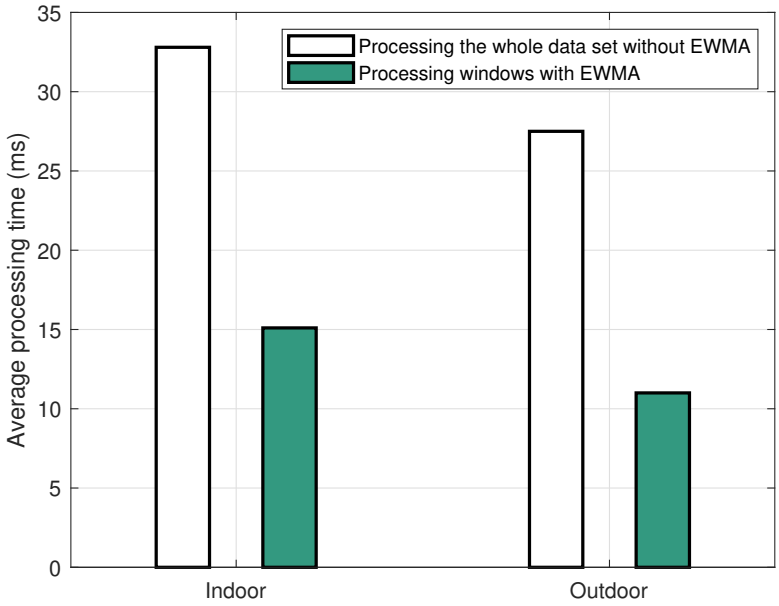

Figure 5.12: Comparison of the average processing time in the cases with and without the EWMA, for indoor and outdoor walking scenarios.

time window comprises 3000 data samples. The processing time to output a value of the step length depends on the number of samples of the data sets to be used each time and whether the EWMA algorithm is used. The measurement technique in Chapter 4 requires the use of the whole data set to estimate the step length; thus the processing time is large. Meanwhile, the processing time is significantly reduced in the EWMA technique due to the shortened time window.

The above conjecture is confirmed in Fig. 5.12, which plots the average processing time of step length estimation for the same data set with and without the proposed EWMA algorithm. In this figure, the white bars are the time required to estimate step length using the whole data set without applying the EWMA algorithm in indoor and outdoor activities. The green bars are the average time of step length estimation required by the proposed EWMA algorithm to process each time window. This figure shows that the processing time is significantly shortened by the EWMA algorithm for both indoor and outdoor scenarios. Initially, the indoor walking case includes more data samples than the outdoor one; thus, the time used to estimate the step length for indoor walking would be longer for outdoor walking without applying the proposed EWMA algorithm. However, with

the application of the EWMA algorithm, the step length could be estimated and updated in each time window. Based on the data samples collected from Chapter 4, the average processing time to estimate a step length was 15.1 ms and 11.0 ms, respectively. In particular, in the indoor walking scenario, the time required to estimate the step length in each time window using the EWMA algorithm is only 46.04% of the total time required for the step length estimation where the EWMA algorithm was not applied. For the outdoor walking case, this number is 40%. In other words, the proposed EWMA algorithm can not only provide comparable accuracy, but also shorten the processing time by 53.96% for indoor walking and by 60% for outdoor walking, compared to our technique proposed in Chapter 4.

5.6 Chapter Summary

In this chapter, we have estimated the human step length for daily indoor and outdoor walking activities based on our developed wearable transceivers and the RSSI method. The RSSI outliers filtering technique has been refined with the proposed EWMA method, so that the thresholds could be updated periodically while the person under test is walking. As a result, the proposed EWMA algorithm facilitates the step length estimation in real-time. In addition, this chapter investigates the optimal γ value in the equation of the upper threshold $Th^{(u)}$ to minimise the estimation errors, by analysing the statistical properties of the collected data sets. The results reveal that the optimal γ for an indoor environment is about 0.9, while this value for an outdoor scenario is around 0.5. With the optimal values of γ, step length estimation can be considered to be accurate with the estimation errors being as small as 1.90% and 0.30% for the indoor and outdoor scenarios, respectively. It is worth noting that this accuracy is achievable without the need of collecting and processing the whole data set as discussed in Chapter 4. In addition, by comparing the processing time required to compute and output a step length estimation for the cases with and without using the proposed EWMA algorithm, it is found that the new method could shorten this processing time by 53.96% for indoor walking and by 56.72% to 60% for outdoor walking, respectively. As a result, the EWMA algorithm could be a promising

candidate technique for measuring the step length in human daily activities in real-time.

Chapter 6

Step Length Measurements using Smart Devices

6.1 Introduction

In previous Chapters 3 - 5, human step length for both indoor and outdoor daily activities has been estimated based on our developed hardware coupled with the proposed RSSI-based estimation algorithms. However, direct comparisons between the features and parameters of our proposed estimation techniques and those of the popularly used wearable devices, such as Apple or Fitbit watches, have not been discussed. Apart from the most basic function in showing the time accurately, smartwatches are able to provide a group of health indexes of the device wearer. For example, Apple watches are able to measure a series of parameters, including one's steps, walking and running distances, walking heart rate average, double support time, walking speed, walking step length, walking asymmetry, stair speed: down, stair speed: up, six-minute walk, and walking steadiness. Thus, in this chapter, we will provide comparisons and analyses between the step length measurements based on our estimation techniques and those measurements shown by Apple and Fitbit watches to users. To this end, we will carry out some experiments using these smartwatches to derive the personal walking step length in daily activities for indoor and outdoor scenarios in Section 6.2. We will then compare the features of step length measurements, including accuracy and feasibility, provided by these smartwatches and by our hardware in Section 6.3. At last, Section 6.4 summarises this chapter.

6.2 Experimental Performance of Smartwatches

In this section, the walking step length of the person under test will be examined in both indoor and outdoor environments using smartwatches combined with the pairing smartphones. There are two groups of experiments. One experiment uses an Apple watch (iWatch) and an iPhone (with a pre-installed application called Health), noted as iWatch + iPhone. The other experiment uses a Fitbit watch and an iPhone (with a pre-installed application called Fitbit), indicated as Fitbit + iPhone. For a fair comparison, these two experiments are conducted in the same indoor and outdoor environments and with the similar settings with those presented previously in Fig. 4.4 and discussed in Chapters 4 and 5. That is to say, the length of the walking path is 71.11 m per round. The person under test will wear the smartwatch on the left wrist while keeping the smartphone in the right pocket, which locates on the front thigh part of the body. Then the person under test walks steadily at a normal speed, along the path for 20 rounds for each set of experiments. At the same time, the person under test counts the total steps of each set in experiments, which will be used to calculate the real walking step length, which is, in turn, used as a reference to compare with the step length measured by the smartwatches.

6.2.1 iWatch + iPhone

In the iWatch + iPhone experiments, the models being used are iWatch 7 and iPhone 11. With the inbuilt Health application, activities, such as steps, and mobilities, such as double support time, walking asymmetry, walking speed and walking step length, can be monitored. Because the finest resolution of the steps and walking step length the users can choose is an hour, we can only do one set of the experiments in each hour. The following figures show an example of one set of experimental outcomes and their appearance on the Health application.

Fig. 6.1 presents the experimental outcomes including step counts in Fig. 6.1(a) and walking step length in Fig. 6.1(b). As shown in this figure, the experiment has been undertaken on 10/02/2023, during the period of 11 am – 12 pm.

Fig. 6.1(a) shows the hourly step distribution for the time duration from 7 am onwards.

(a) Step counts.

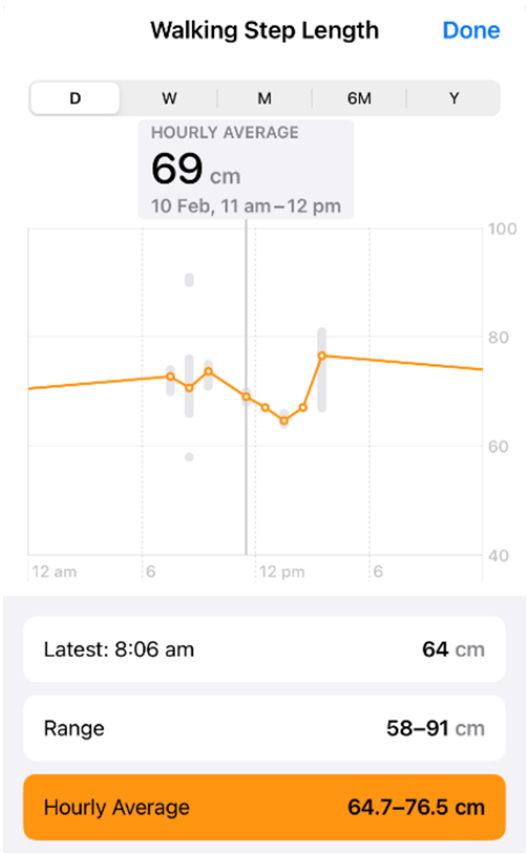

(b) Walking step length.

Figure 6.1: Example of indoor experimental results using iWatch + iPhone.

The step count shown in each bar of this bar graph is the total number of steps counted by the iWatch during the one hour of interest when the person under test wears the watch. The step count for our experiment shown in this figure is 1,980, which is the 5^{th} bar from

Table 6.1: Indoor experimental results based on iWatch + iPhone.

Data set		Indoor 1	Indoor 2	Indoor 3
Date and time		10/02/2023 11 am – 12 pm	11/02/2023 12 pm – 1 pm	11/02/2023 1 pm – 2 pm
Reference	Counted steps	2206 steps	2190 steps	2184 steps
	Real walking step length	64.47 cm	64.94 cm	65.12 cm
iWatch + iPhone	Steps	1980 steps	1933 steps	1980 steps
	Hourly average walking step length	69 cm	71.2 cm	70.2 cm

the left.

Fig. 6.1(b) indicates the average walking step length on an hourly basis. *Hourly Average*, highlighted in orange colour in the application, is actually the range of hourly average walking step length through the day. For example, on 10/02/2023, the range of hourly average walking step length is 64.7 cm – 76.5 cm, which is presented by the solid orange line with hollowed orange circles in the graph. The hollowed orange circles represent the average step length for each hour. If one of the circles was selected, as shown in Fig. 6.1(b), a grey shadowed square appears in the middle of the screen, showing the average walking step length of this hour (i.e., the hourly average walking step length from 11 am to 12 pm is 69 cm).

In tandem with the measurement by iWatch and iPhone, the person under test also records the real number of steps. From the real walking distance and the real number of steps, the real step length in each set of experiments can be calculated, which serves as a reference or ground truth for our experiment.

The same experiments have been carried out for both indoor and outdoor environments. Under each environment, we have done three sets of experiments. The outcomes of experiments with iWatch + iPhone are summarised in the tables below.

From Tables 6.1 and 6.2, it is observed that the number of steps provided by iWatch + iPhone is generally significantly smaller than the actual steps counted by the person under test during each experiment for both indoor and outdoor experiments. As a result, the hourly average walking step length provided by iWatch + iPhone is always bigger than the real walking step length. The absolute step length errors of the 1^{st} – 3^{rd} indoor experiments between the real walking step length and the hourly average ones are

Table 6.2: Outdoor experimental results based on iWatch + iPhone.

Data set		Outdoor 1	Outdoor 2	Outdoor 3
Date and time		11/02/2023 8 am – 9 am	12/02/2023 8 am – 9 am	12/02/2023 9 am – 10 am
Reference	Counted steps	2124 steps	2131 steps	2146 steps
	Real walking step length	66.96 cm	66.74 cm	66.27 cm
iWatch + iPhone	Steps	1840 steps	1824 steps	1784 steps
	Hourly average walking step length	71.5 cm	72.8 cm	70.4 cm

4.53 cm, 6.26 cm, and 5.08 cm, respectively. The corresponding relative errors are 7.03%, 9.64%, and 7.80%. Similarly, the absolute step length errors of the 1st – 3rd outdoor experiments between the real walking step length and the hourly average ones are 4.54 cm, 6.06 cm, and 4.13 cm, respectively. The corresponding relative errors are 6.78%, 9.08%, and 6.23%. From the three sets of experiments, the average absolute walking step length errors for indoor and outdoor cases are 5.29 cm and 4.91 cm, respectively. In addition, it is noticed that the indoor case has lower accuracy than the outdoor case in terms of the errors, and thus the hourly average walking step length. Clearly, the measurement method in the Health application is not transparent and its accuracy is limited.

6.2.2 Fitbit + iPhone

In our experiments using Fitbit and iPhone, the models of equipment are Fitbit Luxe and iPhone 11. With the premium membership in the Fitbit application, the number of steps and travelled distance could be tracked. The resolution can be viewed per day, week, and year. Similar to the experiments carried out with iWatch, the person under test wears the Fitbit on the non-dominant wrist (i.e., the left wrist) and keeps the iPhone in the right pocket while carrying out experiments. It is noticed that although Fitbit is able to count the number of steps, the finest resolution is a day. Thus, two screenshots in each experiment must be taken for the purpose of step length estimation. The first screenshot is taken before the commencement of each experiment, noting down the number of steps and distance at that moment as shown in Fig. 6.2(a). Right after the experiment, the second screenshot is taken as shown in Fig. 6.2(b), recording the updated steps and distance. In this way, the difference between them could be viewed as the number of steps and the

(a) Before the commencement of experiment.

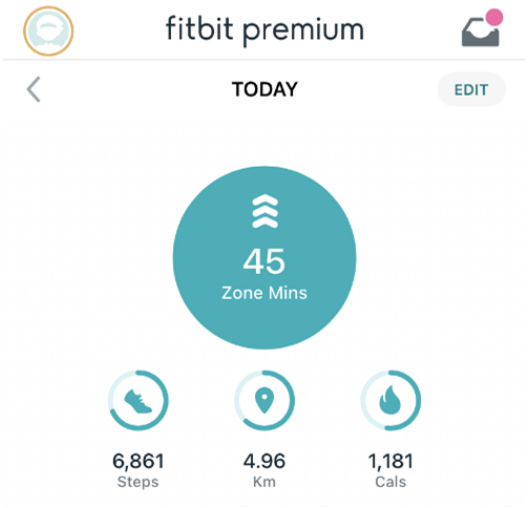

(b) At the end of the experiment.

Figure 6.2: Example of indoor experimental result using Fitbit + iPhone.

travelled distance during each experiment. Thus, the experimental walking step length can be calculated.

It is noticed that the so-called stride length in Fitbit is actually the step length discussed in this thesis. To prevent misunderstanding, the term 'step length' will be used to replace the term 'stride length' in the following discussion when stride length in the Fitbit application is mentioned. The step length in Fitbit is, by default, updated automatically when the motion activity of the Fitbit wearer is tracked. The real step length can be input manually into Fitbit to calibrate the measurements if the real step length is known. The step length shown in the Fitbit application is the number automatically measured by Fitbit

Table 6.3: Indoor experimental results based on Fitbit + iPhone.

Data set		Indoor 1	Indoor 2	Indoor 3
Date and time		18/02/2023 12 pm - 1 pm	18/02/2023 1 pm – 2 pm	18/02/2023 3 pm – 4 pm
Reference	Counted steps	2181 steps	2181 steps	2186 steps
	Real walking step length	65.21 cm	65.21 cm	65.06 cm
Fitbit + iPhone	Steps	2094 steps	2019 steps	2043 steps
	Experimental walking step length	72.11 cm	72.31 cm	72.44 cm

Table 6.4: Outdoor experimental results based on Fitbit + iPhone.

Data set		Outdoor 1	Outdoor 2	Outdoor 3
Date and time		16/02/2023 6 pm – 7 pm	16/02/2023 7 pm – 8 pm	18/02/2023 5 pm – 6 pm
Reference	Counted steps	2172 steps	2177 steps	2121 steps
	Real walking step length	65.48 cm	65.33 cm	67.05 cm
Fitbit + iPhone	Steps	1954 steps	1952 steps	1976 steps
	Experimental walking step length	72.16 cm	72.23 cm	72.37 cm

considering the height of the person under test. For consistency, three sets of experiments are conducted for indoor and outdoor scenarios, respectively. Their results are recorded in Tables 6.3 and 6.4.

From Tables 6.3 and 6.4, a similar observation can be drawn: the number of steps tracked by Fitbit + iPhone is always smaller than the actual steps counted by the person under test during each experiment, resulting in the estimated walking step length being higher than the real walking step length. The absolute step length errors of the 3 indoor experiments between the real walking step length and the experimental walking step length are 6.90 cm, 7.10 cm, and 7.38 cm. The corresponding relative errors are 10.58%, 10.89% and 11.34%. The absolute step length errors of the 1^{st} – 3^{rd} outdoor experiments between the real walking step length and the experimental ones are 6.68 cm, 6.90 cm, and 5.32 cm, while the corresponding relative errors are 10.20%, 10.56% and 7.93%. As a result, the average absolute walking step length errors of the three sets of experiments for indoor and outdoor cases are 7.12 cm and 6.30 cm, respectively. Similar to the iWatch + iPhone experiments, it is noticed that the outdoor cases are more accurate than the indoor cases because they have smaller walking step length estimation errors.

As mentioned previously, the Fitbit application allows users to manually input their reference step length if it is known to calibrate the measurements. Because the real step length cannot be known before the experiment is carried out, in the next experiment, we input the reference step length value of 66 cm, which is our best guess of the real step length of the person under test, into the application. An indoor experiment is then carried out again and the performance is summarised as below. The number of steps counted by the person under test in this experiment is 2104 while the number tracked by Fitbit is 1811. The real walking step length is 67.60 cm while the walking step length calculated by Fitbit is 66.26 cm.

From the above experiment, it is observed that when the real (or near real) step length is input manually as ground truth, the experimental result is improved. We have conducted similar experiments in a similar manner. It is observed that Fitbit will always try to output the step length to be close to the reference value which has been entered into the Fitbit application. It is noted that the Fitbit application only shows the number of steps and the travelled distance, rather than the step length value. The estimated step length value must be calculated by the user from the number of steps and the travelled distance for the time period of interest. Thus, the disadvantages of the Fitbit are: (i) the real step length has to be manually input prior to the usage of the Fitbit application to enhance the accuracy; (ii) the step length cannot be directly measured during the daily activities in human daily life; (iii) the algorithm adopted in Fitbit to calculate the step length based on the manual input is not transparent.

6.3 Comparison between iWatch, Fitbit and the RSSI-based Method

Experiments have been undertaken using smartwatches and smartphones to obtain one's walking step length. In this section, we will compare some main features of step length measurements using an Apple watch, a Fitbit watch, and our developed hardware associated with the novel filtering and EWMA algorithms proposed in this thesis as shown in Table 6.5.

Table 6.5: Comparison between Apple watch, Fitbit watch and RSSI-based method with novel filtering and EWMA algorithms proposed in this thesis.

Features	Apple watch	Fitbit watch	This thesis
Indoor relative estimated error	7.03%	10.58%	1.90%
Outdoor relative estimated error	6.23%	7.93%	0.30%
Output step length directly	✓	×	×
Wearable	✓(wrist)	✓(wrist)	✓(ankle)
Comfortability	High	High	Medium
Cost	High	Medium	Low

All these techniques are able to provide step length values for both indoor and outdoor environments. The most merit of the Apple watch is that it provides an intuitive outcome on the Health application by directly showing the measured hourly average walking step length, while Fitbit and the proposed algorithm in this thesis require further calculation. Both iWatch and Fitbit could be comfortably worn on the user's wrist whereas our proposed equipment might be slightly less comfort as two small pieces of hardware are attached to human ankles. In terms of the estimation accuracy, the relative walking step length estimated errors provided by the RSSI-based method with novel filtering and EWMA algorithm proposed in this thesis, are as small as 1.90% and 0.30% for indoor and outdoor environments, respectively. Under the same scenario, the indoor and outdoor relative walking step length estimated errors measured by iWatch are 7.03% and 6.23%, respectively, and by Fitbit are 10.58% and 7.93%. Clearly, our measurement techniques have much higher accuracy, compared to the iWatch and Fitbit. Regarding the possible cost of the aforementioned techniques, the cost of the iWatch is around 500 AUD, of the Fitbit watch is around 150 AUD, while the equipment proposed in this thesis costs the least, which is around 100 AUD. The cost of our equipment could even be significantly lowered if it is mass-produced.

6.4 Chapter Summary

In this chapter, experiments using commercially available smartwatches, such as iWatch and Fitbit, have been undertaken. Experimental results suggest that step length measured by iWatch could have relative estimation errors of 7.03% and 6.23% for indoor and out-

door environments, respectively. The relative step length estimation errors of Fitbit are slightly larger than those of iWatch, which are 10.58% and 7.93% for indoor and outdoor walking scenarios, respectively. Unlike iWatches, Fitbit watches allow users to enter the reference step length value to calibrate the measurements. However, both iWatches and Fitbit watches are of relatively high costs, and have limited accuracy and non-transparent algorithms in step length measurements. Meanwhile, our developed hardware associated with our novel data filtering and EWMA algorithms proposed in this thesis is more affordable, while it could achieve the relative estimation errors as small as 1.90% and 0.30% for indoor and outdoor environments, respectively.

Chapter 7

Conclusions and Future Works

7.1 Conclusions

This thesis has investigated the approaches for step length estimations and distance measurements. Measuring the human step lengths using wearable equipment while they are performing daily activities is a very challenging task due to the randomness and irregularity of the propagation channel related to these activities.

As shown in this thesis, we have developed portable transceivers utilising Arduino UNO and XBee PRO-S2C chips. The developed hardware transceivers are used to record the RSSI data sets (then converted to path loss values) and to analyse the wireless channel between the two ankles of the subject under test. Unlike existing works, this thesis proposes an unobstructed, non-invasive, less health-concerning, and less space-constrained, but also a relatively accurate and cost-effective methodology for step length estimations in human daily activities. This thesis reveals that the proposed techniques could accurately estimate the step length despite of the random variations superimposed on the wireless channel between the two ankles of the person under test during daily activities.

The thesis has successfully proposed (i) a novel path loss model between two ankles and the optimal configurations of the hardware which is deployed to measure the step length, (ii) novel techniques to estimate human step length in daily activities, and (iii) optimal parameters of these measurement techniques. Specifically, the transceivers composed of Arduino UNO and XBee PRO-S2C modules, are firstly developed. Different configurations are taken into consideration to find the most suitable transmission power

level and data rate for the distance measurement. It is found that the optimal transmitted power is 0 dBm at the transmission data rate of 9600 bps, which are in fact the default settings of the hardware. The developed hardware with the optimal hardware configuration is then attached to the inner side of the ankles of the person under test to measure the RSSI, thus the path loss, between the two ankles. As a result, the characteristics of the wireless channel between the two ankles can be examined. Based on the assessment of the collected data, an experimental path loss model between the two ankles of the subject under test, that jointly considers the non-linearity, shadowing effect, multipath, mismatch loss, and insertion loss, is proposed. To the best of our knowledge, this path loss model is the first model of its kind. The path loss model for the channel between the two ankles is revealed to be the free space model added with a correction factor ΔPL, whose value is found experimentally. This accurate path loss model facilitates our step length estimations in the later phases as mentioned next.

Another significant problem addressed in this thesis is to estimate the step length in different daily activities, such as walking and jogging, in different environments (i.e., indoors and outdoors). This research problem is significant because, in most existing step length tracking or measuring works, the range of activities of the subject under test and the physical locations where the subject under test can be tested are limited, as the candidate must either walks on a sensing mat, on a specially designed treadmill, or, in the specific room equipped with cameras or IR sensors. Moreover, activities other than walking are almost unexplored. Therefore, this thesis considers both walking and jogging activities in either indoors and outdoors. Based on the empirical path loss model proposed previously, the thesis proposes a novel filtering technique, which sets up the two boundaries to eliminate on-ankle path loss outliers. These boundaries are regarded as the lower threshold and the upper threshold. The resulting range of path loss values between the two thresholds is used to estimate the human step length in daily activities for both indoor and outdoor environments. We consider that the histogram of the on-ankle path loss follows a two-term Gaussian distribution, and the upper threshold value could be found from the second hump of this distribution. Mathematically, the upper threshold is found as $\mu + 0.5\sigma$ for

walking or jogging outdoors and as $\mu + \sigma$ for those activities indoors, where μ and σ are the mean and the standard deviation of the second hump of the fitting two-term Gaussian distribution. Meanwhile, the lower threshold could be numerically found to be the path loss value where the survival rate of the measured path loss data is 0.68 for all cases of walking and jogging indoors and outdoors. Numerical results show that the proposed filtering technique achieves an accurate estimation of the step length, with errors of only 10.15 mm and 4.40 mm for walking and jogging in an indoor environment, respectively, and only 4.81 mm and 10.84 mm for the same activities in an outdoor environment.

Next, the thesis proposes a novel EWMA algorithm, which aims to estimate and update the walking step length over short periods of time, rather than having to process the whole data set as in the presumed technique mentioned above. In the proposed EWMA algorithm, the lower and upper thresholds of the path loss, and thus the step length estimation, are updated periodically after each time window. The average step length estimation depends more on the step length estimation in the current time window while the effect of the estimations in the previous windows exponentially reduces. Thus, the proposed EWMA algorithm facilitates the step length estimation process in real-time.

Then, the thesis examines the optimal parameters of the proposed EWMA algorithm. Specifically, we consider the upper threshold as the function $\mu + \gamma\sigma$ where γ is a weighting factor. We examine the influence of the weight γ on the accuracy of the EWMA algorithm. We discover that the optimal value of γ is approximate 0.9 and 0.5 for indoor and outdoor environments, respectively. Numerical results show that, with the optimal γ, the proposed EWMA technique can obtain the accuracy comparable with the previously proposed technique with errors of 1.90% and 0.30% for the indoor and outdoor scenarios, respectively, while the processing time that is used to output the step length estimation is significantly reduced compared to the case when EWMA algorithm is not applied. the proposed EWMA algorithm saves approximately 53.96% and 60% of processing time in the step length estimation for indoor and outdoor walking activities, respectively.

Lastly, a fair comparison is provided in this thesis, addressing the walking step length estimation performance using this thesis-developed hardware and using smartwatches

with paired smartphones such as iWatch and Fitbit. It is observed that the relative walking step length estimation errors provided by iWatch are 7.03% and 6.23% for indoor and outdoor environments, respectively. These numbers are 0.58% and 7.93% if Fitbit was used. Meanwhile, the developed hardware with novel filtering and EWMA algorithms proposed in this thesis achieves relative errors as small as 1.90% and 0.30% with a more affordable price.

7.2 Recommendations

The following recommendations, especially for the experimental procedure, can be derived based on our experience in carrying out experiments in this thesis.

1. Before the commencement of the experiments, it is primary to ensure the related parameters are configured in every transceiver (in both Arduino UNO and XBee PRO-S2C modules), to make sure the transmitter and the receiver are successfully paired.

2. It is suggested to replace or recharge batteries before each new set of experiments. Otherwise, batteries may run out during the experiments because the remaining batteries cannot be observed visually, which leads to an insufficient amount of collected data.

7.3 Future Works

There remain many interesting aspects that could be further studied. For example, the EWMA algorithm proposed in this thesis could be applied to estimate the near-instantaneous step length in mixed walking-and-jogging activities. It is also worth continuing to advance the prototype proposed in this thesis with more functions, such as the detection of human activities, especially those activities which may cause or reflect an individual's health conditions, such as cycling, doing sports and active recreation. Another possible research direction is to deploy the developed transceivers for multiple users in order to estimate the distances between these users, which in turn helps reinforce the social distancing practice

during the COVID pandemic [7]. In addition, the development of lighter, smaller and more cost-effective yet reliable transceivers is worth considering. Advancing the developed hardware proposed techniques to measure other gait parameters, such as gait speed, step width and foot angle, is also an interesting research topic. All the aforementioned research directions require further study, which could be our future work.

Bibliography

[1] H. Ritchie and M. Roser. "Age structure," Our World in Data. (Sep. 2019), [Online]. Available: https://ourworldindata.org/age-structure.

[2] S. Movassaghi, M. Abolhasan, J. Lipman, D. Smith, and A. Jamalipour, "Wireless body area networks: A survey," *IEEE Commun. Surv. Tutor.*, vol. 16, no. 3, pp. 1658–1686, 2014.

[3] Y. Hao and R. Foster, "Wireless body sensor networks for health-monitoring applications," *Physiol. Meas.*, vol. 29, no. 11, R27–R56, Nov. 2008.

[4] J. A. Behar, C. Liu, K. Kotzen, *et al.*, "Remote health diagnosis and monitoring in the time of COVID-19," *Physiol. Meas.*, vol. 41, no. 10, 10TR01, Oct. 2020.

[5] S. S. Vedaei, A. Fotovvat, M. R. Mohebbian, *et al.*, "COVID-SAFE: An IoT-based system for automated health monitoring and surveillance in post-pandemic life," *IEEE Access*, vol. 8, pp. 188 538–188 551, Oct. 2020.

[6] M. M. Khan, S. Mehnaz, A. Shaha, M. Nayem, and S. Bourouis, "IoT-based smart health monitoring system for COVID-19 patients," *Comput. Math. Methods Med.*, vol. 2021, e8591036, Nov. 2021.

[7] L. C. Tran, A. T. Le, X. Huang, S. L. Phung, C. Ritz, and A. Bouzerdoum, "Background on positioning and localization for social distancing," in *Enabling Technologies for Social Distancing: Fundamentals, concepts and solutions*, The IET, 2021.

[8] "IEEE standard for local and metropolitan area networks - part 15.6: Wireless body area networks," *IEEE Std. 802.15.6-2012*, Feb. 2012.

[9] K. Y. Yazdandoost and K. Sayrafian-Pour. "Channel model for body area network (BAN)." (Apr. 2009), [Online]. Available: https://mentor.ieee.org/802.15/dcn/08/15-08-0780-09-0006-tg6-channel-model.pdf.

[10] S. Studenski, S. Perera, K. Patel, *et al.*, "Gait speed and survival in older adults," *JAMA*, vol. 305, no. 1, pp. 50–58, Jan. 2011.

[11] W. H. Organization, *World Health Statistics 2015*. World Health Organization, May 2015.

[12] N. R. Kandula, M. Kersey, and N. Lurie, "Assuring the health of immigrants: What the leading health indicators tell us," *Annu. Rev. Public Health*, vol. 25, no. 1, pp. 357–376, Apr. 2004.

[13] M. Akhtaruzzaman, A. Shafie, and M. R. Khan, "Gair analysis: Systems, technologies, and importance," *J. Mech. Med. Biol.*, vol. 16, no. 7, p. 1 630 003, Mar. 2016.

[14] B. E. Moyer, A. J. Chambers, M. S. Redfern, and R. Cham, "Gait parameters as predictors of slip severity in younger and older adults," *Ergonomics*, vol. 49, no. 4, pp. 329–343, Mar. 2006.

[15] S. Chowdhury and N. Kumar, "Estimation of forces and moments of lower limb joints from kinematics data and inertial properties of the body by using inverse dynamics technique," *J. Rehabil. Robot.*, vol. 1, no. 2, pp. 93–98, Jan. 2013.

[16] H. Sadeghi, P. Allard, F. Prince, and H. Labelle, "Symmetry and limb dominance in able-bodied gait: A review," *Gait & Posture*, vol. 12, no. 1, pp. 34–45, Sep. 2000.

[17] G. Taga, "A model of the neuro-musculo-skeletal system for human locomotion," *Biol. Cybern.*, vol. 73, no. 2, pp. 97–111, Jul. 1995.

[18] Y. Wahab and N. A. Bakar, "Gait analysis measurement for sport application based on ultrasonic system," in *Proc. 15th International Symposium on Consumer Electronics (ISCE)*, Singapore, Jun. 2011, pp. 20–24.

[19] D. V. Thiel and A. K. Sarkar, "Swing profiles in sport: An accelerometer analysis," *Procedia Eng.*, vol. 72, pp. 624–629, Jan. 2014.

[20] S. Schmid, M. Moffat, and G. M. Gutierrez, "Effects of cooling on ground reaction forces, knee kinematics, and jump height in drop jumps," *Athletic Training & Sports Health Care*, vol. 5, no. 1, pp. 29–37, Jan. 2013.

[21] M. J. Johnson, "Recent trends in robot-assisted therapy environments to improve real-life functional performance after stroke," *J. NeuroEng. Rehabil.*, vol. 3, no. 1, p. 29, Dec. 2006.

[22] D. Ferris, G. Sawicki, and A. Domingo, "Powered lower limb orthoses for gait rehabilitation," *Top. Spinal Cord Inj. Rehabil.*, vol. 11, no. 2, pp. 34–49, Sep. 2005.

[23] M. Hassan, H. Kadone, K. Suzuki, and Y. Sankai, "Wearable gait measurement system with an instrumented cane for exoskeleton control," *Sensors*, vol. 14, no. 1, pp. 1705–1722, Jan. 2014.

[24] M. W. Whittle, D. Levine, and J. D. Richards, "Chapter 2 - normal gait," in *Gait Analysis*, 5th ed., Churchill Livingstone, Jan. 2012, pp. 47–100.

[25] A. Rodríguez-Molinero, A. Herrero-Larrea, A. Miñarro, *et al.*, "The spatial parameters of gait and their association with falls, functional decline and death in older adults: A prospective study," *Sci. Rep.*, vol. 9, no. 1, p. 8813, Jun. 2019.

[26] A. Aggarwal, R. Gupta, and R. Agarwal, "Design and development of integrated insole system for gait analysis," in *Proc. Eleventh International Conference on Contemporary Computing (IC3)*, Noida, India, Aug. 2018, pp. 1–5.

[27] P. Padmanabhan, K. S. Rao, S. Gulhar, K. M. Cherry-Allen, K. A. Leech, and R. T. Roemmich, "Persons post-stroke improve step length symmetry by walking asymmetrically," *J. NeuroEng. Rehabil.*, vol. 17, no. 1, pp. 1–14, Aug. 2020.

[28] C. Kirtley, *Clinical Gait Analysis: Theory and Practice*. Elsevier Health Sciences, Jan. 2006.

[29] N. Hauptman. "The average walking stride length," Live Healthy - Chron. (Apr. 2018), [Online]. Available: https://livehealthy.chron.com/average-walking-stride-length-7494.html.

[30] "Stepping science: Estimating someone's height from their walk," Scientific American. (Mar. 2013), [Online]. Available: https://www.scientificamerican.com/article/bring-science-home-estimating-height-walk/.

[31] R. M. Guimaraes and B. Isaacs, "Characteristics of the gait in old people who fall," *Int. Rehabil. Med.*, vol. 2, no. 4, pp. 177–180, Jan. 1980.

[32] M. Schimpl, C. Lederer, and M. Daumer, "Development and validation of a new method to measure walking speed in free-living environments using the actibelt® platform," *PLoS One*, vol. 6, no. 8, e23080, Aug. 2011.

[33] Y. Abe, A. Matsunaga, R. Matsuzawa, *et al.*, "Determinants of slow walking speed in ambulatory patients undergoing maintenance hemodialysis," *PLoS One*, vol. 11, no. 3, e0151037, Mar. 2016.

[34] D. D. Espy, F. Yang, T. Bhatt, and Y.-C. Pai, "Independent influence of gait speed and step length on stability and fall risk," *Gait & Posture*, vol. 32, no. 3, pp. 378–382, Jul. 2010.

[35] A. L. Rosso, M. J. Olson Hunt, M. Yang, *et al.*, "Higher step length variability indicates lower gray matter integrity of selected regions in older adults," *Gait & Posture*, vol. 40, no. 1, pp. 225–230, May 2014.

[36] J. Verghese and X. Xue, "Predisability and gait patterns in older adults," *Gait & Posture*, vol. 33, no. 1, pp. 98–101, Jan. 2011.

[37] Z. Q. Liu and F. Yang, "Obesity may not induce dynamic stability disadvantage during overground walking among young adults," *PLoS One*, vol. 12, no. 1, e0169766, Jan. 2017.

[38] L. Allet, H. Kim, J. Ashton-Miller, T. De Mott, and J. K. Richardson, "Step length after discrete perturbation predicts accidental falls and fall-related injury in elderly people with a range of peripheral neuropathy," *J. Diabetes Complicat.*, vol. 28, no. 1, pp. 79–84, Jan. 2014.

[39] T. J. Daskivich, J. Houman, M. Lopez, *et al.*, "Association of wearable activity monitors with assessment of daily ambulation and length of stay among patients undergoing major surgery," *JAMA Netw. Open*, vol. 2, no. 2, e187673, Feb. 2019.

[40] J. Woo, S. C. Ho, and A. L. M. Yu, "Walking speed and stride length predicts 36 months dependency, mortality, and institutionalization in chinese aged 70 and older," *J. Am. Geriatr. Soc.*, vol. 47, no. 10, pp. 1257–1260, 1999.

[41] M. Cesari, S. B. Kritchevsky, B. W. H. J. Penninx, *et al.*, "Prognostic value of usual gait speed in well-functioning older people—results from the health, aging and body composition study," *J. Am. Geriatr. Soc.*, vol. 53, no. 10, pp. 1675–1680, 2005.

[42] Y. Morio, K. P. Izawa, Y. Omori, *et al.*, "The relationship between walking speed and step length in older aged patients," *Diseases*, vol. 7, no. 1, p. 17, Feb. 2019.

[43] C. Fritsche and A. Klein, "On the performance of hybrid GPS/GSM mobile terminal tracking," in *Proc. IEEE International Conference on Communications Workshops*, Dresden, Germany, Jun. 2009, pp. 1–5.

[44] M. Cabric, *From Corporate Security to Commercial Force: A Business Leader's Guide to Security Economics*. Butterworth-Heinemann, May 2017.

[45] Z. B. Tariq, D. M. Cheema, M. Z. Kamran, and I. H. Naqvi, "Non-GPS positioning systems: A survey," *ACM Comput. Surv.*, vol. 50, no. 4, pp. 1–34, Aug. 2017.

[46] N. M. Nguyen, L. C. Tran, F. Safaei, *et al.*, "Performance evaluation of non-GPS based localization techniques under shadowing effects," *Sensors*, vol. 19, no. 11, p. 2633, Jan. 2019.

[47] S. J. Crane, "Eldercare technology for clinical practitioners," *Mayo Clin. Proc.*, vol. 84, no. 11, p. 1045, Nov. 2009.

[48] X. Cai, G. Han, X. Song, and J. Wang, "Single-camera-based method for step length symmetry measurement in unconstrained elderly home monitoring," *IEEE Trans. Biomed. Eng.*, vol. 64, no. 11, pp. 2618–2627, Nov. 2017.

[49] H. B. Menz, M. D. Latt, A. Tiedemann, M. Mun San Kwan, and S. R. Lord, "Reliability of the GAITRite® walkway system for the quantification of temporo-spatial parameters of gait in young and older people," *Gait & Posture*, vol. 20, no. 1, pp. 20–25, Aug. 2004.

[50] P. Srinivasan, D. Birchfield, G. Qian, and A. Kidané, "A pressure sensing floor for interactive media applications," in *Proc. ACM International Conference Proceeding Series*, vol. 265, Jan. 2005, pp. 278–281.

[51] E. Li, X. Lin, B.-C. Seet, F. Joseph, and J. Neville, "Low profile and low cost textile smart mat for step pressure sensing and position mapping," in *Proc. IEEE International Instrumentation and Measurement Technology Conference (I2MTC)*, Auckland, New Zealand, May 2019, pp. 1–5.

[52] "GAITRite: World leader in temporospatial gait analysis," GAITRite. (2005), [Online]. Available: https://www.gaitrite.com.

[53] A. Muro-de-la-Herran, B. Garcia-Zapirain, and A. Mendez-Zorrilla, "Gait analysis methods: An overview of wearable and non-wearable systems, highlighting clinical applications," *Sensors*, vol. 14, no. 2, pp. 3362–3394, Feb. 2014.

[54] F. Wang, E. Stone, W. Dai, M. Skubic, and J. Keller, "Gait analysis and validation using voxel data," in *Proc. Annual International Conference of the IEEE Engineering in Medicine and Biology Society*, Minneapolis, MN, USA, Sep. 2009, pp. 6127–6130.

[55] R. R. Jensen, R. R. Paulsen, and R. Larsen, "Analyzing gait using a time-of-flight camera," in *Proc. Scandinavian Conference on Image Analysis*, A.-B. Salberg, J. Y. Hardeberg, and R. Jenssen, Eds., vol. 5575, Berlin, Heidelberg: Springer, Jun. 2009, pp. 21–30.

[56] R. Tron and R. Vidal, "Distributed image-based 3-d localization of camera sensor networks," in *Proc. 48h IEEE Conference on Decision and Control (CDC) held jointly with 2009 28th Chinese Control Conference*, Shanghai, China, Dec. 2009, pp. 901–908.

[57] J. Courtney and A. M. De Paor, "A monocular marker-free gait measurement system," *IEEE Trans. Neural Syst. Rehabil. Eng.*, vol. 18, no. 4, pp. 453–460, Aug. 2010.

[58] H. P. Jain, A. Subramanian, S. Das, and A. Mittal, "Real-time upper-body human pose estimation using a depth camera," in *Proc. International Conference on Computer Vision/Computer Graphics Collaboration Techniques and Applications*, vol. 6930, Berlin, Heidelberg, 2011, pp. 227–238.

[59] F. Aubeck, C. Isert, and D. Gusenbauer, "Camera based step detection on mobile phones," in *Proc. International Conference on Indoor Positioning and Indoor Navigation*, Guimaraes, Portugal, Sep. 2011, pp. 1–7.

[60] N. Vishnoi, Z. Duric, and N. L. Gerber, "Markerless identification of key events in gait cycle using image flow," in *Proc. Annual International Conference of the IEEE Engineering in Medicine and Biology Society*, San Diego, CA, USA, Aug. 2012, pp. 4839–4842.

[61] S. Das and S. Meher, "Automatic extraction of height and stride parameters for human recognition," in *Proc. Students Conference on Engineering and Systems (SCES)*, Allahabad, India, Apr. 2013, pp. 1–6.

[62] W. Zhu, B. Anderson, S. Zhu, and Y. Wang, "A computer vision-based system for stride length estimation using a mobile phone camera," in *Proc. 18th International ACM SIGACCESS Conference on Computers and Accessibility*, Reno Nevada USA, Oct. 2016, pp. 121–130.

[63] S. Singhal, C. Neustaedter, T. Schiphorst, A. Tang, A. Patra, and R. Pan, "You are being watched: Bystanders' perspective on the use of camera devices in public spaces," in *Proc. CHI Conference Extended Abstracts on Human Factors in Computing Systems*, New York, NY, USA, May 2016, pp. 3197–3203.

[64] S. Jeong, J. Min, and Y. Park, "Indoor positioning using deep-learning-based pedestrian dead reckoning and optical camera communication," *IEEE Access*, vol. 9, pp. 133 725–133 734, 2021.

[65] F. Wang, E. Stone, M. Skubic, J. M. Keller, C. Abbott, and M. Rantz, "Toward a passive low-cost in-home gait assessment system for older adults," *IEEE J. Biomed. Health Inform.*, vol. 17, no. 2, pp. 346–355, Mar. 2013.

[66] I. Pachoulakis and K. Kourmoulis, "Building a gait analysis framework for parkinson's disease patients: Motion capture and skeleton 3d representation," in *Proc. International Conference on Telecommunications and Multimedia (TEMU)*, Heraklion, Greece, Jul. 2014, pp. 220–225.

[67] Q. Wang, L. Ye, H. Luo, A. Men, F. Zhao, and Y. Huang, "Pedestrian stride-length estimation based on LSTM and denoising autoencoders," *Sensors*, vol. 19, no. 4, p. 840, Feb. 2019.

[68] Q. Wang, H. Luo, L. Ye, *et al.*, "Personalized stride-length estimation based on active online learning," *IEEE Internet Things J.*, vol. 7, no. 6, pp. 4885–4897, Jun. 2020.

[69] S. Vandermeeren, H. Bruneel, and H. Steendam, "Feature selection for machine learning based step length estimation algorithms," *Sensors*, vol. 20, no. 3, p. 778, Jan. 2020.

[70] J. Li, Z. Li, G. Tyson, and G. Xie, "Your privilege gives your privacy away: An analysis of a home security camera service," in *Proc. IEEE INFOCOM 2020 - IEEE Conference on Computer Communications*, Toronto, ON, Canada, Jul. 2020, pp. 387–396.

[71] S. Ohta, H. Nakamoto, Y. Shinagawa, and T. Tanikawa, "A health monitoring system for elderly people living alone," *J. Telemed. Telecare*, vol. 8, no. 3, pp. 151–156, Feb. 2002.

[72] Z. Xue, D. Ming, W. Song, B. Wan, and S. Jin, "Infrared gait recognition based on wavelet transform and support vector machine," *Pattern Recognition*, vol. 43, no. 8, pp. 2904–2910, Aug. 2010.

[73] Z. Fang, Z. Zhao, P. Guo, and Y.-G. Zhang, "Analysis of distance measurement based on RSSI," *Chin. J. Sens. Actuators*, vol. 20, no. 11, pp. 2526–2530, Nov. 2007.

[74] Z. Qiu, Y. Lu, and Z. Qiu, "Review of ultrasonic ranging methods and their current challenges," *Micromachines*, vol. 13, no. 4, p. 520, Apr. 2022.

[75] S. Zihajehzadeh and E. J. Park, "A gaussian process regression model for walking speed estimation using a head-worn IMU," in *Proc. 39th Annual International Conference of the IEEE Engineering in Medicine and Biology Society (EMBC)*, Jeju, Korea (South), Jul. 2017, pp. 2345–2348.

[76] Y. Song, S. Shin, S. Kim, D. Lee, and K. H. Lee, "Speed estimation from a tri-axial accelerometer using neural networks," in *Proc. 29th Annual International Conference of the IEEE Engineering in Medicine and Biology Society*, Lyon, France, Aug. 2007, pp. 3224–3227.

[77] W. Zijlstra and A. L. Hof, "Assessment of spatio-temporal gait parameters from trunk accelerations during human walking," *Gait & Posture*, vol. 18, no. 2, pp. 1–10, Oct. 2003.

[78] D. Alvarez, R. C. Gonzalez, A. Lopez, and J. C. Alvarez, "Comparison of step length estimators from weareable accelerometer devices," in *Proc. International Conference of the IEEE Engineering in Medicine and Biology Society*, New York, NY, USA, Aug. 2006, pp. 5964–5967.

[79] R. C. Gonzalez, D. Alvarez, A. M. Lopez, and J. C. Alvarez, "Modified pendulum model for mean step length estimation," in *Proc. 29th Annual International Conference of the IEEE Engineering in Medicine and Biology Society*, Lyon, France, Aug. 2007, pp. 1371–1374.

[80] A. Köse, A. Cereatti, and U. Della Croce, "Bilateral step length estimation using a single inertial measurement unit attached to the pelvis," *J. Neuroeng. Rehabilitation*, vol. 9, no. 1, p. 9, Dec. 2012.

[81] H. Xing, J. Li, B. Hou, Y. Zhang, and M. Guo, "Pedestrian stride length estimation from IMU measurements and ANN based algorithm," *J. Sens.*, vol. 2017-2, pp. 1–10, 2017.

[82] V. Renaudin, M. Susi, and G. Lachapelle, "Step length estimation using handheld inertial sensors," *Sensors*, vol. 12, no. 7, pp. 8507–8525, Jul. 2012, Number: 7 Publisher: Molecular Diversity Preservation International.

[83] M. Bertschi, P. Celka, R. Delgado-Gonzalo, *et al.*, "Accurate walking and running speed estimation using wrist inertial data," in *Proc. 37th Annual International Conference of the IEEE Engineering in Medicine and Biology Society (EMBC)*, Milan, Italy, Aug. 2015, pp. 8083–8086.

[84] S. Miyazaki, "Long-term unrestrained measurement of stride length and walking velocity utilizing a piezoelectric gyroscope," *IEEE Trans. Biomed. Eng.*, vol. 44, no. 8, pp. 753–759, Aug. 1997.

[85] E. M. Diaz and A. L. M. Gonzalez, "Step detector and step length estimator for an inertial pocket navigation system," in *Proc. International Conference on Indoor Positioning and Indoor Navigation (IPIN)*, Busan, Korea (South), Oct. 2014, pp. 105–110.

[86] Q. Li, M. Young, V. Naing, and J. M. Donelan, "Walking speed estimation using a shank-mounted inertial measurement unit," *J. Biomech.*, vol. 43, no. 8, pp. 1640–1643, May 2010.

[87] S. Yang and Q. Li, "Ambulatory walking speed estimation under different step lengths and frequencies," in *Proc. IEEE/ASME International Conference on Advanced Intelligent Mechatronics*, Montreal, QC, Canada, Jul. 2010, pp. 658–663.

[88] S. Zihajehzadeh and E. J. Park, "Experimental evaluation of regression model-based walking speed estimation using lower body-mounted IMU," in *Proc. 38th Annual International Conference of the IEEE Engineering in Medicine and Biology Society (EMBC)*, Orlando, FL, USA, Aug. 2016, pp. 243–246.

[89] ——, "Regression model-based walking speed estimation using wrist-worn inertial sensor," *PLoS One*, vol. 11, no. 10, e0165211, Oct. 2016.

[90] A. Nouriani, R. A. McGovern, and R. Rajamani, "Step length estimation using inertial measurements units," in *Proc. American Control Conference (ACC)*, New Orleans, LA, USA, May 2021, pp. 666–671.

[91] J. Zhang, M. Sun, and X. Wang, "Dynamic distance estimation method based on RSSI and LQI," *Electronic Measurement Technology*, vol. 30, no. 2, pp. 142–145, Feb. 2007.

[92] J. Liu, Z. Wang, M. Yao, and Z. Qiu, "VN-APIT: Virtual nodes-based range-free APIT localization scheme for WSN," *Wirel. Netw.*, vol. 22, no. 3, pp. 867–878, Apr. 2016.

[93] J. Wang and H. Jin, "Improvement on APIT localization algorithms for wireless sensor networks," in *Proc. International Conference on Networks Security, Wireless Communications and Trusted Computing*, vol. 1, Wuhan, China, Apr. 2009, pp. 719–723.

[94] S. Kumar, K. Kislay, M. K. Singh, and R. M. Hegde, "A range-free tracking algorithm in vehicular ad-hoc networks," in *Proc. Twentieth National Conference on Communications (NCC)*, Kanpur, India, Feb. 2014, pp. 1–6.

[95] D. Zhang, F. Xia, Z. Yang, L. Yao, and W. Zhao, "Localization technologies for indoor human tracking," in *Proc. 5th International Conference on Future Information Technology*, Busan, Korea (South), May 2010, pp. 1–6.

[96] M. Sugano, "Indoor localization system using rssi measurement of wireless sensor network based on zigbee standard," *Wireless and Optical Communications*, vol. 538, pp. 1–6, 2006.

[97] X. Zhu and Y. Feng, "RSSI-based algorithm for indoor localization," *Communications and Network*, vol. 05, no. 2, pp. 37–42, May 2013.

[98] S. Hamdoun, A. Rachedi, and A. Benslimane, "Comparative analysis of RSSI-based indoor localization when using multiple antennas in wireless sensor networks," in *Proc. International Conference on Selected Topics in Mobile and Wireless Networking (MoWNeT)*, Montreal, QC, Canada, Aug. 2013, pp. 146–151.

[99] L. Altoaimy, I. Mahgoub, and M. Rathod, "Weighted localization in vehicular ad hoc networks using vehicle-to-vehicle communication," in *Proc. Global Information Infrastructure and Networking Symposium (GIIS)*, Montreal, QC, Canada, Sep. 2014, pp. 1–5.

[100] J.-R. Jiang, C.-M. Lin, F.-Y. Lin, and S.-T. Huang, "ALRD: AoA localization with RSSI differences of directional antennas for wireless sensor networks," *Int. J. Distrib. Sens. Netw.*, vol. 9, no. 3, p. 529 489, Mar. 2013.

[101] V. Kumar, R. Arablouei, R. Jurdak, B. Kusy, and N. W. Bergmann, "RSSI-based self-localization with perturbed anchor positions," in *Proc. IEEE 28th Annual International Symposium on Personal, Indoor, and Mobile Radio Communications (PIMRC)*, Montreal, QC, Canada, Oct. 2017, pp. 1–6.

[102] X. Li, "RSS-based location estimation with unknown pathloss model," *IEEE Trans. Wireless Commun.*, vol. 5, no. 12, pp. 3626–3633, Jan. 2007.

[103] L. Pormante, C. Rinaldi, M. Santic, and S. Tennina, "Performance analysis of a lightweight RSSI-based localization algorithm for wireless sensor networks," in *Proc. International Symposium on Signals, Circuits and Systems ISSCS2013*, Iasi, Romania, Jul. 2013, pp. 1–4.

[104] F. Yaghoubi, A.-A. Abbasfar, and B. Maham, "Energy-efficient RSSI-based localization for wireless sensor networks," *IEEE Commun. Lett.*, vol. 18, no. 6, pp. 973–976, Jun. 2014.

[105] J. Zheng, C. Wu, H. Chu, and Y. Xu, "An improved RSSI measurement in wireless sensor networks," *Procedia Eng.*, vol. 15, pp. 876–880, Jan. 2011.

[106] H. Wang, J. Wan, and R. Liu, "A novel ranging method based on RSSI," *Energy Procedia*, vol. 12, pp. 230–235, Dec. 2011.

[107] P. K. Sahu, E. H.-K. Wu, and J. Sahoo, "DuRT: Dual RSSI trend based localization for wireless sensor networks," *IEEE Sens. J.*, vol. 13, no. 8, pp. 3115–3123, Aug. 2013.

[108] H. Shi, "A new weighted centroid localization algorithm based on RSSI," in *Proc. IEEE International Conference on Information and Automation*, Shenyang, China, Jun. 2012, pp. 137–141.

[109] B. Mukhopadhyay, S. Sarangi, and S. Kar, "Performance evaluation of localization techniques in wireless sensor networks using RSSI and LQI," in *Proc. Twenty First National Conference on Communications (NCC)*, Mumbai, India, Feb. 2015, pp. 1–6.

[110] Z. Jianwu and Z. Lu, "Research on distance measurement based on RSSI of ZigBee," in *Proc. ISECS International Colloquium on Computing, Communication, Control, and Management*, vol. 3, Sanya, China, Aug. 2009, pp. 210–212.

[111] Z. Zhang, X. Zhou, W. Zhang, *et al.*, "I am the antenna: Accurate outdoor AP location using smartphones," in *Proc. 17th annual international conference on Mobile computing and networking*, New York, NY, USA, Sep. 2011, pp. 109–120.

[112] J. Seberry, L. C. Tran, A. Mertins, and T. A. Wysocki, *Complex Orthogonal Space-Time Processing in Wireless Communications*. Springer Science & Business Media, 2007.

[113] L. C. Tran, T. A. Wysocki, J. Seberry, A. Mertins, and S. S. Adams, "Novel constructions of improved square complex orthogonal designs for eight transmit antennas," *IEEE Trans. Inf. Theory*, vol. 55, no. 10, pp. 4439–4448, Oct. 2009.

[114] T. S. Rappaport, *Wireless communications: principles and practice*. Prentice Hall PTR, 1996, vol. 2.

[115] Y. Wang, X. Yang, Y. Zhao, Y. Liu, and L. Cuthbert, "Bluetooth positioning using RSSI and triangulation methods," in *Proc. IEEE 10th Consumer Communications and Networking Conference (CCNC)*, Las Vegas, NV, Jan. 2013, pp. 837–842.

[116] H. Zhang, F. Safaei, and L. C. Tran, "Measurement-based characterizations of on-body channel in the human walking scenario," in *Proc. IEEE 85th Vehicular Technology Conference (VTC Spring)*, Sydney, NSW, Australia, Jun. 2017, pp. 1–5.

[117] J. Xu, W. Liu, F. Lang, Y. Zhang, and C. Wang, "Distance measurement model based on RSSI in WSN," *Wirel. Sens. Netw.*, vol. 02, no. 8, pp. 606–611, Aug. 2010.

[118] A. J. Yves and P. Hao, "RSSI-based indoor localization using RSSI-with-angle-based localization estimation algorithm," *Int. J. Sens. Netw.*, vol. 04, no. 122, 2015.

[119] M. Jais, P. Ehkan, R. Ahmad, I. Ismail, T. Sabapathy, and M. Jusoh, "Review of angle of arrival (AOA) estimations through received signal strength indication (RSSI) for wireless sensors network (WSN)," in *Proc. International Conference on Computer, Communications, and Control Technology (I4CT)*, Kuching, Malaysia, Apr. 2015, pp. 354–359.

[120] F. Gu, K. Khoshelham, C. Yu, and J. Shang, "Accurate step length estimation for pedestrian dead reckoning localization using stacked autoencoders," *IEEE Trans. Instrum. Meas.*, vol. 68, no. 8, pp. 2705–2713, Oct. 2018.

[121] I. Klein and O. Asraf, "StepNet—deep learning approaches for step length estimation," *IEEE Access*, vol. 8, pp. 85 706–85 713, May 2020.

[122] M. Vezočnik and M. B. Juric, "Average step length estimation models' evaluation using inertial sensors: A review," *IEEE Sens. J.*, vol. 19, no. 2, pp. 396–403, Jan. 2019.

[123] S. H. Shin and C. G. Park, "Adaptive step length estimation algorithm using optimal parameters and movement status awareness," *Med. Eng. Phys.*, vol. 33, no. 9, pp. 1064–1071, Nov. 2011.

[124] S. Díaz, S. Disdier, and M. A. Labrador, "Step length and step width estimation using wearable sensors," in *Proc. 9th IEEE Annual Ubiquitous Computing, Electronics & Mobile Communication Conference (UEMCON)*, New York, NY, USA, Nov. 2018, pp. 997–1001.

[125] A. A. Perez and M. A. Labrador, "A smartphone-based system for clinical gait assessment," in *Proc. IEEE International Conference on Smart Computing (SMARTCOMP)*, St. Louis, MO, USA, May 2016, pp. 1–8.

[126] H. Zhang, F. Safaei, and L. C. Tran, "A novel cooperation-based network coding scheme for walking scenarios in WBANs," *Wirel. Commun. Mob. Comput.*, vol. 2017, pp. 1–20, Sep. 2017.

[127] ——, "Channel autocorrelation-based dynamic slot scheduling for body area networks," *Eurasip J. Wirel. Commun. Netw.*, vol. 2018, no. 1, pp. 1–7, Dec. 2018.

[128] ——, "Joint transmission power control and relay cooperation for WBAN systems," *Sensors*, vol. 18, no. 12, p. 4283, Dec. 2018.

[129] Z. Yang, L. C. Tran, and F. Safaei, "Step length measurements using the received signal strength indicator," *Sensors*, vol. 21, no. 2, p. 382, Jan. 2021.

[130] H. Friis, "A note on a simple transmission formula," *Proc. IRE*, vol. 34, no. 5, pp. 254–256, May 1946.

[131] DIGI. "XBee/XBee-PRO® s2c zigbee® RF module user guide." (2020), [Online]. Available: https://www.digi.com/resources/documentation/digidocs/pdfs/90002002.pdf.

[132] D. M. Pozar, *Microwave Engineering*. John Wiley & Sons, Nov. 2011.

[133] A. Poulose, J. Kim, and D. S. Han, "A sensor fusion framework for indoor localization using smartphone sensors and wi-fi RSSI measurements," *Applied Sciences*, vol. 9, no. 20, p. 4379, Jan. 2019.

[134] Z. Yang, L. C. Tran, and F. Safaei, "Step length estimation using the RSSI method in walking and jogging scenarios," *Sensors*, vol. 22, no. 4, p. 1640, Jan. 2022.

[135] "IEEE standard for information technology– local and metropolitan area networks– specific requirements– part 15.4: Wireless medium access control (MAC) and physical layer (PHY) specifications for low-rate wireless personal area networks (WPANs): Amendment 1: Add alternate PHYs," *IEEE Std. 802.15.4a-2007*, Aug. 2007.